Terahertz wave phase stabilization for ultra-high frequency wireless communication

アマリナ アティラ ビンティ イブラヒム

出版情報：九州大学, 2023, 博士（学術）, 課程博士

TERAHERTZ WAVE PHASE STABILIZATION FOR ULTRA-HIGH FREQUENCY WIRELESS COMMUNICATION

AMALINA ATHIRA BINTI IBRAHIM

KYUSHU UNIVERSITY

A thesis submitted in fulfilment of the
requirements for the award of the degree of
Doctor of Philosophy

Thesis Committee:

Supervisor	:	Prof. Yuji Oki
Co-Supervisor	:	Prof. Shunji Kimura
Co-Supervisor	:	Prof. Kazutoshi Kato
Date	:	31 JULY 2023

TERAHERTZ WAVE PHASE STABILIZATION FOR ULTRA-HIGH FREQUENCY WIRELESS COMMUNICATION

AMALINA ATHIRA BINTI IBRAHIM

A thesis submitted in fulfillment of the
requirements for the award of the degree of
Doctor of Philosophy

Department of Electrical and Electronic Engineering
Graduate School of Information Science and Electrical Engineering
Kyushu University

JULY 2023

DEDICATION

For my beloved family and Malaysia-Japan relationship.

ACKNOWLEDGEMENT

I would like to express my deep gratitude to all those who have contributed significantly to the preparation and completion of this thesis. Their guidance, support, and contributions have been invaluable to my academic journey. First and foremost, my heartfelt appreciation goes to my academic supervisor, Prof. Kazutoshi Kato, for his unwavering commitment, vast knowledge, insightful ideas, and constructive criticism throughout this research. I am truly grateful for his guidance. I am also indebted to my external academic supervisor, Prof. Osamu Mikami, for his valuable guidance and inspiration in shaping my research direction and methodology. Sincere gratitude goes to Dr. Yuya Mikami, an assistant professor, for his invaluable guidance, inspirational insights, and valuable suggestions that significantly enhanced the quality of this research project.

Furthermore, I would like to acknowledge and extend my gratitude to Prof. Yuji Oki and Prof. Shunji Kimura for their invaluable contributions as members of my thesis committee. Their expertise, feedback, and valuable suggestions have greatly enriched the content of this thesis and improved its overall quality.

I am immensely grateful to the Japan International Cooperation Agency (JICA) for their sponsorship under the 4th Innovative Asia program, enabling me to pursue this research and fostering academic growth.

I would like to acknowledge and thank my postgraduate friends, whose support and camaraderie have been invaluable. I express my gratitude to Takashi Shiramizu, Hanwei Chen, Shenghong Ye, Bo Li, Kazuya Kondo, Qingjie Song, Naoya Seiki, Ruo Yamamoto, Yuki Matsuo, Yusuke Kawai, Momone Ida, Chengyuan Qian, Naoto Masutomi, Ryo Doi, Haolan Tang, Chong Zhang, Aoi Asano, and Hussein Ssali for their friendship and shared experiences. Furthermore, I extend my appreciation to Dr. Ming Che, a research fellow in our lab, for his valuable insights and contributions, as well as Ms. Ikumi Fukamachi, our laboratory's secretary, for her exceptional support and organizational skills.

To my beloved family, especially my parents, Mr. Ibrahim Mohamad and Dr. Nor Rizah Abdul Rashid, thank you for your unwavering support and encouragement. I am also grateful to my siblings, Siti Nabila Aishah, Amirul Al-Amin, Al-Muizzuddin Hakim, Amirah Syazana, and Aqilah Nabighah, for their continuous belief in me. Lastly, I would like to extend my deepest gratitude to my friends Dr. Fatin Hazwani and Zihong Ye, whose help and support made this academic journey more enjoyable. To all those whose names couldn't be mentioned, your contributions have not gone unnoticed. I am truly grateful for the assistance and encouragement from each and every one of you. Finally, I dedicate this thesis as a testament to my efforts and as a token of appreciation to all those who have supported and believed in me. Thank you for being an integral part of my academic journey.

ABSTRACT

As a high-frequency carrier, the Terahertz (THz) wave is essential for achieving high-data-rate wireless transmission due to its ultra-wide bandwidth. Phase stabilization becomes crucial to enable phase-shift-based multilevel modulation for high-speed data transmission. A Mach-Zehnder interferometric phase stabilization technique for photomixing is developed, which has proved a promising method for phase-stable continuous THz-wave generation. However, this method faces inefficiencies in generating phase-modulated THz waves due to the impact of the phase modulator on the phase stabilization system. By photomixing, which is a promising method for generating terahertz waves, the phase of the generated waves can be controlled in the optical domain, so that the stability of the generated THz wave can be controlled by photonics technologies. Thus, a novel phase stabilization approach using backward-directional lightwave is devised, which is overlapped with the THz wave generation system. This study presents a conceptual and experimental framework for stabilizing the phases of optical carrier signals at different frequencies. I compare the optical domain and transmission performances between forward-directional and backward-directional phase stabilization methods. Remarkably, our results demonstrate error-free transmission at a modulation frequency of 3 Gbit/s and higher.

概要

本研究では、超広帯域性を有するテラヘルツ（THz）波を高データレートの無線伝送に不可欠な高周波キャリアとして位置付けています。高速データ伝送のためには位相シフトを利用した多値変調を用いるため、位相安定化が重要です。我々は、連続的な THz 波生成において有望な手法とされているフォトミキシングシステムをマッハ-ツェンダ干渉計として動作させる位相安定化技術を開発しました。この手法は THz の位相を光ドメインで検出、制御することで THz 波の位相安定化が可能というフォトミキシングの利点を用いたものです。しかし、このシステムで THz 波を位相変調すると、位相変調による干渉効率の低下が課題となります。そこで、私は THz 波生成システムに逆方向光波を用いた新しい位相安定化手法を提案しました。本研究では、異なる周波数での光キャリア信号の位相を安定化するための概念的および実験的なフレームワークを提示しています。さらに、進行方向と逆方向の位相安定化手法の伝送特性を比較しました。これらの結果をもとに 3 Gbit/s 以上の変調周波数におけるエラーフリー伝送を実証しました。

TABLE OF CONTENTS

LIST OF TABLES

LIST OF FIGURES

CHAPTER 1
INTRODUCTION

1.1 Research Background

In the 21st century, mobile device usage has increased dramatically, which is quite amazing. New gadgets with improved capabilities and intelligence are introduced every year, and this leads to their market adoption. This is a result of the continually strong demand and the industry rapid rate of innovation. The rise of machine-to-machine (M2M) applications including video surveillance, healthcare monitoring, transportation systems, and device tracking systems is also contributing to this explosion in mobile devices. The development of devices and connections is significantly influenced by these M2M applications. Cisco Annual Internet reports that M2M connections increased significantly from 2018 to 2023 [1], as seen in Figure 1.1. The number of M2M devices are more than doubling in number by 2023 compared to 2018.

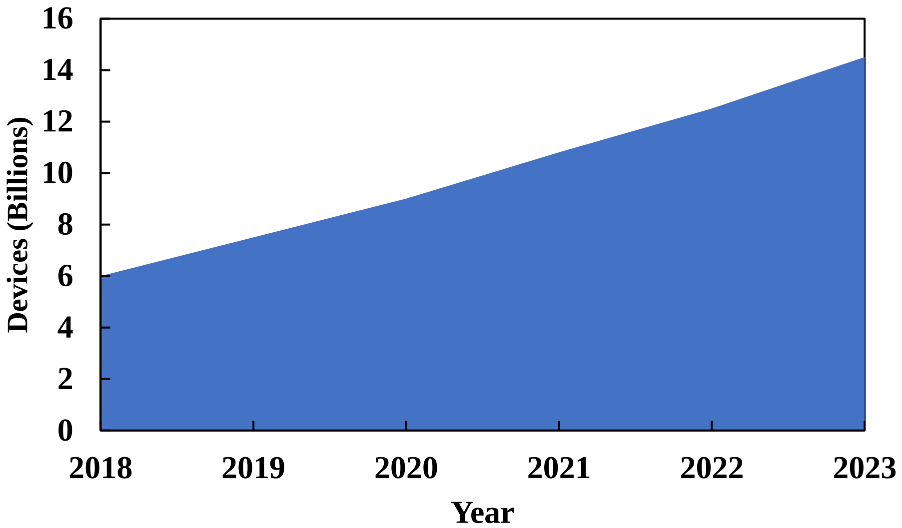

Figure 1.1 Global trend of M2M from 2018 to 2023

In response to the increasing demand and the need to enhance service capabilities, there has been a race to improve data rates. Boosting data rates is crucial to meet the ever-growing service requirements. This phenomenon aligns with Edholm's Law, which states that bandwidth and data rates double every 18 months. This law has proven to be remarkably accurate in predicting the ongoing progress of data transmission speeds. In 1995, wireless transmission operated at approximately 5 to 10 kbit/s, which significantly increased to 100 kbit/s by 2004 [2]. The transition from 3G technologies during 2000-2010 witnessed data rates ranging from several Mbit/s, followed by 4G LTE offering download speeds of up to 100 Mbit/s within 2010-2020. Today, the deployment of 5G networks has expected to reach the speed up to 10 Gbit/s, as illustrated in the Figure 1.2, aligning with Edholm's law. Furthermore, by 2030, the industry aims to reach a peak data rate of 1,000 Gbit/s (1 Tbit/s) for in 6G.

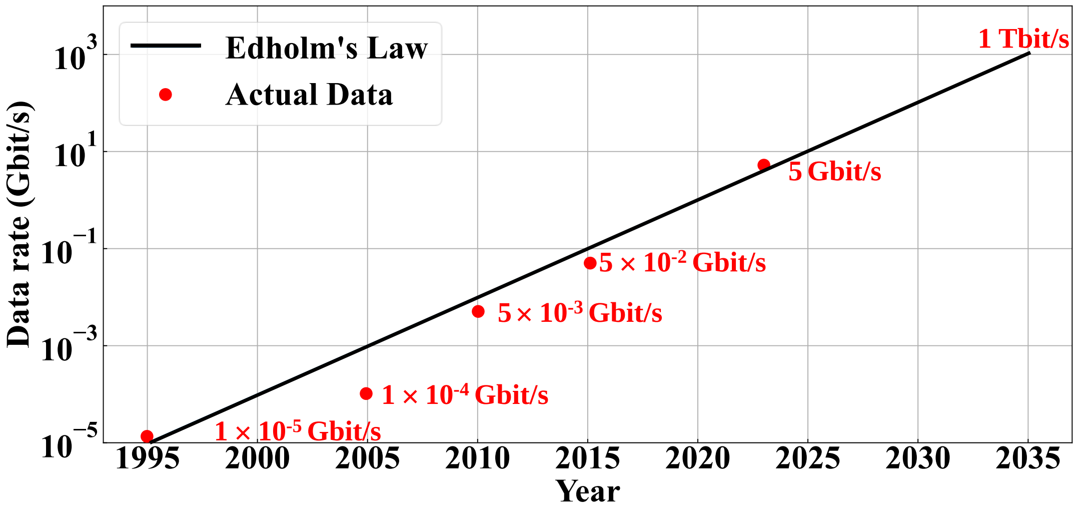

Figure 1.2 The data rate of wireless communication from 1995 up to 2035

This situation of racing to increase bandwidth is also aimed at enabling mobile life beyond 2030. This aligns with the target of evolving modes of communication between 2022 and 2030, as reported by the Ericsson White Paper shown in the Figure 1.3. Today, communication based on audio-visual digital communication is transitioning towards additional sensory experiences. By 2030, digital experiences will become more immersive, starting with extended reality (XR) and progressing towards holographic communication. Beyond 2030, multisensory extension will gradually enhance the level of immersion beyond audio-visual, incorporating other senses such as touch, taste, and smell [3].

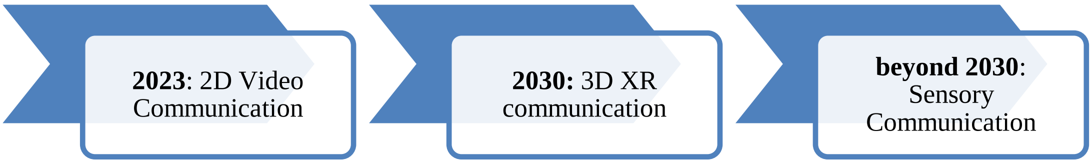

Figure 1.3 Evolving mode of communication from 2023 and beyond

1.2 THz Waves: Meeting High-Speed Communication Needs

Attention is being drawn to the Terahertz (THz) frequency band as a potential answer to the growing need for high-speed wireless communication. Since the 2000s, THz waves have been referred to as submillimeter waves since they fall between microwaves and infrared light waves in the electromagnetic spectrum. The term "THz waves" now refers to frequencies between 0.1 THz and 10 THz. [4]. These THz bands offer ultra-wide bandwidth, making them suitable for numerous application areas that require high data rates exceeding tens of Gbps, including communication at both nano-scale and macro-scale levels [5]. As result, THz communication has the potential to provide ultra-wide bandwidth, enabling extremely high transmission rates [6]. This makes it suitable for high-capacity wireless communication systems and potential future technologies like 6G access networks.

To assess the potential data capacity of a communication channel, the Shannon-Hartley theorem provides a fundamental mathematical equation that correlates the channel capacity, *C* with the available bandwidth, *B* and the signal, *S*-to-noise, *N* ratio the channel. The theorem is expressed as follows:

$$C = B\, log_2\left(1 + \frac{S}{N}\right) \tag{1}$$

In principle, the Shannon-Hartley theorem establishes that the capacity (transmission rate), C of a communication channel is directly proportional to the bandwidth and the logarithm of the signal-to-noise ratio. The bandwidth, B denotes the range of frequencies allocated for communication, while the signal-to-noise ratio quantifies the ratio of desired signal power to background noise power within the channel.

In practical terms, this means that the transmission rate is directly influenced by the available bandwidth. Same situation as the signal-to-noise ratio improves, the transmission rate increases. However, the rate of increase becomes smaller as the signal-to-noise ratio reaches higher levels. This is because the relationship between the signal-to-noise ratio and the transmission rate is logarithmic, meaning that the gains achieved become gradually smaller with each improvement in the ratio. To achieve significant increases in the transmission rate, it is more effective to focus on increasing the available bandwidth, as wider bandwidths have linear impact on the transmission rate.

By using higher frequencies, which enable wider bandwidths, the transmission rate can be significantly improved. Current 5G technology also use higher frequency range than conventional radio wave, 400 MHz to 52.6 GHz to achieve their target data rate at 20 Gbit/s [7]. Similarly, for the future 6G communication systems aiming to achieve data rates of up to 1 Tbit/s, higher frequency ranges such as the THz wave frequency range will be required.

1.3 THz Wave Generation Method

Terahertz wave is generated by either all-electronic approach employing electronics devices for both THz emitter and receiver and opto-electronics approach which based on photonic generation on high-speed THz signal. Here, the summarize up-to date of THz wave generation method in Table 1 for all-electronics and opto-electronics approach and the explanation of each approach. First, there are several methods based on all-electronic approach. There is Heterojunction Bipolar Transistors (HBTs), Field-Effect Transistors (FETs), Schottky Diodes and High Electron Mobility Transistors (HEMTs). Meanwhile, in opto-electronics approach, there are some approaches such as Photonic Integrated Circuits (PICs), Quantum Cascade Lasers (QCLs) and photomixer. The simplified configuration of both main approaches can be illustrated as in Figure 1.4.

The all-electronics approach relies solely on electronic devices in its configuration, as shown in Figure 1.4 (a). This approach offers notable advantages such as excellent resolution and adaptability for THz applications. However, certain applications require THz measurements for wideband and high-speed signals that exceed the speed and bandwidth capabilities of electronic devices [8]. In such cases, photonics-based methods can provide a solution with wider bandwidths [9]. The opto-electronic approach in Figure 1.4 (b) utilizes a fiber optic configuration, enabling seamless connectivity between fiber optic and wireless communication networks. This approach offers the potential for generating THz waves with wider bandwidths and higher speeds compared to purely electronic methods. Taking these factors into account, opto-electronics THz generation method is chosen for this research. Specifically, the photomixing technique is employed as a key method for generating THz waves.

Table 1 Technology of all-electronic and electronic-photonic approaches for generating THz wave

	Approach	Explanation	References
All-Electronics	Heterojunction Bipolar Transistors (HBTs)	HBTs can be employed to generate THz waves by exploiting their high-frequency capabilities. By biasing the transistor appropriately, THz waves can be emitted through the interaction of charge carriers within the device.	[10], [11]
	Field-Effect Transistors (FETs)	FETs can be utilized to generate THz waves by leveraging their high-frequency response. By applying suitable electrical signals and biasing conditions to the FET, THz waves can be generated through the modulation and interaction of charge carriers within the device.	[12], [13]
	Schottky Diodes	Schottky diodes can be utilized to generate THz waves by exploiting their nonlinear characteristics. By applying an appropriate electrical signal to the diode, THz waves can be generated through the mixing and rectification of high-frequency signals.	[14], [15]
	High Electron Mobility Transistors (HEMTs)	HEMTs can be employed to generate THz waves by leveraging their high-frequency capabilities and high electron mobility. By controlling the biasing conditions and applying suitable electrical signals, THz waves can be generated through the interaction of charge carriers within the device.	[16], [17]
Optoelectronics	Photonic Integrated Circuits (PICs)	PICs offer a compact and integrated platform for generating and manipulating THz waves. They leverage the principles of photonics to generate and control THz signals within a chip-scale device. The components within the PIC work together to generate THz waves through processes such as optical-to-electrical conversion and modulation.	[18]–[20]
	Quantum Cascade Lasers (QCLs)	QCLs are semiconductor lasers specifically designed to emit THz waves. They employ quantum cascade structures that enable the emission of THz radiation through intersubband transitions within the semiconductor layers. The QCL setup typically includes a power supply and temperature control to maintain optimal operation.	[21], [22]
	Photomixers	**Photomixers generate THz waves through the process of optical mixing. The setup involves two optical waves, typically generated by lasers, which are combined in a photomixer device. The mixing of these optical waves within the photomixer leads to the generation of THz radiation.**	[23]–[26]

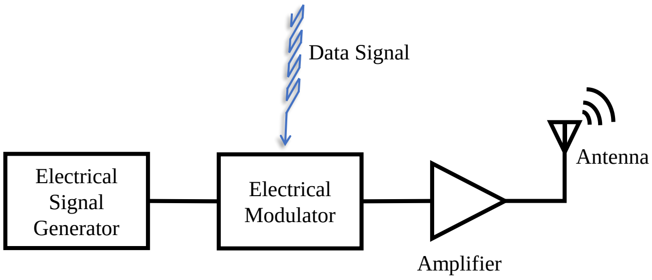

(a)

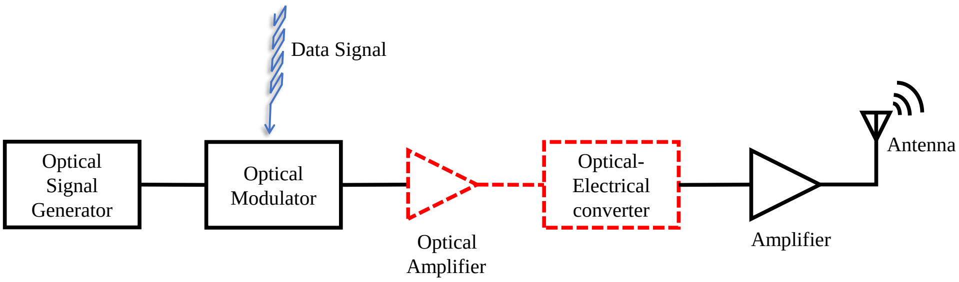

(b)

Figure 1.4 THz wave generation approaches; (a) all-electronics and (b) opto-electronics.

Photomixing is a technique that involves the use of a specific device called a photomixer, which can convert optical signals into electrical signals and generate THz waves as shown in Figure 1.5. By introducing two continuous lightwaves with different frequency of f_1 and f_2 into the photomixer, such as a photoconductor or photodiode, the optical-to-electrical conversion occurs, resulting in the generation of THz waves. The frequency and phase of the generated THz wave depend on the difference of $f_1 - f_2$ and phase difference of $\varphi_1 - \varphi_2$ between the original two lightwaves. Among the various types of photomixer available, the uni-traveling carrier photodiode (UTC-PD) is commonly used due to its high-speed response and efficient conversion of optical signals into THz waves. The UTC-PD offers advantages such as higher operation current and lower operation voltage [27].

THz waves have a lot of appeal for communication because of the large bandwidth and promise for high-capacity wireless data transmission. When utilizing the wide bandwidth of THz waves for data communication, multilevel modulation

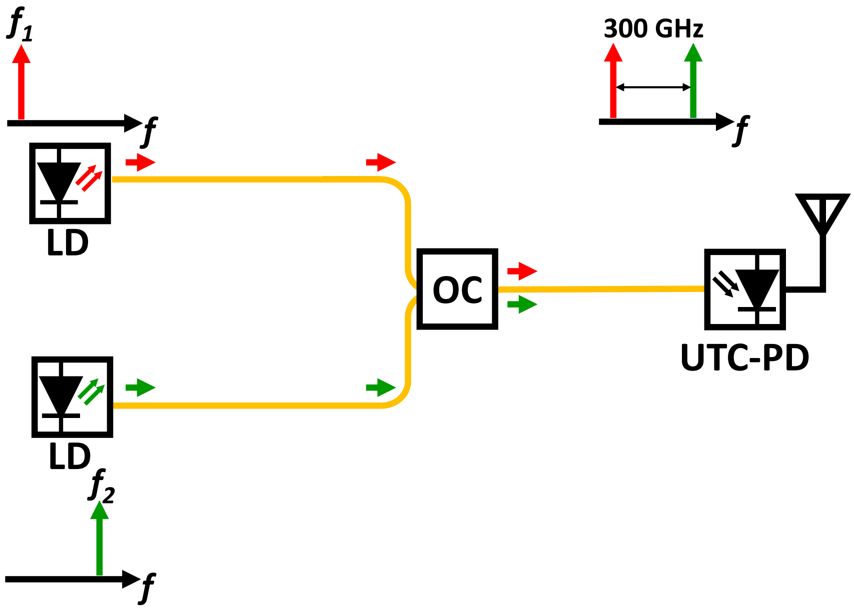

Figure 1.5 Basic system of photomixing technique

becomes essential. By employing multilevel modulation techniques, frequency utilization efficiency can be increased and enable unique applications such as ultra-high-speed stream data transmission.

1.4 Development Trend in Multilevel Modulation Technique

In this sub-chapter will explore the development trends in multilevel modulation from recent research papers published in the last five years up to June 2023 made by various countries with carrier frequencies of 100 GHz as in Table 2.

Table 2 Publication of papers on wireless communication with carrier frequency above 100 GHz, achievable modulation rate and modulation scheme applied in recent five years up to June 2023

Carrier frequency (GHz)	Modulation rate (Gbit/s)	Modulation scheme	Approach	Technology	Country/ Region	Year	Reference
80, 120, 160	0.1	BPSK	Opto-Electronic	PD	Netherland	2020	[28]
92-105	10	OOK	Opto-Electronic	UTCPD	Spain	2019	[29]
100	10	OOK	Alternative Approach	Metasurface	China	2023	[30]
110-170	48	QAM	All-Electronic	HBT	India	2017	[31]
125, 175, 225	4, 10	QAM	Opto-Electronic	PD	Taiwan	2022	[32]
130	36	QPSK	All-Electronic	HBT	USA	2018	[33]
149	0.01	OOK	All-Electronic	Transistor-Based Oscillators	USA	2022	[34]
150	30	PAM4	All-Electronic	CMOS	USA	2020	[35]
196	20, 40	BPSK	All-Electronic	Transistor-Based Oscillators	France	2023	[36]
220-260	110	16QAM	All-Electronic	HBT	Germany	2020	[37]
240	30, 50	BPSK, QPSK	All-Electronic	HBT	China	2022	[38]
300	13	QPSK	Opto-Electronic	Photomixer	Japan	2018	[39]
300	16	QPSK	All-Electronic	CMOS	Japan	2021	[40]
300	25	PAM4	Opto-Electronic	PIC	Japan	2022	[41]
300	48	PAM4	Opto-Electronic	RTD UTCPD	Japan	2022	[42]
300	56	64-QAM	All-Electronic	CMOS and InP-HEMT	Japan	2021	[43]
300	100	16-QAM, 32-QAM	Opto-Electronic	UTCPD	Japan	2023	[44]
300	104	OOK, QAM	Alternative Approach	Metasurface	Italy	2022	[45]
300	160	OOK, QAM	Opto-Electronic	PIC	Germany	2022	[46]
300	50, 100	QPSK	Opto-Electronic	UTCPD	Japan	2020	[47]
310	60	PAM4	Opto-Electronic	UTCPD	China	2021	[48]
320	84.4	QAM	Opto-Electronic	Optoelectronic Devices	China	2023	[49]
325	140	QPSK, 16-QAM, 64-QAM	Opto-Electronic	UTCPD	China	2022	[50]
339	124.8	256-QAM	Opto-Electronic	UTCPD	China	2022	[51]
350-475	120	QPSK	Opto-Electronic	UTCPD	China	2017	[52]
375-500	120	QPSK	Opto-Electronic	Photomixer	China	2018	[53]
441.5	3.5	OOK	All-Electronic	Transistor-Based Oscillator	China	2017	[54]
450	16	QPSK	Opto-Electronic	Photomixer	China	2017	[55]
450	132	64QAM	Opto-Electronic	UTCPD	China	2019	[56]
500	144	OOK, QPSK	Opto-Electronic	Optoelectronic Devices	China	2022	[57]

In particular, Table 2 summarizes advancements in wireless communication research with carrier frequencies above 100 GHz, highlighting achievable modulation rates and applied modulation schemes. Notably, the focus has been on exploring the scope of THz waves, pushing the boundaries of carrier frequencies, modulation rates, and modulation scheme levels. This progress has been achieved through the integration of opto-electronic and all-electronic approaches for achieving higher modulation levels.

In 2017, the all-electronic approach utilizing Heterojunction Bipolar Transistors (HBT) demonstrated successful modulation of QPSK at frequencies ranging from 110 GHz to 170 GHz, achieving a transmission rate of 48 Gbit/s. However, it was in 2018 that the opto-electronic approach employing a photomixer technology enabled the transmission of QPSK at 300 GHz, showcasing a significant leap in both frequency and modulation rate. Since then, the exploration of opto-electronic technologies has gained traction. In 2020, the utilization of opto-electronic BPSK modulation achieved a modest modulation rate of 0.1 Gbit/s at carrier frequencies of 80 GHz, 120 GHz, and 160 GHz by the Photodiode (PD) technology. Moreover, an alternative approach utilizing metasurface technology enabled OOK modulation at 100 GHz with a 10 Gbit/s modulation rate, marking a novel achievement in wireless communication research.

Then, the significant advancements in both modulation rates and scheme levels is observed. In 2021, the all-electronic approach combined CMOS and InP-HEMT technologies to achieve an impressive modulation rate of 56 Gbit/s using 64-QAM modulation at 300 GHz. Additionally, opto-electronic approach by the UTC-PD technology facilitated the transmission of 104 Gbit/s at the same frequency, employing various modulation schemes including OOK and QAM. Furthermore, the opto-electronic approach proved in achieving higher modulation scheme levels. In 2022, Photonic Integrated Circuit (PIC) technology allowed for 160 Gbit/s modulation rates with combined OOK and QAM schemes at 300 GHz. Similarly, advancements in UTC-PD technology pushed the modulation scheme level to 256-QAM at 339 GHz, achieving a remarkable 124.8 Gbit/s modulation rate.

Figure 1.6 shows the comprehensive visual representation of the relationship between modulation rate and the year of paper publications, showcasing the progression of research efforts in achieving higher transmission speeds. Each data point on the graph represents a specific combination of modulation scheme, approach, and year. The x-axis spans from 2017 to June 2023, providing a timeline of research progress, while the y-axis represents the achieved modulation rate in Gbit/s. Different multilevel modulation schemes are denoted by various symbols assigned to each data point, including OOK/BPSK, QPSK/QAM, PAM4, 16-QAM, 32-QAM, 64-QAM, and 256-QAM. The graph use colors to differentiate between the different approaches utilized in the research.

The graph shows that an increasing transmission speeds progress over time that employed various approaches, both all-electronic and opto-electronic, to achieve higher modulation rates. Significantly, the graph highlights the highest data rate achieved during this period, which reached 160 Gbit/s using the OOK/BPSK scheme in 2022. Moreover, it signifies the prominent contribution of opto-electronic approaches in increasing the transmission rates via different multilevel techniques.

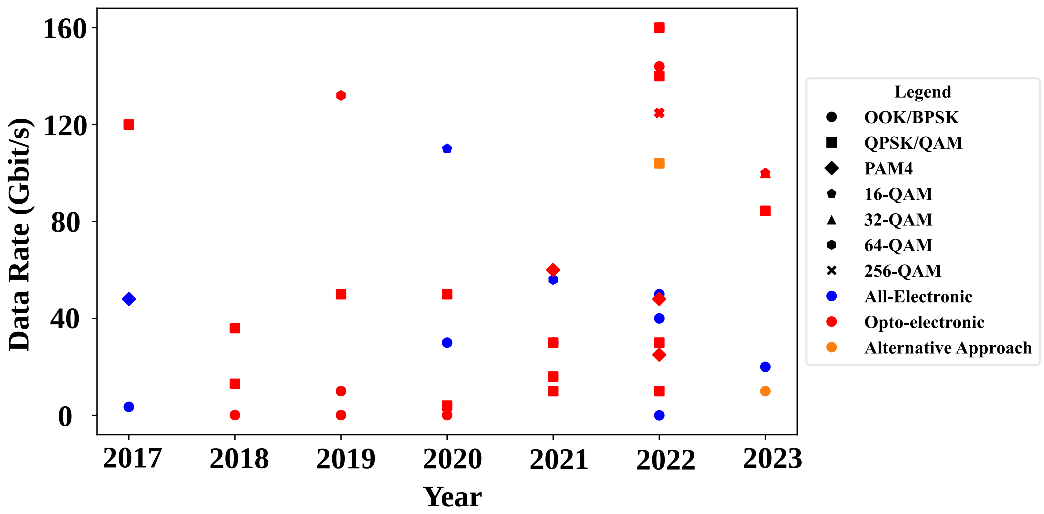

Figure 1.6 Progress of data rate from 2017 up to June 2023 with different modulation schemes and approaches

Figure 1.7 illustrates the relationship between data rate and carrier frequency. It shows that the carrier frequency has been increased up to 500 GHz in order to explore more available bandwidth in higher frequency band for carrying high-speed information. It shows that the opto-electronic approaches have significantly contributed to achieving very high transmission rates, particularly above 80 Gbit/s. The graph indicates that frequencies above 300 GHz are predominantly addressed using opto-electronic approaches. Among all-electronics approaches, the highest transmission bit rate of 110 Gbit/s has been achieved at 220 GHz, while the opto-electronics approach has achieved 140 Gbit/s at 500 GHz. Besides that, as the carrier frequency increases proportionally the data rate can be achieved the same modulation scheme. For instance, the OOK/BPSK modulation scheme, with a symbol of ●, attains 0.1 Gbit/s at 100 GHz and 140 Gbit/s at 500 GHz.

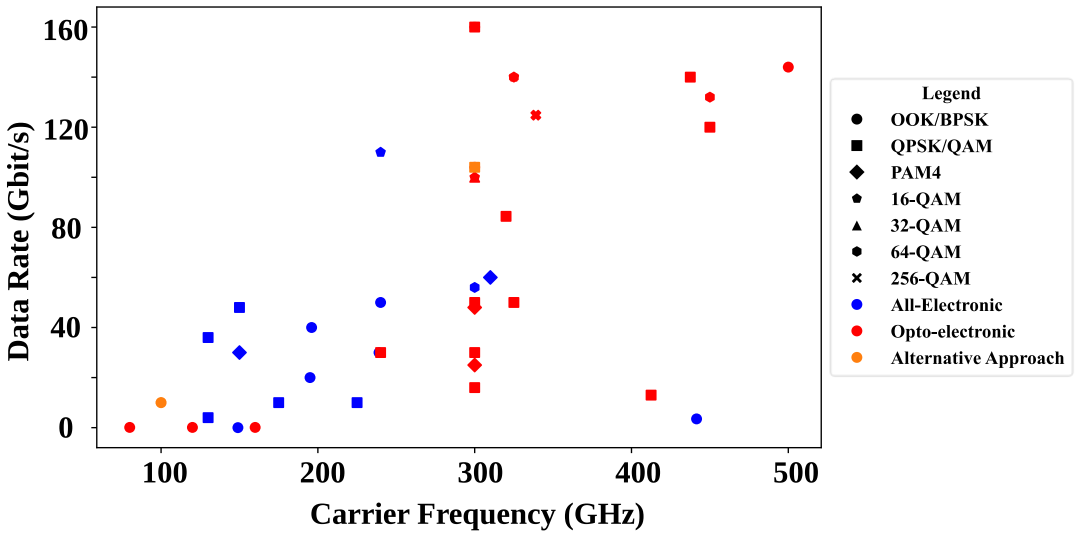

Figure 1.7 Relationship between carrier frequency and transmission rate

Therefore, the relationship between the achieved data rate and the bits per symbol to elucidate multilevel modulation is analyzed in Figure 1.8 . The graph indicates an accumulation of data points at 1 and 2 bits per symbol for the modulation schemes of OOK/ BPSK and QPSK/ QAM/ PAM4, respectively. Furthermore, the graph indicates that the opto-electronics approach achieves the highest bit per symbol. To date, the highest achieved bit per symbol is 8, achieved by 256-QAM at 120 Gbit/s.

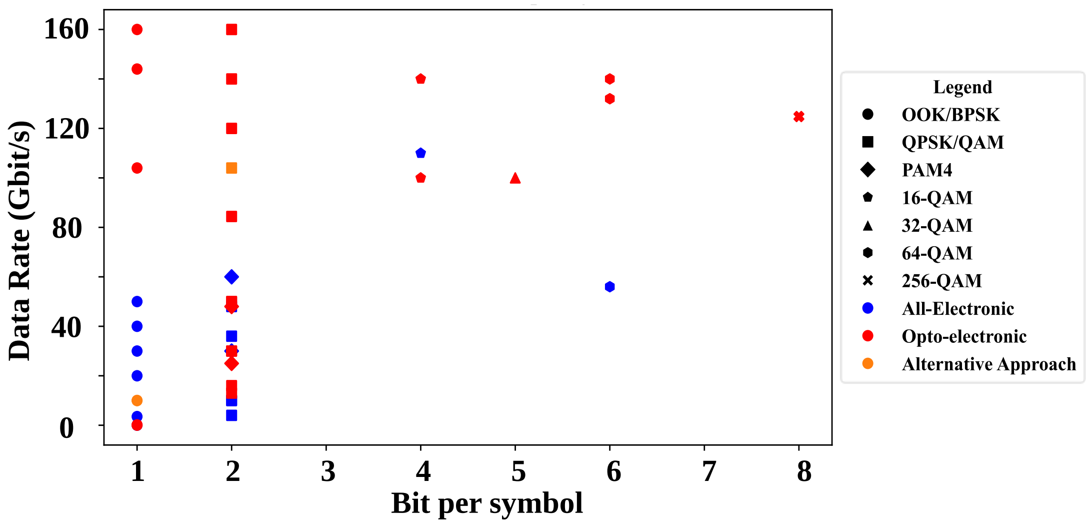

Figure 1.8 Relationship between data rate and the bit per symbol

1.5 Proposal of Generating Phase Modulated THz Wave by Photomixing Approach

As discussed earlier, photomixing has gained attention due to its ability to achieve high-frequency THz wave generation with excellent spectral purity and wide tunability. The UTC-PD, as a photomixer, being a key component in this technique, where it converts the optical power of the input lightwaves into a current. By introducing two continuous lightwaves with different frequencies of f_1 and f_2 into the photomixer, resulted in the generation of THz waves. Let's say the initial lightwave is given below,

$$E_1 = A_1\, e^{i(2\pi f_1 t + \varphi_1)} \tag{2}$$

$$E_2 = A_2\, e^{i(2\pi f_2 t + \varphi_2)} \tag{3}$$

the frequency and phase of the generated THz wave depend on the frequency difference of $f_1 - f_2$ and the phase difference of $\varphi_1 - \varphi_2$ between the original two lightwaves, as shown in the equation below.

$$E_{THz} \propto |E_1 + E_2|^2 \propto A_1{}^2 + A_2{}^2 + 2A_1A_2\cos\big(2\pi(f_1 - f_1)t + (\varphi_1 - \varphi_2)\big) \tag{4}$$

One advantage of photomixing is offering a flexible and tunable approach to THz wave generation. By adjusting the frequencies of the input lightwaves, the generated THz frequency is controllable, allowing for versatile applications in different communication scenarios. However, despite its promise, photomixing faces challenges that need to be addressed for practical implementation. One significant challenge is the phase stability of the lightwave, particularly for implementing multilevel phase modulation.

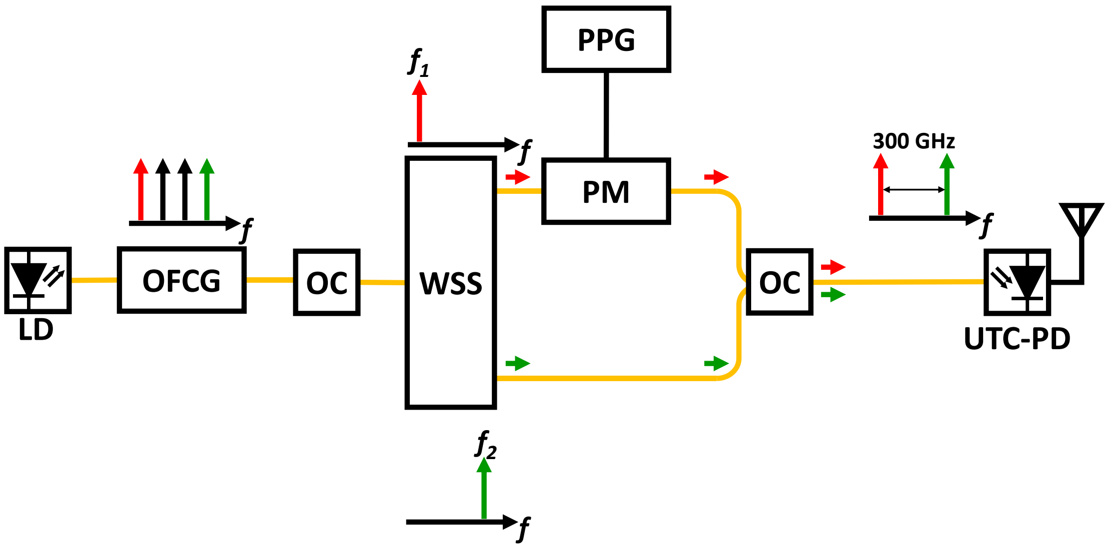

Figure 1.9 OFC-based technique of photomixing.

Figure 1.9 shows an optical frequency comb (OFC)-based photomixing technique for THz wave generation [58], [59]. In this technique, two lightwaves, whose optical frequencies are denoted as f_1 and f_2, are extracted from the OFC using a wavelength selective switch (WSS). The extracted lightwaves are passing through phase modulator (PM) that has been introduced electrical signal by the pulse pattern generator (PPG) on the upper path then combined with lightwave lower path using an optical coupler (OC). Although the initial phase locking of f_1 and f_2 is achieved, the

$$E_{THz} = {A_1}^2 + {A_2}^2 + 2A_1A_2\cos\left(2\pi(f_1 - f_1)t + (\varphi_1 - \varphi_2 + \varphi_{noise})\right) \qquad (5)$$

generated THz wave may experience phase fluctuations, φ_{noise}, due to path length variations in the optical fibers between the optical filter and the OC. THz wave will always change based on the φ_{noise} as shown in the above. Therefore, phase stabilization techniques for the lightwaves are necessary to ensure the stability and reliability of the THz wave generated through photomixing.

A phase stabilization system using the Mach-Zehnder Interferometric (MZI) phase stabilization method [60]–[62] is developed. This method involved introducing a pilot lightwave, f_o, which can be represent as,

$$E_o = A_o \, e^{i(2\pi f t + \varphi)} \quad (6)$$

into the THz wave generation system, which can be considered an MZI, as in Figure 1.10. As the pilot lightwaves from the top,

$$E_{o1} = A_o \, e^{i(2\pi f t + (\varphi + \varphi_{noise}))} \quad (7)$$

and bottom path,

$$E_{o2} = A_o \, e^{i(2\pi f t + \varphi)} \quad (8)$$

interfere after OC, the φ_{noise} is expected can be detected and to be corrected. The interference signal,

$$P_{interference} = 2{A_o}^2 (\, 1 + cos(\varphi_{noise}) \,) \quad (9)$$

is then converted into an electrical signal and introduced into optical.

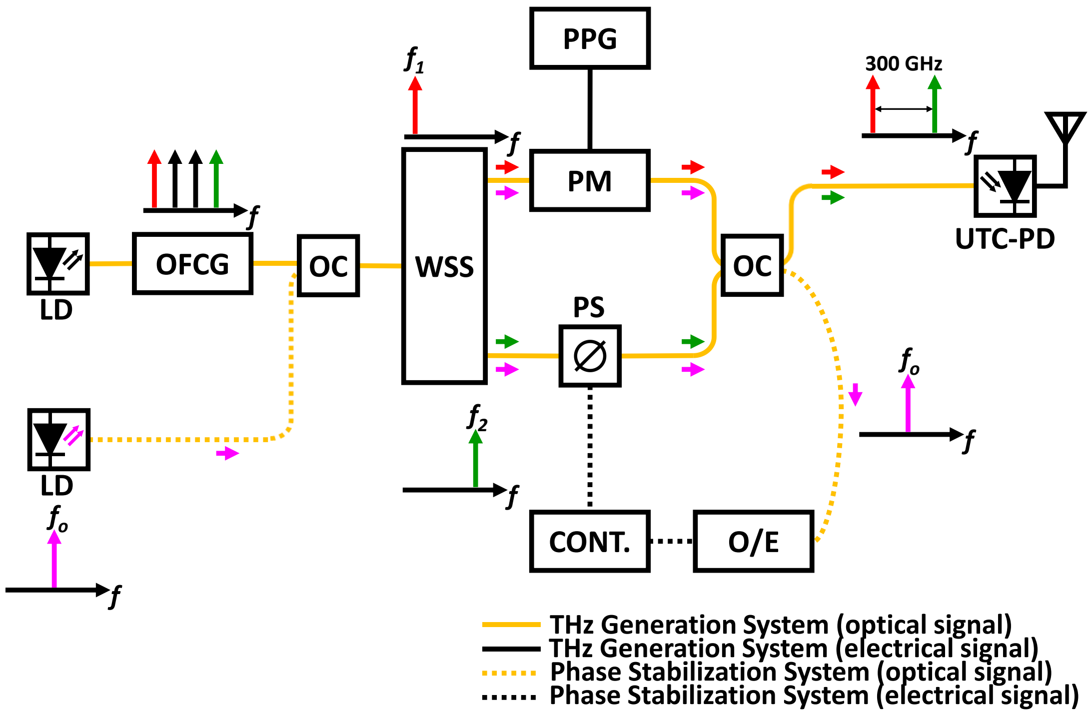

Figure 1.10 MZI phase stabilization method

By controlling the intensity interference of the pilot lightwave at a specific value, the stabilization of the THz wave generation system was achieved.

This approach was successfully demonstrated the transmission of THz-wave data using intensity modulation-coherent detection. However, it is this method is not suitable for THz-wave phase modulation (PM), which is necessary for implementing multilevel PM schemes such as quadrature phase shift keying (QPSK) or 16-state quadrature amplitude modulation (16QAM). However, the pilot lightwave used in the MZI-based stabilization system would also undergo phase modulation, making it unable to accurately detect and compensate for phase fluctuations.

Thus, this thesis came up with a novel phase stabilization technique for a photomixing-based THz-wave phase modulation system which the pilot lightwave being introduced from the backward direction of the generation system. This study will be discussed more in next chapter.

1.6 Topics in This Thesis

In chapter 2 will discuss the development of the novel phase stabilization technique for a photomixing-based THz-wave phase modulation system started with the phase detection method using MZI method, channel setting of Wavelength Selective Switch (WSS), and the phase modulator mechanism. This study has been presented in International Workshop on Plasma Application and Hybrid Functional Materials (March 2022), IEEE International Semiconductor Laser Conference (October 2022) and the 27th OptoElectronics and Communications Conference (OECC) and 2022 International Conference on Photonics in Switching and Computing (PSC) (July 2022).

In Chapter 3 proceed by employing the new phase stabilization system into the THz wave generation setup. This stage in to validate the phase stabilization system in optical domain of THz wave generation system. This study also has been presented in 27th Microoptics Conference (MOC2022) (September 2022), URSI GASS 2023 (August 2023) and MDPI Electronics.

In Chapter 4 procced by generating the phase modulated THz wave and validate the detected signal stability. This result has also being presented in 2022 Asia-Pacific Microwave Conference (APMC) (November 2022), TeraTech (September 2023) and MDPI Electronics.

Finally conclude this thesis in Chapter 5.

REFERENCES

[1] I. Cisco Systems, “Cisco Visual Networking Index: Forecast and Trends, 2017–2022 White Paper,” *Cisco Forecast Methodol.*, pp. 2017–2022, 2019.

[2] S. Cherry, “Edholm’s law of bandwidth,” *IEEE Spectr.*, vol. 41, no. 7, p. 50, 2004.

[3] E. W. Paper, “6G spectrum - enabling the future mobile life beyond 2030,” no. March, 2023.

[4] Z. Li *et al.*, “Terahertz band range adjustable hyperbolic metamaterial refractive index sensor,” *Results Phys.*, vol. 49, no. April, p. 106477, 2023, doi: 10.1016/j.rinp.2023.106477.

[5] K. Tekbıyık, A. R. Ekti, G. K. Kurt, and A. Görçin, “Terahertz band communication systems: Challenges, novelties and standardization efforts,” *Phys. Commun.*, vol. 35, p. 100700, 2019, doi: 10.1016/j.phycom.2019.04.014.

[6] W. Hao, F. Zhou, M. Zeng, O. A. Dobre, and N. Al-Dhahir, “Ultra Wideband THz IRS Communications: Applications, Challenges, Key Techniques, and Research Opportunities,” *IEEE Netw.*, vol. 36, no. 6, pp. 214–220, 2022, doi: 10.1109/MNET.110.2100664.

[7] A. B. Belguidoum, M. L. Tounsi, and S. Mekaoui, “Analysis of 5G Radio Parameters and their Impact on the Peak Data Rate,” *Proc. - 2019 3rd Eur. Conf. Electr. Eng. Comput. Sci. EECS 2019*, pp. 66–71, 2019, doi: 10.1109/EECS49779.2019.00025.

[8] T. Nagatsuma, G. Ducournau, and C. C. Renaud, “Advances in terahertz communications accelerated by photonics,” *Nat. Photonics*, vol. 10, no. 6, pp. 371–379, 2016, doi: 10.1038/nphoton.2016.65.

[9] J. Yao and J. Capmany, “Microwave photonics,” *Sci. China Inf. Sci.*, vol. 65, no. 12, pp. 314–335, 2022, doi: 10.1007/s11432-021-3524-0.

[10] H. G. Yu, S. H. Choi, S. Jeon, and M. Kim, "300 GHz InP HBT amplifier with 10 mW output power," *Electron. Lett.*, vol. 50, no. 5, pp. 377–379, 2014, doi: 10.1049/el.2013.3288.

[11] M. Seo *et al.*, "InP HBT IC technology for terahertz frequencies: Fundamental oscillators Up to 0.57 THz," *IEEE J. Solid-State Circuits*, vol. 46, no. 10, pp. 2203–2214, 2011, doi: 10.1109/JSSC.2011.2163213.

[12] S. H. Kim, T. H. Jang, D. M. Kang, and C. S. Park, "A 120 GHz Wideband CMOS I/Q Transmitter for Short-Range Wireless Device-to-Device Communication," *Asia-Pacific Microw. Conf. Proceedings, APMC*, vol. 2020-Decem, pp. 39–41, 2020, doi: 10.1109/APMC47863.2020.9331594.

[13] T. A. Vu and M. Fujishima, "A 300 GHz CMOS transmitter front-end for ultrahigh-speed wireless communications," *Int. J. Electr. Comput. Eng.*, vol. 7, no. 4, pp. 2278–2286, 2017, doi: 10.11591/ijece.v7i4.pp2278-2286.

[14] J. V. Siles and J. Grajal, "Physics-based design and optimization of Schottky diode frequency multipliers for terahertz applications," *IEEE Trans. Microw. Theory Tech.*, vol. 58, no. 7 PART 2, pp. 1933–1942, 2010, doi: 10.1109/TMTT.2010.2050103.

[15] Y. Zhang, W. Zhao, Y. Wang, T. Ren, and Y. Chen, "A 220 GHz subharmonic mixer based on schottky diodes with an accurate terahertz diode model," *Microw. Opt. Technol. Lett.*, vol. 58, no. 10, pp. 2311–2316, Oct. 2016, doi: https://doi.org/10.1002/mop.30032.

[16] H. Hamada *et al.*, "300-GHz 120-Gb/s Wireless Transceiver with High-Output-Power and High-Gain Power Amplifier Based on 80-nm InP-HEMT Technology," *2019 IEEE BiCMOS Compd. Semicond. Integr. Circuits Technol. Symp. BCICTS 2019*, pp. 2019–2022, 2019, doi: 10.1109/BCICTS45179.2019.8972756.

[17] H. Hamada *et al.*, "300-GHz. 100-Gb/s InP-HEMT Wireless Transceiver Using a 300-GHz Fundamental Mixer," *IEEE MTT-S Int. Microw. Symp. Dig.*, vol. 2018-June, pp. 1480–1483, 2018, doi: 10.1109/MWSYM.2018.8439850.

[18] L. Hou, S. Tang, B. Hou, and J. H. Marsh, “Photonic integrated circuits for terahertz source generation,” *IET Optoelectron.*, vol. 14, no. 3, pp. 136–142, 2020, doi: 10.1049/iet-opt.2019.0089.

[19] W. Lee *et al.*, “Coherent terahertz wireless communication using dual-parallel MZM-based silicon photonic integrated circuits,” *Opt. Express*, vol. 30, no. 2, p. 2547, 2022, doi: 10.1364/oe.446516.

[20] G. Carpintero *et al.*, “Photonic integrated circuits for terahertz communication: The hybrid integrated microwave photonic approach,” *Opt. InfoBase Conf. Pap.*, no. Mmi, pp. 6–7, 2021, doi: 10.1364/ofc.2021.f4f.4.

[21] T. Alam *et al.*, “Wideband, high-resolution terahertz spectroscopy by light-induced frequency tuning of quantum-cascade lasers,” *Opt. Express*, vol. 27, no. 4, p. 5420, 2019, doi: 10.1364/oe.27.005420.

[22] H. W. Hübers, H. Richter, and M. Wienold, “High-resolution terahertz spectroscopy with quantum-cascade lasers,” *J. Appl. Phys.*, vol. 125, no. 15, 2019, doi: 10.1063/1.5084105.

[23] T. Shiramizu *et al.*, “Feasibility Demonstration of THz Wave Generation/Modulation Based on Photomixing Using a Single Wavelength-Tunable Laser,” *Photonics*, vol. 10, no. 4, 2023, doi: 10.3390/photonics10040369.

[24] S. Preu, G. H. Dhler, S. Malzer, L. J. Wang, and A. C. Gossard, “Tunable, continuous-wave Terahertz photomixer sources and applications,” *J. Appl. Phys.*, vol. 109, no. 6, 2011, doi: 10.1063/1.3552291.

[25] K. Li *et al.*, “16-QAM Vector Terahertz-Wave Signal Generation by Simple MZM-Based Optical Frequency Comb,” *IEEE Photonics J.*, vol. 13, no. 1, 2021, doi: 10.1109/JPHOT.2020.3045058.

[26] K. Kondo, M. Che, and K. Kato, “Generation and Enhancement of Pulsed THz Waves by Arrayed UTC-PDs,” *OECC/PSC 2022 - 27th Optoelectron. Commun. Conf. Conf. Photonics Switch. Comput. 2022*, no. 2, pp. 1–4, 2022, doi: 10.23919/OECC/PSC53152.2022.9849992.

[27] E. Peytavit, G. Ducournau, and J. Lampin, “THz Photomixers,” 2021, pp. 137–186.

[28] A. Morales, G. I. Nazarikov, S. Rommel, C. Okonkwo, and I. T. Monroy, “All-Photonic Heterodyne sub-THz Wireless Transmission at 80 GHz, 120 GHz and 160 GHz Carrier Frequencies,” in *2020 45th International Conference on Infrared, Millimeter, and Terahertz Waves (IRMMW-THz)*, 2020, pp. 1–2, doi: 10.1109/IRMMW-THz46771.2020.9370506.

[29] E. García-Muñoz *et al.*, “Photonic-based integrated sources and antenna arrays for broadband wireless links in terahertz communications,” *Semicond. Sci. Technol.*, vol. 34, no. 5, 2019, doi: 10.1088/1361-6641/aaf8f2.

[30] H. Yang *et al.*, “A THz-OAM Wireless Communication System Based on Transmissive Metasurface,” *IEEE Trans. Antennas Propag.*, vol. 71, no. 5, pp. 1–1, 2023, doi: 10.1109/tap.2023.3255539.

[31] S. Carpenter *et al.*, “A D-Band 48-Gbit/s 64-QAM/QPSK Direct-Conversion I/Q Transceiver Chipset,” *IEEE Trans. Microw. Theory Tech.*, vol. 64, no. 4, pp. 1285–1296, 2016, doi: 10.1109/TMTT.2016.2533491.

[32] P. Torkaman *et al.*, “A 5G/Sub-Terahertz Heterogeneous Communication Network,” *IEEE Access*, vol. 10, pp. 65572–65584, 2022, doi: 10.1109/ACCESS.2022.3184312.

[33] M. Sawaby, N. Dolatsha, B. Grave, C. Chen, and A. Arbabian, “A fully packaged 130-GHz QPSK transmitter with an integrated PRBS generator,” *IEEE Solid-State Circuits Lett.*, vol. 1, no. 7, pp. 166–169, 2018, doi: 10.1109/LSSC.2019.2895571.

[34] E. F. Garay, D. J. Munzer, and H. Wang, “A 150 GHz Lens-Free Large FoV Regenerative 2 × 2 Transceiver Array With 31% DC-to-EIRP Efficiency and -70 dBm Sensitivity for a 70 cm Bidirectional Peer-to-Peer Link,” *IEEE J. Solid-State Circuits*, vol. 57, no. 7, pp. 2102–2113, 2022, doi: 10.1109/JSSC.2022.3149526.

[35] Y. Kim *et al.*, “150-GHz CMOS TX/RX with Digitally Predistorted PAM-4

Modulation for Terahertz Contactless/Plastic Waveguide Communications," *IEEE Trans. Terahertz Sci. Technol.*, vol. 10, no. 4, pp. 370–382, 2020, doi: 10.1109/TTHZ.2020.2991303.

[36] L. Chen, M. Taba, A. Cathelin, and E. Afshari, "A Low-Power 20Gb/s 196GHz BPSK Wireless Transmitter with Energy Efficiency FoM of 0.15pJ/bit/cm," *Proc. Cust. Integr. Circuits Conf.*, vol. 2023-April, pp. 1–2, 2023, doi: 10.1109/CICC57935.2023.10121306.

[37] P. Rodriguez-Vazquez, J. Grzyb, B. Heinemann, and U. R. Pfeiffer, "A QPSK 110-Gb/s Polarization-Diversity MIMO Wireless Link with a 220-255 GHz Tunable LO in a SiGe HBT Technology," *IEEE Trans. Microw. Theory Tech.*, vol. 68, no. 9, pp. 3834–3851, 2020, doi: 10.1109/TMTT.2020.2986196.

[38] J. Grzyb, P. R. Vazquez, N. Sarmah, B. Heinemann, and U. R. Pfeiffer, "A 240 GHz high-speed transmission link with highly-integrated transmitter and receiver modules in SiGe HBT technology," in *2017 42nd International Conference on Infrared, Millimeter, and Terahertz Waves (IRMMW-THz)*, 2017, pp. 1–2, doi: 10.1109/IRMMW-THz.2017.8066869.

[39] C. Wang, J. Yu, X. Li, P. Gou, and W. Zhou, "Fiber-THz-Fiber Link for THz Signal Transmission," *IEEE Photonics J.*, vol. 10, no. 2, pp. 1–6, 2018, doi: 10.1109/JPHOT.2018.2809433.

[40] T. Hagiwara *et al.*, "A 258-GHz CMOS Transmitter with Phase-Shifting Architecture for Phased-Array Systems," *IEEE MTT-S Int. Microw. Symp. Dig.*, vol. 2021-June, pp. 705–708, 2021, doi: 10.1109/IMS19712.2021.9574976.

[41] K. Takiguchi, "PAM4 wireless communication in 300 GHz-band using integrated-optic PAM signal emulator," *2022 Conf. Lasers Electro-Optics, CLEO 2022 - Proc.*, pp. 1–2, 2022, doi: 10.1364/cleo_si.2022.stu5l.7.

[42] A. Oshiro *et al.*, "PAM4 48-Gbit/s wireless communication using a resonant tunneling diode in the 300-GHz band," *IEICE Electron. Express*, vol. 19, no. 2, pp. 1–6, 2022, doi: 10.1587/elex.18.20210494.

[43] I. Abdo, H. Hamada, H. Nosaka, A. Shirane, and K. Okada, "64QAM wireless

link with 300 GHz InP-CMOS hybrid transceiver,” *IEICE Electron. Express*, vol. 18, no. 17, pp. 1–4, 2021, doi: 10.1587/ELEX.18.20210314.

[44] K. Maekawa, Y. Kawamoto, T. Nakashita, and T. Yoshioka, “300-GHz-band Wireless Link Using Photonics-based Ultralow-noise Transmitter and Receiver,” *2023 Opt. Fiber Commun. Conf. Exhib.*, pp. 15–17, 2023, doi: 10.23919/OFC49934.2023.10116279.

[45] D. Pirrone *et al.*, “Metasurface-Based Filters for High Data Rate THz Wireless Communication: Experimental Validation of a 14 Gbps OOK and 104 Gbps QAM-16 Wireless Link in the 300 GHz Band,” *IEEE Trans. Wirel. Commun.*, vol. 21, no. 10, pp. 8688–8697, 2022, doi: 10.1109/TWC.2022.3168399.

[46] S. Nellen *et al.*, “Coherent Wireless Link at 300 GHz with 160 Gbit/s Enabled by a Photonic Transmitter,” *J. Light. Technol.*, vol. 40, no. 13, pp. 4178–4185, 2022, doi: 10.1109/JLT.2022.3160096.

[47] L. Yi *et al.*, “300-GHz-band wireless communication using a low phase noise photonic source,” in *2019 49th European Microwave Conference (EuMC)*, 2019, pp. 816–819, doi: 10.23919/EuMC.2019.8910724.

[48] M. Qiao *et al.*, “60 Gbit/s PAM-4 wireless transmission in the 310 GHz band with nonlinearity tolerant signal processing,” *Opt. Commun.*, vol. 492, no. June 2020, p. 126988, 2021, doi: 10.1016/j.optcom.2021.126988.

[49] J. Shi *et al.*, “4096-QAM OFDM THz-over-fiber MIMO transmission using delta-sigma modulation,” *IEEE Photonics Technol. Lett.*, vol. 35, no. 13, pp. 741–744, 2023, doi: 10.1109/LPT.2023.3271907.

[50] Y. Tan *et al.*, “Transmission of High-Frequency Terahertz Band Signal Beyond 300 GHz Over Metallic Hollow Core Fiber,” *J. Light. Technol.*, vol. 40, no. 3, pp. 700–707, 2022, doi: 10.1109/JLT.2021.3123473.

[51] J. Ding *et al.*, “104-m Terahertz-Wave Wireless Transmission Employing 124.8-Gbit/s PS-256QAM Signal,” *Opt. InfoBase Conf. Pap.*, vol. 1, no. c, pp. 1–3, 2022, doi: 10.1364/ofc.2022.m3c.3.

[52] S. Jia *et al.*, “120 Gb/s multi-channel THz wireless transmission and THz receiver performance analysis,” *IEEE Photonics Technol. Lett.*, vol. 29, no. 3, pp. 310–313, 2017, doi: 10.1109/LPT.2016.2647280.

[53] X. Li *et al.*, “120 Gb/s wireless terahertz-wave signal delivery by 375 GHz-500 GHz multi-carrier in a 2 × 2 MIMO system,” *J. Light. Technol.*, vol. 37, no. 2, pp. 606–611, 2019, doi: 10.1109/JLT.2018.2862356.

[54] M. Zhao, W. Zhou, and J. Yu, “3.5 Gbit/s OOK THz signal delivery over 88 cm free-space at 441.504 GHz,” *Microw. Opt. Technol. Lett.*, vol. 60, no. 6, pp. 1435–1439, 2018, doi: 10.1002/mop.31176.

[55] X. Li, J. Yu, K. Wang, W. Zhou, and J. Zhang, “Photonics-aided 2 × 2 MIMO wireless terahertz-wave signal transmission system with optical polarization multiplexing,” *Opt. Express*, vol. 25, no. 26, p. 33236, 2017, doi: 10.1364/oe.25.033236.

[56] X. Li *et al.*, “132-Gb/s photonics-aided single-carrier wireless terahertz-wave signal transmission at 450GHz enabled by 64QAM modulation and probabilistic shaping,” *Opt. InfoBase Conf. Pap.*, vol. Part F160-, pp. 10–12, 2019.

[57] X. Liu *et al.*, “Demonstration of 144-Gbps Photonics-Assisted THz Wireless Transmission at 500 GHz Enabled by Joint DBN Equalizer,” *Micromachines*, vol. 13, no. 10, 2022, doi: 10.3390/mi13101617.

[58] Y. Yoshimizu, S. Hisatake, S. Kuwano, J. Terada, N. Yoshimoto, and T. Nagatsuma, “Wireless transmission using coherent terahertz wave with phase stabilization,” *IEICE Electron. Express*, pp. 10–20130578, 2013.

[59] L. Gonzalez-Guerrero and G. Carpintero, “Coherent photonic Terahertz transmitters compatible with direct comb modulation,” *Sci. Rep.*, vol. 12, no. 1, pp. 1–10, 2022, doi: 10.1038/s41598-022-13618-y.

[60] K. Sakuma *et al.*, “First demonstration of Mach-Zehnder-interferometric phase-stabilization at optoelectronic carrier generation for phase-shift keying signal,” *2015 Opto-Electronics Commun. Conf. OECC 2015*, pp. 1–3, 2015, doi:

10.1109/OECC.2015.7340086.

[61] S. Takeuchi, K. Kato, Y. Yoshimizu, Y. Yasuda, S. Hisatake, and T. Nagatsuma, "Coherent sub-THz carrier frequency transmission with novel pseudo-Mach-Zehnder interferometric phase stabilization," in *Microwave Photonics (MWP) and the 2014 9th Asia-Pacific Microwave Photonics Conference (APMP) 2014 International Topical Meeting on*, Oct. 2014, pp. 208–210, doi: 10.1109/MWP.2014.6994532.

[62] S. Takeuchi *et al.*, "Novel lightwave-interferometric phase detection for phase stabilization of two-tone coherent millimeter-wave/microwave carrier generation," *IEICE Trans. Electron.*, vol. E99C, no. 9, pp. 1048–1055, 2016, doi: 10.1587/transele.E99.C.1048.

[63] M.-C. Lo *et al.*, "Foundry-fabricated dual-DFB PIC injection-locked to optical frequency comb for high-purity THz generation," in *Optical Fiber Communication Conference*, 2019, pp. W1B-3.

[64] G. K. M. Hasanuzzaman, H. Shams, C. C. Renaud, J. Mitchell, and S. Iezekiel, "Photonic THz Generation using Optoelectronic Oscillator-driven Optical Frequency Comb Generator," in *2018 International Topical Meeting on Microwave Photonics (MWP)*, 2018, pp. 1–4, doi: 10.1109/MWP.2018.8552892.

[65] T. Nagatsuma *et al.*, "Terahertz wireless communications based on photonics technologies," *Opt. Express*, vol. 21, no. 20, pp. 23736–23747, Oct. 2013, doi: 10.1364/OE.21.023736.

[66] S. Takeuchi *et al.*, "Novel lightwave-interferometric phase detection for phase stabilization of two-tone coherent millimeter-wave/microwave carrier generation," *IEICE Trans. Electron.*, vol. E99C, no. 9, pp. 1048–1055, 2016, doi: 10.1587/transele.E99.C.1048.

[67] Y. Ma, L. Stewart, J. Armstrong, I. G. Clarke, and G. Baxter, "Recent progress of wavelength selective switch," *J. Light. Technol.*, vol. 39, no. 4, pp. 896–903, 2020.

[68] A. A. Ibrahim, T. Shiramizu, S. Ye, Y. Mikami, and K. Kato, “Pilot-Lightwave-based Terahertz Wave Phase Stabilization,” *Conf. Dig. - IEEE Int. Semicond. Laser Conf.*, vol. 2022-Octob, no. Ld, pp. 2022–2023, 2022, doi: 10.23919/ISLC52947.2022.9943347.

[69] T. Shiramizu, A. A. Ibrahim, S. Ye, Y. Mikami, and K. Kato, “Photonic Phase Stabilization Control System for Terahertz-Wave Phase Modulation,” in *2022 27th OptoElectronics and Communications Conference (OECC) and 2022 International Conference on Photonics in Switching and Computing (PSC)*, 2022, pp. 1–4, doi: 10.23919/OECC/PSC53152.2022.9850107.

[70] A. A. Ibrahim, H. Chen, T. Shiramizu, Y. Mikami, and K. Kato, “Terahertz-Wave Phase Modulation Enabled by Optical Interferometric Phase Stabilization,” in *2022 Asia-Pacific Microwave Conference (APMC)*, Nov. 2022, pp. 943–945.

CHAPTER 2
DEVELOPMENT OF A NEW METHOD OF PHASE STABILIZATION FOR PHOTOMIXING SETUP

2.1 Introduction

The generation of THz waves using photomixing has emerged as a promising technique. However, the quality of the phase-modulated lightwave and the resulting THz wave is significantly impacted by phase fluctuations. In this chapter, a novel method for phase stabilization of a photomixing setup is presented. The proposed method utilizes a MZI system, wavelength selective switch (WSS) and introduces the pilot lightwave from the backward direction as understanding the phase modulator mechanism to stabilize the phase of the THz wave carrier generation system. The effectiveness of the phase stabilization system is experimentally demonstrated.

2.2 Phase Stabilization System Using Mach-Zehnder Interferometer (MZI)

Two of the most practical methods of the lightwave for photomixing are the free-running laser-based approach [63] and the optical frequency comb (OFC)-based technique [64]. For the free-running laser-based approach, the optical frequencies of the two lasers are not constant and the optical phases fluctuated independently [58]. In contrast, in the OFC-based approach, two optical frequency signals are extracted by an optical filter at a series of optical frequency signals originating from a single lightwave [65]. Thus, both optical signals would be in the same phase. However, the problem with this method is that temperature variation and acoustic noise cause the fluctuation of the path length difference between two optical fibers and then it generates a phase noise on the carrier [66]. Therefore, phase detection based on the MZI technique was systematically investigated in this study. The fluctuation of the path length difference is detected by using a pilot light and deducing relative optical phase fluctuations. As a result, the noises are successfully eliminated using a programming-based feedback controller at the experimental demonstrations.

2.2.1 Phase Stabilization of Two-Tone Lightwave in Photomixing

Figure 2.1 shows the conceptual diagram of the THz wave carrier generation system with our proposed phase detection method in which two optical paths are configured as the MZI. For the THz wave generation system represented by the solid line which is started with a laser diode (LD) introduced to the optical frequency comb generator (OFCG), in which the OFC is generated. From the OFC, the two lightwaves of different frequencies are then extracted into two different optical paths using a special optical filter called as Wavelength Selective Switch (WSS). On the upper path, the lightwave will be modulated by the phase modulator (PM) and then coupled with the lightwave on the lower path at the optical coupler (OC). Finally, the output of the OC is connected to UTC-PD. Here, the THz wave carrier is generated with the same frequency as the frequency difference between two different frequencies earlier.

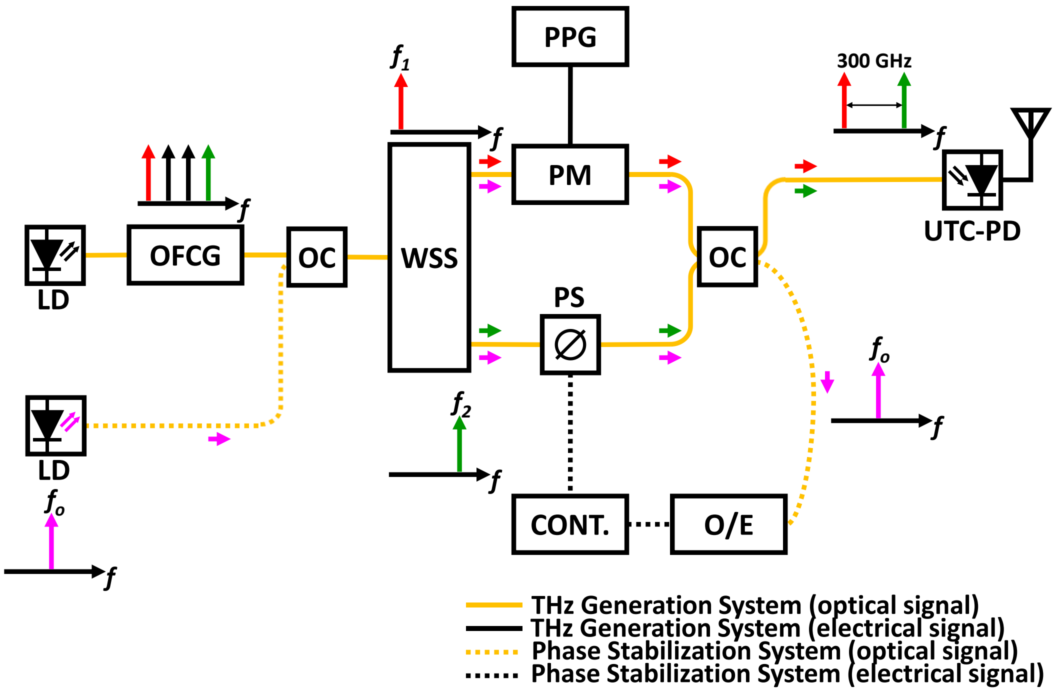

Figure 2.1 Conceptual diagram of Mach- Zehnder Interferometric (MZI) phase detection for phase stabilization system

While the dotted line represented the phase stabilization system, a method uses lightwave as a pilot light phase detection. The lightwave from the pilot laser diode (LD) is passed WSS and traveled through both optical paths in upper and lower paths and coupled back at OC. These two optical paths between the WSS and OC are almost equal in their length to work as the MZI. The combined light after the OC would be interfered with and detected by the Optical-to-Electrical (O/E) converter. Hence, by monitoring the intensity of the interfered light of frequency pilot, the relative optical phase fluctuation which causes the phase fluctuation on the generated millimeter-wave carrier can be detected. The feedback controller (CONT.) cancels the detected relative phase fluctuation using a phase shifter (PS). If the interfered light intensity is controlled at a certain value, the phase difference between the lightwaves of two optical paths could be kept at constant.

2.2.2 Phase Stabilization System

Figure 2.2 shows the experimental setup block diagram for the phase detection for the stabilization system. From the left side, there is a single-frequency laser with an optical frequency f_o of 193.50 THz. First, this pilot lightwave is split into two optical paths using the optical coupler. Then, these lightwaves combined at one more OC on the left side. The interference intensity is detected by the O/E converted at 531V/W. The

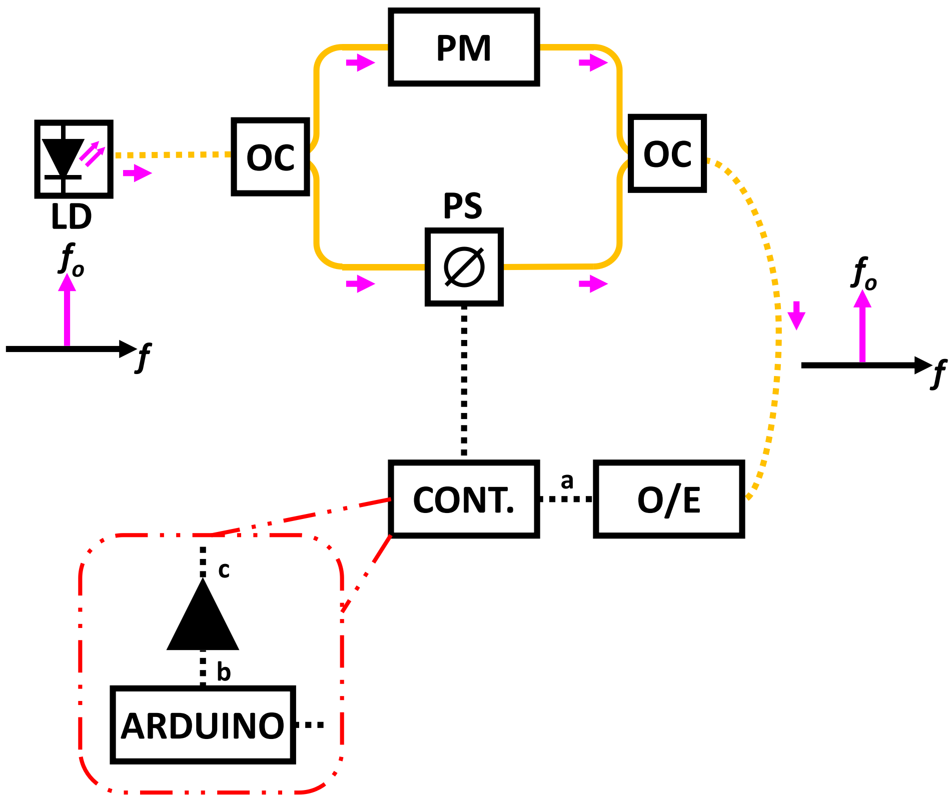

Figure 2.2 Block diagram of the preliminary experimental set up for the phase detection and stabilization

converted voltage is then read by the Arduino MKR, an open-source hardware which works as the proportional–integral–derivative (PID) controller as the feedback controller in this experiment. The controlled voltage value was then amplified with a gain of 9 to integrate with the PS. The PS required at least 14V to shift for π radian to control the value of the intensity interference. The controlled voltage value cancelled the detected interference intensity and kept the read voltage value constant.

2.2.2.1 Controller Design

The feedback control was designed as in Figure 2.3. The PS phase shifter need more than 14 V to shift a π. However, the Arduino only can output 3.3V. Under this circumstance, an operational amplifier of AD818 with gain of 9 is used to amplify the voltage of Arduino. Even though the maximum output of the amplifier is only about 17 V, it proves to be sufficient to drive the phase shifter and achieve a phase shift of π. Our measurements have revealed that the phase fluctuations caused by environmental noises remain minimal, fluctuating less than π. As a result, an output amplifier of up to 17 V proves to be more than adequate for our purposes.

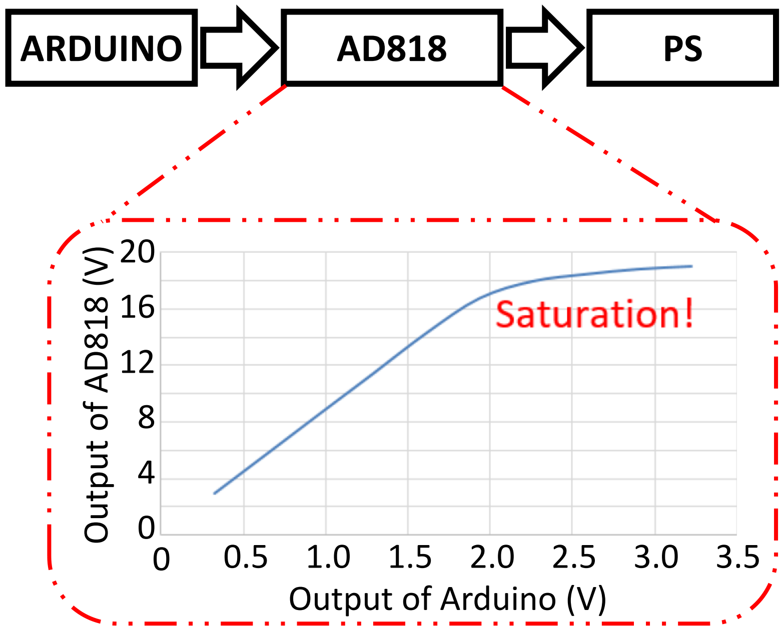

Figure 2.3 Controller design

2.2.2.2 Feedback control

Now, the controller is clearly can output a very high voltage to drive the phase shifter. Next, to design the PID control system, the feedback controller. In this PID control implementation using an Arduino as shown in Figure 2.4, the objective is to regulate the V_{ouput} (position) of the phase shifter towards a V_{target} (setpoint).

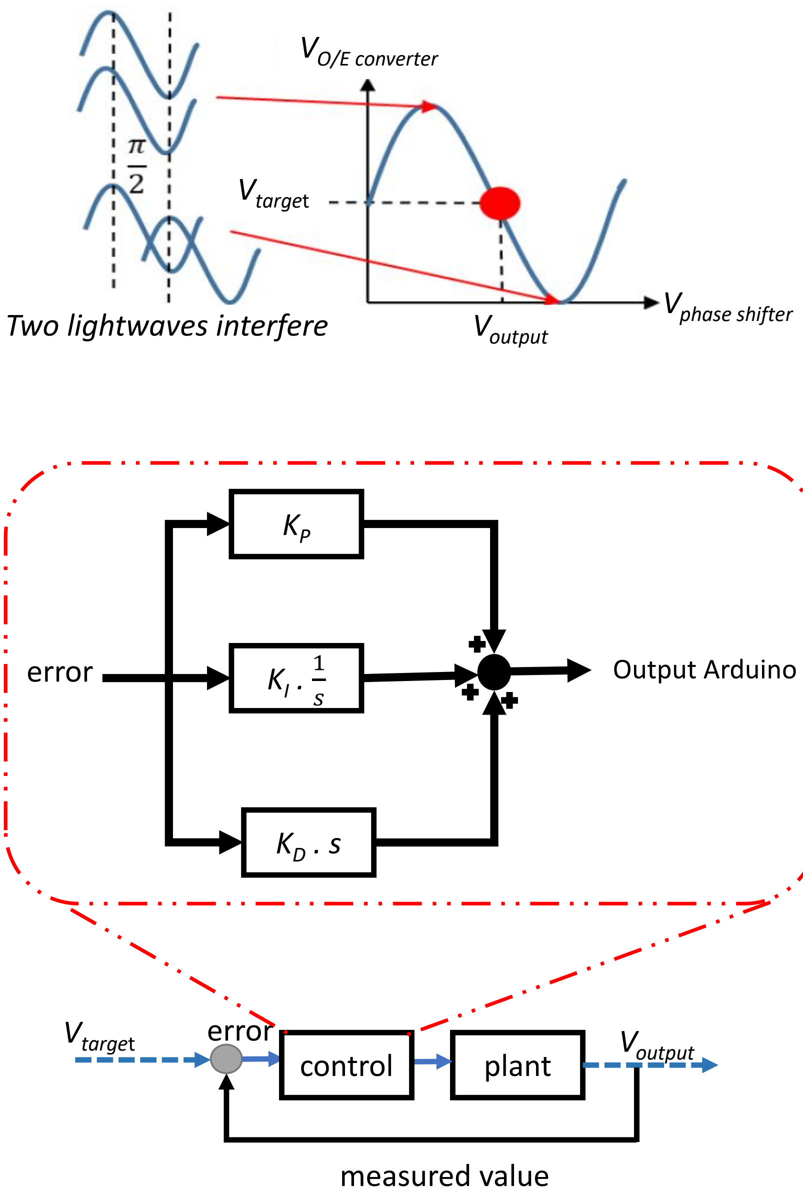

Figure 2.4 Feedback control

The control algorithm operates within the Arduino microcontroller, calculating the error, which represents the deviation between the desired V_{target} and the measured

V_{ouput} of the phase shifter. The error is computed as the difference between the V_{target} and the measured V_{ouput} ($e(k) = V_{target} - V_{ouput}$).

$$\Delta u(k) = K_P\,[e(k) - e(k-1)] + K_I\, e(k) + K_D\,[e(k) - 2e(k-1) + e(k-2)] \qquad (10)$$

The control signal ($\Delta u(k)$) is then determined incrementally using the Proportional (P), Integral (I), and Derivative (D) components of the PID controller. The Proportional component ($K_P * [e(k) - e(k-1)]$) contributes to the control signal proportionally to the current error, while the Integral component ($K_I * e(k)$) accumulates past errors to eliminate steady-state error and bring the phase shifter to the desired V_{target}. The Derivative component ($K_D * [e(k) - 2 * e(k-1) + e(k-2)]$) anticipates future errors based on the rate of change of the error, helping to dampen the phase shifter's response and reduce overshooting. By adjusting the PID gains (K_P, K_I, K_D), the Arduino fine-tunes the response to optimize performance for the specific phase shifter under control. The PID control algorithm incrementally updates the control signal at each time step, and the Arduino outputs the resulting voltage signal ($\Delta u(k)$) to the phase shifter, guiding it towards the V_{target} and effectively maintaining the V_{ouput} of the phase shifter at the setpoint which resulting as the phase difference always at same value.

2.2.3 Results and Discussion

Figure 2.5 depicts the voltage value at various points in the initial experimental configuration for phase detection and stabilization, both with and without a feedback controller. Point a, represented by the yellow line, corresponds to the converted interference intensity. Point b, represented by the green line, indicates the controlled voltage value, while point c, represented by the blue line, reflects the voltage value received by the phase shifter. In Figure 2.5 (a), the voltage value of the converted interference intensity (yellow) exhibits instability, fluctuating over time. This instability is attributed to the absence of a controlled voltage value provided by the phase shifter. Conversely, in Figure 2.5 (b) the converted interference intensity's (yellow) voltage value remains stable within a narrow range of 400 mV – 500 mV. The converted voltage value reads 1.35 V (green), and the amplified voltage received by the phase shifter amounts to 13.5 V.

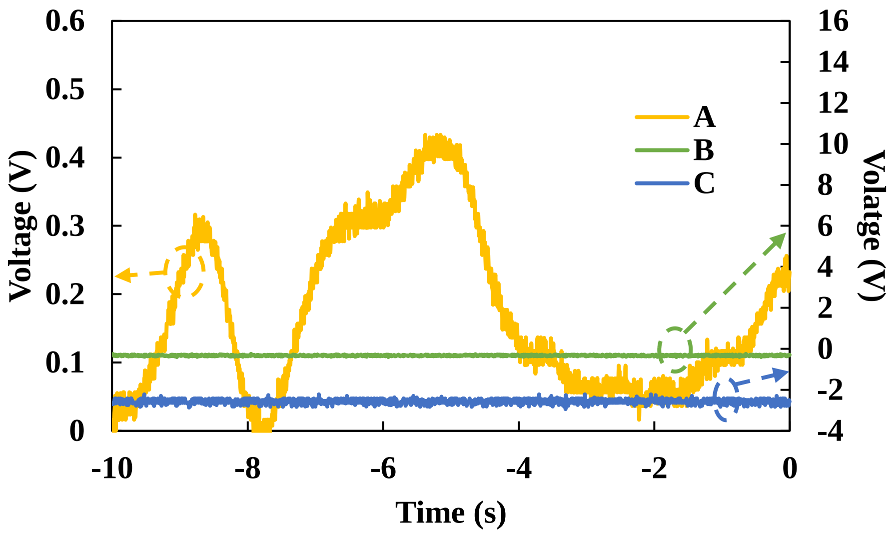

(a)

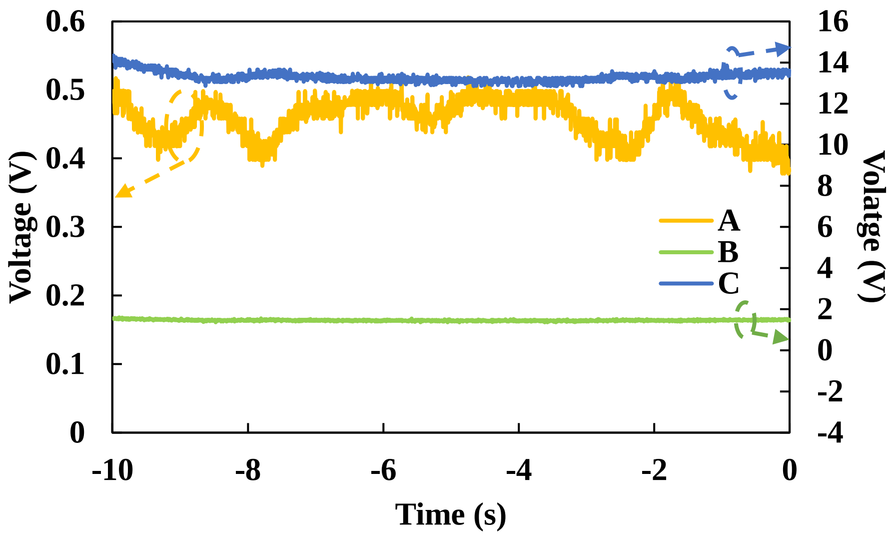

(b)

Figure 2.5 Interference intensity (a) without and (b) with a feedback controller

As conclusion, a phase stabilization system utilizing a lightwave interferometric technique has been developed. The stabilization of phase fluctuation is achieved through the implementation of the MZI method, where a controlled phase shifter is employed in conjunction with a PID controller. The experimental results demonstrate the successful stabilization of phase fluctuations. As a result of this approach, the interfered optical intensity experiences a decrease and remains stable within a consistent range of 450 mV. Based on these outcomes, it can be concluded that the proposed method is suitable and effective for both phase detection and stabilization purposes.

2.3 Wavelength Selective Switch Channel Settings Technique

In continuation of the preceding system, the feasibility of implementing phase stabilization using a pilot lightwave in the THz wave generation system has been established. However, a challenge arises with the conventional Wavelength Selective Switch (WSS), which cannot output lightwaves of the same frequency at both output ports. To address this issue, a novel channel settings technique has been devised. Leveraging the overlapping nature of the filter channels, the pilot lightwave (f_{pilot}) can be output at both output ports [67]. This technique enables the alignment of f_{pilot} with f_1 and f_2, on different output ports, which is essential for the lightwave interferometric phase stabilization system. The WSS, known as an optical switch by name, the WSS exhibits inherent filtering properties, as evidenced by its ability to generate lightwaves of same frequency at two-channel outputs, facilitated by the special channel setting technique. This novel approach contributed to the phase stabilization system of the THz wave carrier generation. The fluctuation of the path length difference can easily be controlled by the feedback control and lastly, the phase of the lightwave or that of the THz wave is always identical.

2.3.1 Channels Settings Technique at WSS

The Wavelength Selective Switch (WSS) is an optical switch designed to manipulate light input that has been dispersed in wavelength, eliminating the need for the input light to be demultiplexed into separate ports [67]. Additionally, the WSS has the capability to output multiple frequencies through the same output port by selectively choosing the desired filter channel and directing it to the designated output port. This functionality proves to be highly advantageous in the context of the stabilized THz wave generation system, where three distinct optical frequencies must be efficiently produced by the WSS; f_1, f_2, *and* f_{pilot}. f_1 and f_2 are required for the THz wave carrier generation, while the f_{pilot} is necessary for the stabilization. f_{pilot} is needed to be output aligned with both f_1 and f_2 on different output ports. However, the WSS output ports cannot output the same frequency signal. A new technique in order the overcome this problem is develop by utilizing the fact that each filter channel is overlapping to the adjacent channels. In this technique, f_{pilot} can be output in both output ports by selecting overlapped filter channel value, as shown in Figure 2.6(a). In this case, f_{pilot} can be found in both WSS output ports. Figure 2.6(b) shows the transmittance output of WSS output ports of f_1, f_2, and f_{pilot}. Here, f_1 and f_{pilot} can be found at the output port 1, while, f_2, *and* f_{pilot} can be found at the output Port 2. Thus, this technique can be applied to the lightwave interferometric phase stabilization system.

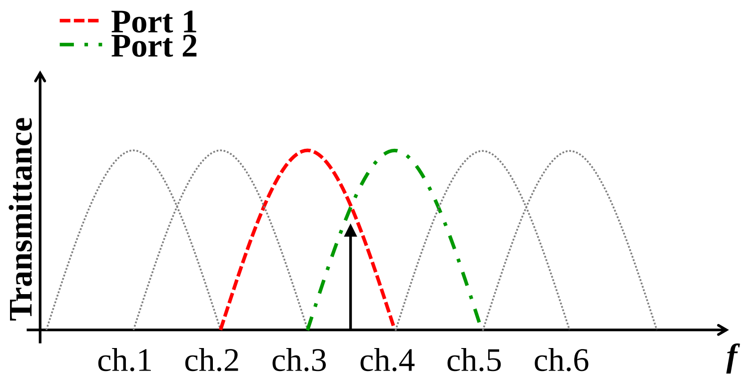

(a)

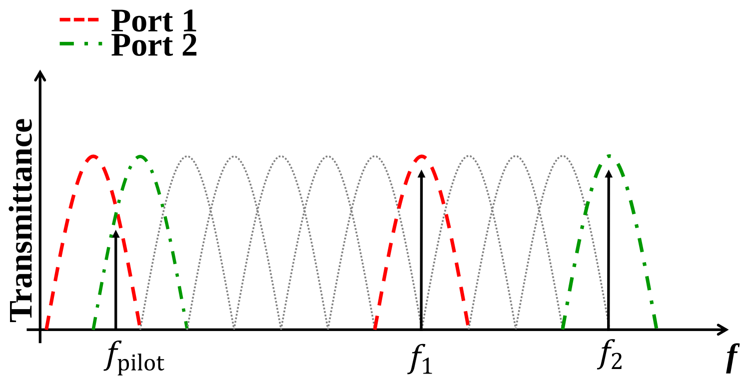

(b)

Figure 2.6 (a) Overlapped filter channel that can output the same frequency on both output ports (b) The light output wavelength based on the output ports

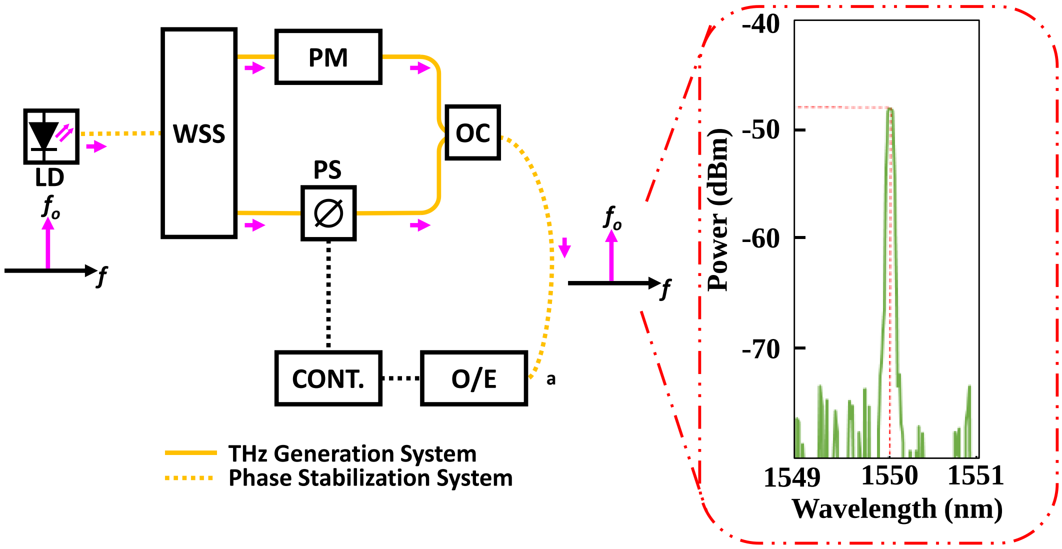

Figure 2.7 illustrates the block diagram of the experimental setup for THz wave generation based on photomixing using the WSS with a channel spacing of 25 GHz. The proposed phase stabilization configuration involves the introduction of a pilot lightwave into the system. An LD emitting light at an optical frequency of 193.0125 THz (corresponding to 1550 nm) serves as the pilot lightwave. The pilot lightwave is split into two optical paths by the WSS, with one path at 193.0 THz and the other at 193.025 THz. These lightwaves are then combined using an optical coupler (OC), resulting in an interfered signal. The interfered lightwave, which is expected to have the same optical frequency as the pilot, is monitored using an optical spectrum analyzer (OSA). The OC is connected to an O/E converter, where the interfered signal is detected and converted into an electrical signal at a sensitivity of 531 V/W. This electrical signal is then fed into a feedback controller for processing. The output of the feedback controller is amplified and sent to the phase shifter to stabilize the interfered

signal in the system. and applied to the phase shifter to stabilize the system's interfered signal.

2.3.2 Results and Discussion

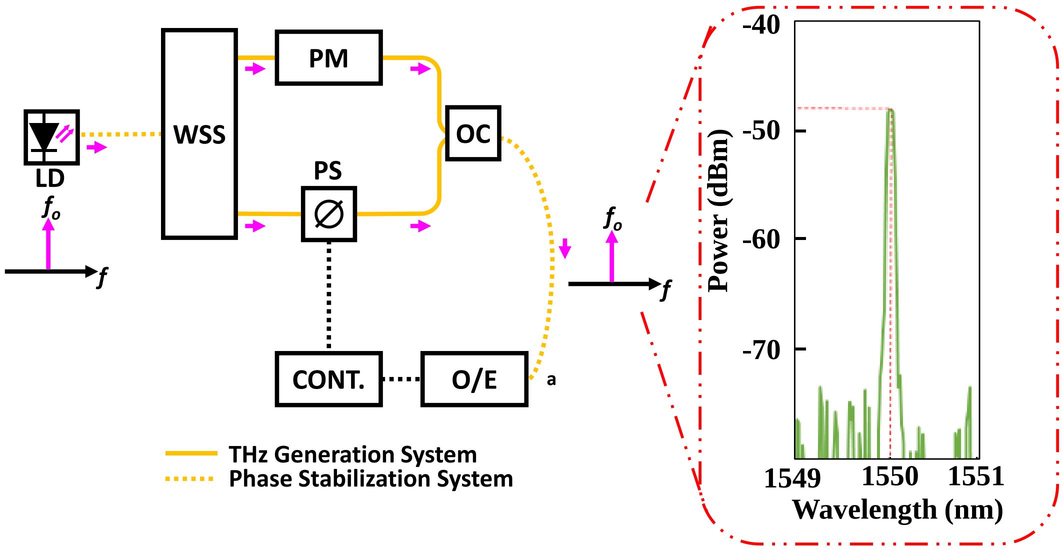

Figure 2.7 WSS-pilot lightwave-based phase stabilization system and detected interference signal

The WSS is an optical switch for operating Figure 2.8 shows the voltage value before and after WSS-pilot lightwave-based phase stabilization system. The interfered signal before feedback control is unstable and changes over time between 0.1 to 0.9 V This instability is due to external disturbances that contributed to the phase fluctuation and resulted in unstable interfered signal voltage values. While the voltage value of interfered signal after feedback control is stable at almost the same range value, 0.5V. The experimental result successfully demonstrates the feasibility of the proposed configuration and channel setting technique at the WSS.

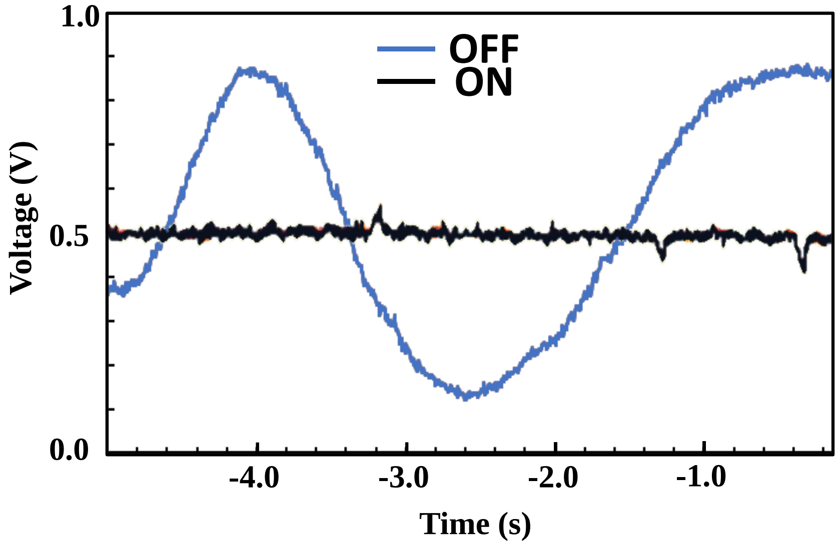

Figure 2.8 The interfered signal before (OFF) and after (ON) the phase stabilization system

2.4 Phase Modulator Mechanism

Continuing from the previous development of the phase stabilization system, it may seem promising for implementation in the THz generation system. However, an additional challenge arises. Since the pilot lightwave travels in the same direction as the lightwave used for generating THz waves, the pilot lightwave is also being modulated, hindering its main purpose for phase detection for phase stabilization system.

2.4.1 The Mechanism of Phase Modulator

The THz wave phase modulation system based on photomixing consists of a commercially available lithium niobate (LN) phase modulator with a length of 100 mm, whose schematic structure is shown in Figure 2.9. The modulation process involves applying an electrical signal to the phase modulator, causing a change in the refractive index of LN and subsequently shifting the phase of the lightwave [66]. As the electrical signal and lightwave are synchronized to travel at the same speed, the voltage of the electrical signal effectively modulates the phase of the lightwave during its passage through the LN modulator.

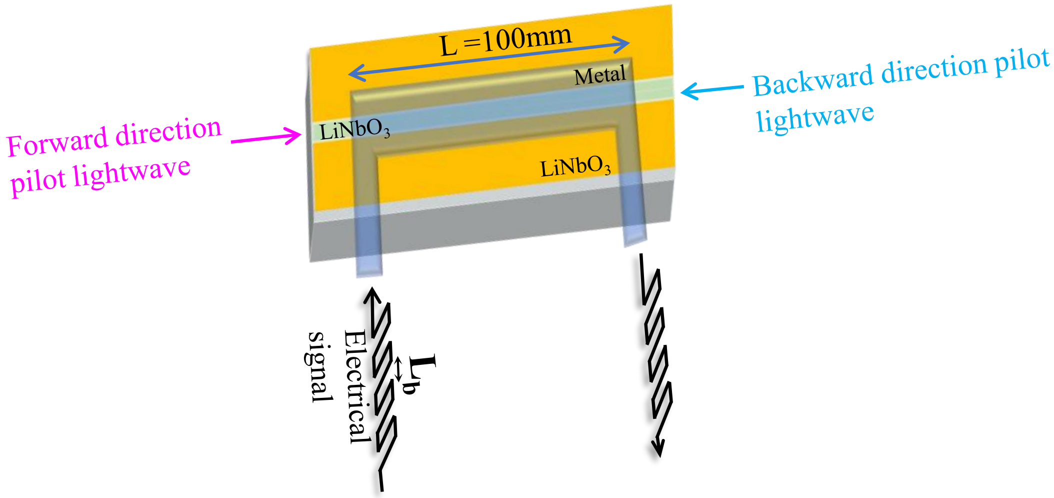

Figure 2.9 Diagram of LN phase modulator, where L_b is bit length.

In the THz-wave phase modulation system shown, one of the two lightwaves needs to be modulated. The phase difference between these lightwaves is subject to fluctuations due to variations in the path length. To address this, a previous development involved an interferometric phase detection method using a pilot lightwave introduced from the same direction (forward direction) as the two lightwaves. This approach successfully detected phase difference fluctuations without requiring an electrical signal to the LN modulator.

However, a new challenge arose as the phase of the pilot lightwave was also modulated by the electrical signal, resulting in a blurred signal, making it challenging to detect fluctuations accurately. To resolve this issue, a solution was devised by introducing a pilot lightwave from the backward direction. By injecting the pilot lightwave into a phase modulator from the backward direction, it experiences a randomly changing electrical signal voltage. If the bit length of the electrical signal is less than the length of the phase modulator, the optical lightwave traveling backward will not be modulated. This occurs when the lightwave encounters a constantly switching electrical signal voltage, causing the phase shift to be effectively averaged out and stay unchanged. It should be observed, however, that the longer electrical bit will modulate the pilot lightwave.

This fluctuation can be represented by a time-varying function *V(t)* which represents the voltage applied to the phase modulator at time *t* with constant *k*. Considering the phase modulation equation $\Delta\varphi \propto kVL$ where *L* is the the length of the phase modulator and L_b is bit length L_b, the phase shift experienced by the backward pilot lightwave as:

$$\Delta\varphi_{backward}(t) \propto kV(t)L_b. \tag{11}$$

Since $V(t)$ constantly switches within the short bit length, the integral of $V(t)$ over that duration is expected to be averaged. Therefore, the phase shift $\Delta\varphi_{backward}$, which the backward lightwave experienced, can be effectively averaged out as well, resulting in no significant phase modulation:

$$\Delta\varphi_{backward} \propto \int \{kV(t)L\}dt \approx 0. \tag{12}$$

This backward-direction pilot lightwave technique proves to be more effective, especially when using a higher bit-rate electrical signal.

Figure 2.10 shows a simulated result of the phase change experienced by the backward-direction pilot lightwave, assuming a mark ratio of 50% for the electrical signal. The mathematical equation used to simulate the phase modulation behaviour of the phase modulator is as follow:

$$\varphi(x) = (2 * len\_light - \lfloor 2 * x / length\_signal \rfloor * length\_signal) / (2 * len\_light) - 0.5] \tag{13}$$

where $\varphi(x)$ represents the phase shift at position x along the phase modulator's length, *len_light* is the effective length of the phase modulator due to the refractive index of the material, ⌊⌋ denotes the floor function, which rounds the value inside the brackets down to the nearest integer and *length_signal* is the length of the optical signal for the specific bit rate (bps).

At lower bit rates less than 1 Gbit/s, the bit length is longer. In this scenario, the phase of the lightwave after passing through the LN modulator undergoes a change of either -½ π or ½ π, depending on the timing of the data. This behaviour is similar to what is observed with forward-direction lightwaves. This is because, at lower bit rates, the ON or OFF of the electrical signal persists throughout the entire path of the LN modulator. As the bit rate of the electrical signal increases to approximately 3 Gbit/s and the bit length of the signal matches that of the LN modulator, the phase of the lightwave changes within the range of -½ π to ½ π, depending on the timing of the data. However, when the bit rate of the signal surpasses 10 Gbit/s, the length of a bit in the signal becomes significantly shorter than that of the LN modulator, resulting in a much smaller phase change of the lightwave, which approaches zero.

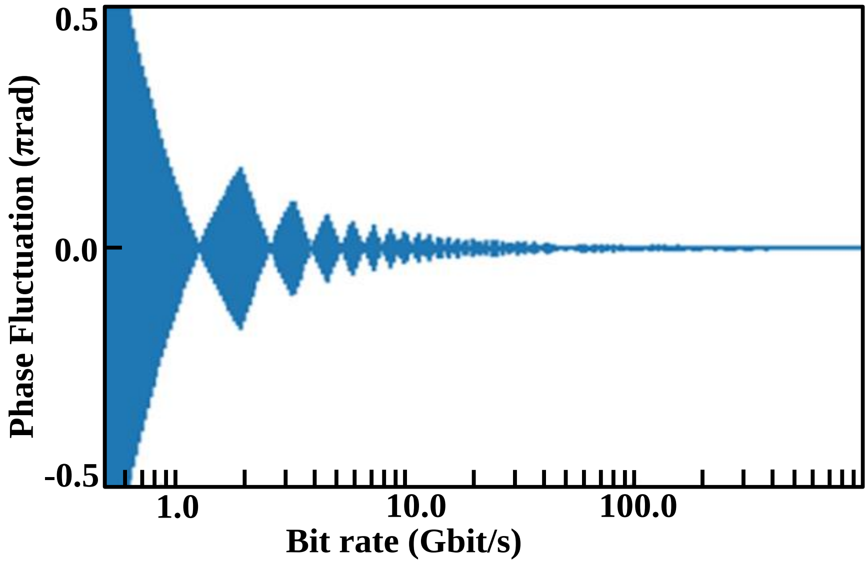

Figure 2.10 Simulated phase change as a function of the bit rate of the signal

Then, proceed with the experimental setup. The block diagram of the experimental setup for phase detection and stabilization is shown in Figure 2.11. From the right side, a pilot lightwave with an optical frequency of 193.50 THz is introduced through the OC. The pilot lightwave is split into two optical paths by the OC. Then, at the upper optical path in the figure, the pilot lightwave passes through the PM backwardly while at the lower optical path it passes through the piezo-electric PS. The

PM is injected with 10 Gbit/s pulse signal from PPG. Both lightwaves are then combined at the WSS and interfered by themselves. The interfered intensity is detected by the OE converter with a responsivity of 531 mV/mW. The feedback controller changes the applied voltage (control voltage) to the phase shifter to keep the interfered intensity at a constant so that the PS cancels the difference between phase fluctuations at both optical paths.

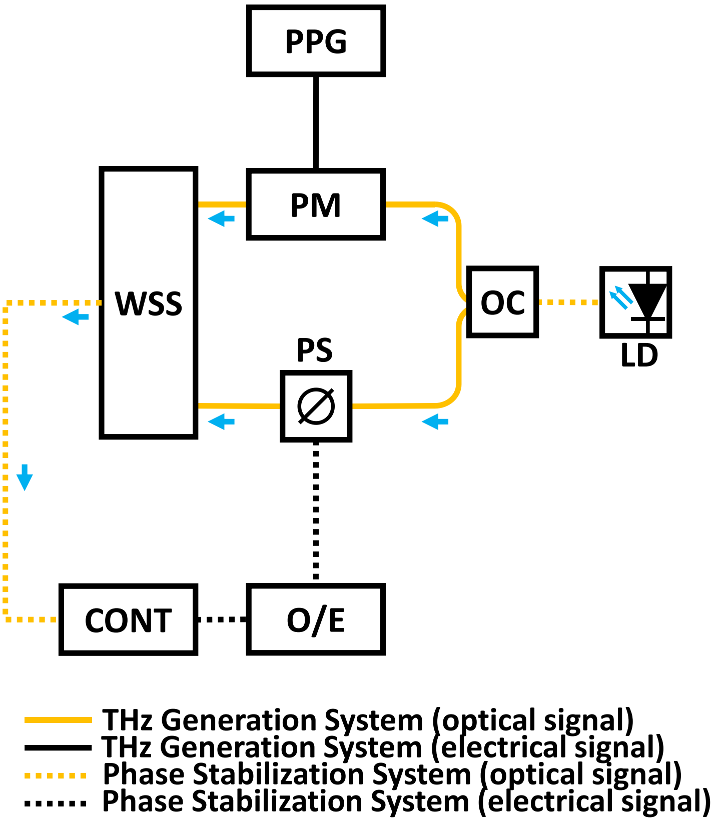

Figure 2.11 Experimental setup for phase detection and stabilization

2.4.2 Results and Discussion

Figure 2.12 shows the voltage detected from the OE converter with and without the feedback control. The interference voltage is unstable between 250 and 530 mV without the feedback control. On the other side, with the FB control, the control voltage changes so that the voltage from the OE converter or the interfered intensity becomes settled at around a target value of 400 mV. The experimental result is consistent with the expectations based on the simulation and shows the effectiveness of the proposed system.

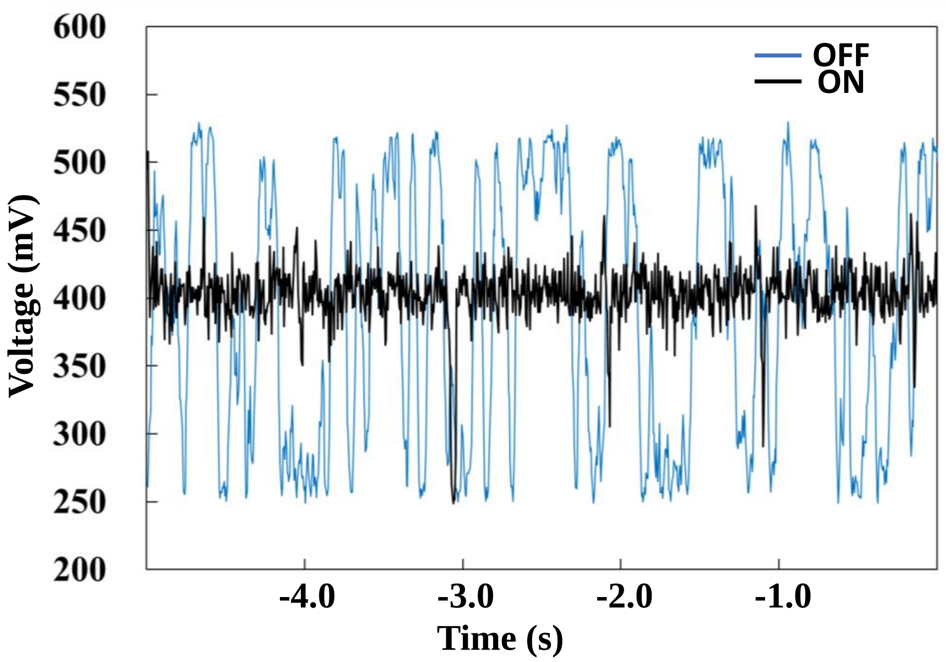

Figure 2.12 The interfered signal before (OFF) and after (ON) the backward phase stabilization system

2.5 Conclusions

In conclusion, a novel method for phase stabilization of a photomixing setup is presented. The use of a wavelength selective switch and a pilot lightwave from the backward direction allows for effective phase stabilization of the THz wave carrier generation system. The experimental results demonstrate the successful stabilization of the phase fluctuation using a feedback controller. This method proves to be suitable for the phase stabilization system, enhancing the overall quality of the photomixing method for THz wave generation [68], [69]. In the next chapter, this phase stabilization system will be implemented into THz wave generation system.

REFERENCES

[1] I. Cisco Systems, “Cisco Visual Networking Index: Forecast and Trends, 2017–2022 White Paper,” *Cisco Forecast Methodol.*, pp. 2017–2022, 2019.

[2] S. Cherry, “Edholm’s law of bandwidth,” *IEEE Spectr.*, vol. 41, no. 7, p. 50, 2004.

[3] E. W. Paper, “6G spectrum - enabling the future mobile life beyond 2030,” no. March, 2023.

[4] Z. Li *et al.*, “Terahertz band range adjustable hyperbolic metamaterial refractive index sensor,” *Results Phys.*, vol. 49, no. April, p. 106477, 2023, doi: 10.1016/j.rinp.2023.106477.

[5] K. Tekbıyık, A. R. Ekti, G. K. Kurt, and A. Görçin, “Terahertz band communication systems: Challenges, novelties and standardization efforts,” *Phys. Commun.*, vol. 35, p. 100700, 2019, doi: 10.1016/j.phycom.2019.04.014.

[6] W. Hao, F. Zhou, M. Zeng, O. A. Dobre, and N. Al-Dhahir, “Ultra Wideband THz IRS Communications: Applications, Challenges, Key Techniques, and Research Opportunities,” *IEEE Netw.*, vol. 36, no. 6, pp. 214–220, 2022, doi: 10.1109/MNET.110.2100664.

[7] A. B. Belguidoum, M. L. Tounsi, and S. Mekaoui, “Analysis of 5G Radio Parameters and their Impact on the Peak Data Rate,” *Proc. - 2019 3rd Eur. Conf. Electr. Eng. Comput. Sci. EECS 2019*, pp. 66–71, 2019, doi: 10.1109/EECS49779.2019.00025.

[8] T. Nagatsuma, G. Ducournau, and C. C. Renaud, “Advances in terahertz communications accelerated by photonics,” *Nat. Photonics*, vol. 10, no. 6, pp. 371–379, 2016, doi: 10.1038/nphoton.2016.65.

[9] J. Yao and J. Capmany, “Microwave photonics,” *Sci. China Inf. Sci.*, vol. 65, no. 12, pp. 314–335, 2022, doi: 10.1007/s11432-021-3524-0.

[10] H. G. Yu, S. H. Choi, S. Jeon, and M. Kim, “300 GHz InP HBT amplifier with 10 mW output power,” *Electron. Lett.*, vol. 50, no. 5, pp. 377–379, 2014, doi: 10.1049/el.2013.3288.

[11] M. Seo *et al.*, “InP HBT IC technology for terahertz frequencies: Fundamental oscillators Up to 0.57 THz,” *IEEE J. Solid-State Circuits*, vol. 46, no. 10, pp. 2203–2214, 2011, doi: 10.1109/JSSC.2011.2163213.

[12] S. H. Kim, T. H. Jang, D. M. Kang, and C. S. Park, “A 120 GHz Wideband CMOS I/Q Transmitter for Short-Range Wireless Device-to-Device Communication,” *Asia-Pacific Microw. Conf. Proceedings, APMC*, vol. 2020-Decem, pp. 39–41, 2020, doi: 10.1109/APMC47863.2020.9331594.

[13] T. A. Vu and M. Fujishima, “A 300 GHz CMOS transmitter front-end for ultrahigh-speed wireless communications,” *Int. J. Electr. Comput. Eng.*, vol. 7, no. 4, pp. 2278–2286, 2017, doi: 10.11591/ijece.v7i4.pp2278-2286.

[14] J. V. Siles and J. Grajal, “Physics-based design and optimization of Schottky diode frequency multipliers for terahertz applications,” *IEEE Trans. Microw. Theory Tech.*, vol. 58, no. 7 PART 2, pp. 1933–1942, 2010, doi: 10.1109/TMTT.2010.2050103.

[15] Y. Zhang, W. Zhao, Y. Wang, T. Ren, and Y. Chen, “A 220 GHz subharmonic mixer based on schottky diodes with an accurate terahertz diode model,” *Microw. Opt. Technol. Lett.*, vol. 58, no. 10, pp. 2311–2316, Oct. 2016, doi: https://doi.org/10.1002/mop.30032.

[16] H. Hamada *et al.*, “300-GHz 120-Gb/s Wireless Transceiver with High-Output-Power and High-Gain Power Amplifier Based on 80-nm InP-HEMT Technology,” *2019 IEEE BiCMOS Compd. Semicond. Integr. Circuits Technol. Symp. BCICTS 2019*, pp. 2019–2022, 2019, doi: 10.1109/BCICTS45179.2019.8972756.

[17] H. Hamada *et al.*, “300-GHz. 100-Gb/s InP-HEMT Wireless Transceiver Using a 300-GHz Fundamental Mixer,” *IEEE MTT-S Int. Microw. Symp. Dig.*, vol. 2018-June, pp. 1480–1483, 2018, doi: 10.1109/MWSYM.2018.8439850.

[18] L. Hou, S. Tang, B. Hou, and J. H. Marsh, “Photonic integrated circuits for terahertz source generation,” *IET Optoelectron.*, vol. 14, no. 3, pp. 136–142, 2020, doi: 10.1049/iet-opt.2019.0089.

[19] W. Lee *et al.*, “Coherent terahertz wireless communication using dual-parallel MZM-based silicon photonic integrated circuits,” *Opt. Express*, vol. 30, no. 2, p. 2547, 2022, doi: 10.1364/oe.446516.

[20] G. Carpintero *et al.*, “Photonic integrated circuits for terahertz communication: The hybrid integrated microwave photonic approach,” *Opt. InfoBase Conf. Pap.*, no. Mmi, pp. 6–7, 2021, doi: 10.1364/ofc.2021.f4f.4.

[21] T. Alam *et al.*, “Wideband, high-resolution terahertz spectroscopy by light-induced frequency tuning of quantum-cascade lasers,” *Opt. Express*, vol. 27, no. 4, p. 5420, 2019, doi: 10.1364/oe.27.005420.

[22] H. W. Hübers, H. Richter, and M. Wienold, “High-resolution terahertz spectroscopy with quantum-cascade lasers,” *J. Appl. Phys.*, vol. 125, no. 15, 2019, doi: 10.1063/1.5084105.

[23] T. Shiramizu *et al.*, “Feasibility Demonstration of THz Wave Generation/Modulation Based on Photomixing Using a Single Wavelength-Tunable Laser,” *Photonics*, vol. 10, no. 4, 2023, doi: 10.3390/photonics10040369.

[24] S. Preu, G. H. Dhler, S. Malzer, L. J. Wang, and A. C. Gossard, “Tunable, continuous-wave Terahertz photomixer sources and applications,” *J. Appl. Phys.*, vol. 109, no. 6, 2011, doi: 10.1063/1.3552291.

[25] K. Li *et al.*, “16-QAM Vector Terahertz-Wave Signal Generation by Simple MZM-Based Optical Frequency Comb,” *IEEE Photonics J.*, vol. 13, no. 1, 2021, doi: 10.1109/JPHOT.2020.3045058.

[26] K. Kondo, M. Che, and K. Kato, “Generation and Enhancement of Pulsed THz Waves by Arrayed UTC-PDs,” *OECC/PSC 2022 - 27th Optoelectron. Commun. Conf. Conf. Photonics Switch. Comput. 2022*, no. 2, pp. 1–4, 2022, doi: 10.23919/OECC/PSC53152.2022.9849992.

[27] E. Peytavit, G. Ducournau, and J. Lampin, “THz Photomixers,” 2021, pp. 137–186.

[28] A. Morales, G. I. Nazarikov, S. Rommel, C. Okonkwo, and I. T. Monroy, “All-Photonic Heterodyne sub-THz Wireless Transmission at 80 GHz, 120 GHz and 160 GHz Carrier Frequencies,” in *2020 45th International Conference on Infrared, Millimeter, and Terahertz Waves (IRMMW-THz)*, 2020, pp. 1–2, doi: 10.1109/IRMMW-THz46771.2020.9370506.

[29] E. García-Muñoz *et al.*, “Photonic-based integrated sources and antenna arrays for broadband wireless links in terahertz communications,” *Semicond. Sci. Technol.*, vol. 34, no. 5, 2019, doi: 10.1088/1361-6641/aaf8f2.

[30] H. Yang *et al.*, “A THz-OAM Wireless Communication System Based on Transmissive Metasurface,” *IEEE Trans. Antennas Propag.*, vol. 71, no. 5, pp. 1–1, 2023, doi: 10.1109/tap.2023.3255539.

[31] S. Carpenter *et al.*, “A D-Band 48-Gbit/s 64-QAM/QPSK Direct-Conversion I/Q Transceiver Chipset,” *IEEE Trans. Microw. Theory Tech.*, vol. 64, no. 4, pp. 1285–1296, 2016, doi: 10.1109/TMTT.2016.2533491.

[32] P. Torkaman *et al.*, “A 5G/Sub-Terahertz Heterogeneous Communication Network,” *IEEE Access*, vol. 10, pp. 65572–65584, 2022, doi: 10.1109/ACCESS.2022.3184312.

[33] M. Sawaby, N. Dolatsha, B. Grave, C. Chen, and A. Arbabian, “A fully packaged 130-GHz QPSK transmitter with an integrated PRBS generator,” *IEEE Solid-State Circuits Lett.*, vol. 1, no. 7, pp. 166–169, 2018, doi: 10.1109/LSSC.2019.2895571.

[34] E. F. Garay, D. J. Munzer, and H. Wang, “A 150 GHz Lens-Free Large FoV Regenerative 2 × 2 Transceiver Array With 31% DC-to-EIRP Efficiency and -70 dBm Sensitivity for a 70 cm Bidirectional Peer-to-Peer Link,” *IEEE J. Solid-State Circuits*, vol. 57, no. 7, pp. 2102–2113, 2022, doi: 10.1109/JSSC.2022.3149526.

[35] Y. Kim *et al.*, “150-GHz CMOS TX/RX with Digitally Predistorted PAM-4

Modulation for Terahertz Contactless/Plastic Waveguide Communications," *IEEE Trans. Terahertz Sci. Technol.*, vol. 10, no. 4, pp. 370–382, 2020, doi: 10.1109/TTHZ.2020.2991303.

[36] L. Chen, M. Taba, A. Cathelin, and E. Afshari, "A Low-Power 20Gb/s 196GHz BPSK Wireless Transmitter with Energy Efficiency FoM of 0.15pJ/bit/cm," *Proc. Cust. Integr. Circuits Conf.*, vol. 2023-April, pp. 1–2, 2023, doi: 10.1109/CICC57935.2023.10121306.

[37] P. Rodriguez-Vazquez, J. Grzyb, B. Heinemann, and U. R. Pfeiffer, "A QPSK 110-Gb/s Polarization-Diversity MIMO Wireless Link with a 220-255 GHz Tunable LO in a SiGe HBT Technology," *IEEE Trans. Microw. Theory Tech.*, vol. 68, no. 9, pp. 3834–3851, 2020, doi: 10.1109/TMTT.2020.2986196.

[38] J. Grzyb, P. R. Vazquez, N. Sarmah, B. Heinemann, and U. R. Pfeiffer, "A 240 GHz high-speed transmission link with highly-integrated transmitter and receiver modules in SiGe HBT technology," in *2017 42nd International Conference on Infrared, Millimeter, and Terahertz Waves (IRMMW-THz)*, 2017, pp. 1–2, doi: 10.1109/IRMMW-THz.2017.8066869.

[39] C. Wang, J. Yu, X. Li, P. Gou, and W. Zhou, "Fiber-THz-Fiber Link for THz Signal Transmission," *IEEE Photonics J.*, vol. 10, no. 2, pp. 1–6, 2018, doi: 10.1109/JPHOT.2018.2809433.

[40] T. Hagiwara *et al.*, "A 258-GHz CMOS Transmitter with Phase-Shifting Architecture for Phased-Array Systems," *IEEE MTT-S Int. Microw. Symp. Dig.*, vol. 2021-June, pp. 705–708, 2021, doi: 10.1109/IMS19712.2021.9574976.

[41] K. Takiguchi, "PAM4 wireless communication in 300 GHz-band using integrated-optic PAM signal emulator," *2022 Conf. Lasers Electro-Optics, CLEO 2022 - Proc.*, pp. 1–2, 2022, doi: 10.1364/cleo_si.2022.stu5l.7.

[42] A. Oshiro *et al.*, "PAM4 48-Gbit/s wireless communication using a resonant tunneling diode in the 300-GHz band," *IEICE Electron. Express*, vol. 19, no. 2, pp. 1–6, 2022, doi: 10.1587/elex.18.20210494.

[43] I. Abdo, H. Hamada, H. Nosaka, A. Shirane, and K. Okada, "64QAM wireless

link with 300 GHz InP-CMOS hybrid transceiver," *IEICE Electron. Express*, vol. 18, no. 17, pp. 1–4, 2021, doi: 10.1587/ELEX.18.20210314.

[44] K. Maekawa, Y. Kawamoto, T. Nakashita, and T. Yoshioka, "300-GHz-band Wireless Link Using Photonics-based Ultralow-noise Transmitter and Receiver," *2023 Opt. Fiber Commun. Conf. Exhib.*, pp. 15–17, 2023, doi: 10.23919/OFC49934.2023.10116279.

[45] D. Pirrone *et al.*, "Metasurface-Based Filters for High Data Rate THz Wireless Communication: Experimental Validation of a 14 Gbps OOK and 104 Gbps QAM-16 Wireless Link in the 300 GHz Band," *IEEE Trans. Wirel. Commun.*, vol. 21, no. 10, pp. 8688–8697, 2022, doi: 10.1109/TWC.2022.3168399.

[46] S. Nellen *et al.*, "Coherent Wireless Link at 300 GHz with 160 Gbit/s Enabled by a Photonic Transmitter," *J. Light. Technol.*, vol. 40, no. 13, pp. 4178–4185, 2022, doi: 10.1109/JLT.2022.3160096.

[47] L. Yi *et al.*, "300-GHz-band wireless communication using a low phase noise photonic source," in *2019 49th European Microwave Conference (EuMC)*, 2019, pp. 816–819, doi: 10.23919/EuMC.2019.8910724.

[48] M. Qiao *et al.*, "60 Gbit/s PAM-4 wireless transmission in the 310 GHz band with nonlinearity tolerant signal processing," *Opt. Commun.*, vol. 492, no. June 2020, p. 126988, 2021, doi: 10.1016/j.optcom.2021.126988.

[49] J. Shi *et al.*, "4096-QAM OFDM THz-over-fiber MIMO transmission using delta-sigma modulation," *IEEE Photonics Technol. Lett.*, vol. 35, no. 13, pp. 741–744, 2023, doi: 10.1109/LPT.2023.3271907.

[50] Y. Tan *et al.*, "Transmission of High-Frequency Terahertz Band Signal Beyond 300 GHz Over Metallic Hollow Core Fiber," *J. Light. Technol.*, vol. 40, no. 3, pp. 700–707, 2022, doi: 10.1109/JLT.2021.3123473.

[51] J. Ding *et al.*, "104-m Terahertz-Wave Wireless Transmission Employing 124.8-Gbit/s PS-256QAM Signal," *Opt. InfoBase Conf. Pap.*, vol. 1, no. c, pp. 1–3, 2022, doi: 10.1364/ofc.2022.m3c.3.

[52] S. Jia *et al.*, “120 Gb/s multi-channel THz wireless transmission and THz receiver performance analysis,” *IEEE Photonics Technol. Lett.*, vol. 29, no. 3, pp. 310–313, 2017, doi: 10.1109/LPT.2016.2647280.

[53] X. Li *et al.*, “120 Gb/s wireless terahertz-wave signal delivery by 375 GHz-500 GHz multi-carrier in a 2 × 2 MIMO system,” *J. Light. Technol.*, vol. 37, no. 2, pp. 606–611, 2019, doi: 10.1109/JLT.2018.2862356.

[54] M. Zhao, W. Zhou, and J. Yu, “3.5 Gbit/s OOK THz signal delivery over 88 cm free-space at 441.504 GHz,” *Microw. Opt. Technol. Lett.*, vol. 60, no. 6, pp. 1435–1439, 2018, doi: 10.1002/mop.31176.

[55] X. Li, J. Yu, K. Wang, W. Zhou, and J. Zhang, “Photonics-aided 2 × 2 MIMO wireless terahertz-wave signal transmission system with optical polarization multiplexing,” *Opt. Express*, vol. 25, no. 26, p. 33236, 2017, doi: 10.1364/oe.25.033236.

[56] X. Li *et al.*, “132-Gb/s photonics-aided single-carrier wireless terahertz-wave signal transmission at 450GHz enabled by 64QAM modulation and probabilistic shaping,” *Opt. InfoBase Conf. Pap.*, vol. Part F160-, pp. 10–12, 2019.

[57] X. Liu *et al.*, “Demonstration of 144-Gbps Photonics-Assisted THz Wireless Transmission at 500 GHz Enabled by Joint DBN Equalizer,” *Micromachines*, vol. 13, no. 10, 2022, doi: 10.3390/mi13101617.

[58] Y. Yoshimizu, S. Hisatake, S. Kuwano, J. Terada, N. Yoshimoto, and T. Nagatsuma, “Wireless transmission using coherent terahertz wave with phase stabilization,” *IEICE Electron. Express*, pp. 10–20130578, 2013.

[59] L. Gonzalez-Guerrero and G. Carpintero, “Coherent photonic Terahertz transmitters compatible with direct comb modulation,” *Sci. Rep.*, vol. 12, no. 1, pp. 1–10, 2022, doi: 10.1038/s41598-022-13618-y.

[60] K. Sakuma *et al.*, “First demonstration of Mach-Zehnder-interferometric phase-stabilization at optoelectronic carrier generation for phase-shift keying signal,” *2015 Opto-Electronics Commun. Conf. OECC 2015*, pp. 1–3, 2015, doi:

10.1109/OECC.2015.7340086.

[61] S. Takeuchi, K. Kato, Y. Yoshimizu, Y. Yasuda, S. Hisatake, and T. Nagatsuma, "Coherent sub-THz carrier frequency transmission with novel pseudo-Mach-Zehnder interferometric phase stabilization," in *Microwave Photonics (MWP) and the 2014 9th Asia-Pacific Microwave Photonics Conference (APMP) 2014 International Topical Meeting on*, Oct. 2014, pp. 208–210, doi: 10.1109/MWP.2014.6994532.

[62] S. Takeuchi *et al.*, "Novel lightwave-interferometric phase detection for phase stabilization of two-tone coherent millimeter-wave/microwave carrier generation," *IEICE Trans. Electron.*, vol. E99C, no. 9, pp. 1048–1055, 2016, doi: 10.1587/transele.E99.C.1048.

[63] M.-C. Lo *et al.*, "Foundry-fabricated dual-DFB PIC injection-locked to optical frequency comb for high-purity THz generation," in *Optical Fiber Communication Conference*, 2019, pp. W1B-3.

[64] G. K. M. Hasanuzzaman, H. Shams, C. C. Renaud, J. Mitchell, and S. Iezekiel, "Photonic THz Generation using Optoelectronic Oscillator-driven Optical Frequency Comb Generator," in *2018 International Topical Meeting on Microwave Photonics (MWP)*, 2018, pp. 1–4, doi: 10.1109/MWP.2018.8552892.

[65] T. Nagatsuma *et al.*, "Terahertz wireless communications based on photonics technologies," *Opt. Express*, vol. 21, no. 20, pp. 23736–23747, Oct. 2013, doi: 10.1364/OE.21.023736.

[66] S. Takeuchi *et al.*, "Novel lightwave-interferometric phase detection for phase stabilization of two-tone coherent millimeter-wave/microwave carrier generation," *IEICE Trans. Electron.*, vol. E99C, no. 9, pp. 1048–1055, 2016, doi: 10.1587/transele.E99.C.1048.

[67] Y. Ma, L. Stewart, J. Armstrong, I. G. Clarke, and G. Baxter, "Recent progress of wavelength selective switch," *J. Light. Technol.*, vol. 39, no. 4, pp. 896–903, 2020.

[68] A. A. Ibrahim, T. Shiramizu, S. Ye, Y. Mikami, and K. Kato, “Pilot-Lightwave-based Terahertz Wave Phase Stabilization,” *Conf. Dig. - IEEE Int. Semicond. Laser Conf.*, vol. 2022-Octob, no. Ld, pp. 2022–2023, 2022, doi: 10.23919/ISLC52947.2022.9943347.

[69] T. Shiramizu, A. A. Ibrahim, S. Ye, Y. Mikami, and K. Kato, “Photonic Phase Stabilization Control System for Terahertz-Wave Phase Modulation,” in *2022 27th OptoElectronics and Communications Conference (OECC) and 2022 International Conference on Photonics in Switching and Computing (PSC)*, 2022, pp. 1–4, doi: 10.23919/OECC/PSC53152.2022.9850107.

[70] A. A. Ibrahim, H. Chen, T. Shiramizu, Y. Mikami, and K. Kato, “Terahertz-Wave Phase Modulation Enabled by Optical Interferometric Phase Stabilization,” in *2022 Asia-Pacific Microwave Conference (APMC)*, Nov. 2022, pp. 943–945.

CHAPTER 3
PHASE STABILIZATION OF THE OPTICAL DOMAIN

3.1 Phase Stabilization System of the Optical Domain

Building upon the earlier discussed research, the current focus is to compare the phase stabilization system based on the Mach-Zehnder Interferometer (MZI) technique by utilizing forward and backward-direction pilot lightwaves. Introducing a pilot lightwave into two optical paths, the combined lightwaves at the output coupler undergo interference. By precisely controlling the intensity of the interfered lightwave, a constant phase difference can be maintained between the lightwaves of the two optical paths. This comparative study aims to assess the stability and reliability of different phase stabilization methods in stabilizing the THz wave generation system, with emphasis on the direction of the pilot lightwave introduced into the system.

In the forward-direction phase stabilization system, the pilot lightwave is launched from the input of the THz wave generation system. On the other hand, in the backward-direction phase stabilization system, the pilot lightwave is fed from the output of the THz wave generation system. This setup enables an investigation of the impact of the pilot lightwave direction on the stability of the system. These analyses are crucial for enhancing the stability of the THz wave phase modulation system and driving improvements in generating phase-modulated THz waves for high-speed data transmission.

In this chapter, the experimental setup for the MZI phase detection method will be presented, both for the forward and backward-direction pilot lightwaves. The details of the setup, including the components used to evaluate the system's stability, will be explained. Subsequently, the detection of interference intensity and the stability of the system in the optical domain will be studied. By investigating the performance and effectiveness of the forward and backward-direction pilot lightwaves in the phase stabilization system, the goal is to identify the most reliable and stable approach for generating a stable phase-modulated THz wave.

3.2 Experimental Setup

The experimental setup of a newly devised phase stabilization technique for THz wave phase modulation system with a backward pilot lightwave is constructed as well as that with a forward pilot lightwave as a reference.

3.2.1 Forward Pilot Lightwave System

Figure 3.1 illustrates the block diagram of a reference experiment conducted to generate phase-modulated THz waves using a forward pilot lightwave in the phase stabilization system. In this THz-wave PM generation system (solid line), a single lightwave with a frequency *f* of 193.4125 THz (1550 nm) (orange arrow) is introduced from the left side instead of utilizing two lightwaves with different optical frequencies. Th lightwave is then passed through the optical coupler (OC). Here marked as the input of the THz wave generation system. The lightwave is then introduced to the Wavelength Selective Switch (WSS). The upper path involves the lightwave traveling through a traveling-wave optical phase modulator (PM) and being phase modulated by the pulse-pattern generator (PPG) at various bit rates using a constant pseudorandom binary sequence (PRBS) of 7. The lower path comprises the lightwave passing through the phase shifter (PS). The lightwaves from these two paths are combined at the OC, here are marked as the output of TH wave generation system. The graph of the input and output lightwaves into the MZI shows that the input power of the *f* into the MZI is 12 dBm and the output is -2.42 dBm. The observed loss may result from various factors in our complex experimental setup, in-cluding fiber-to-waveguide connections, as well as certain devices that introduce considerable inefficiencies. The coupled signal is introduced to an optical-electrical (O/E) converter, resulting in the modulated signal. The phase stability modulated signal in the THz-wave generation system is observed by comparing it with the initial signal injected into the PM using an oscilloscope (OSC).

In contrast, the phase stabilization system (dotted line) operates as follows: the pilot lightwave (pink arrow) originates from a laser with an optical frequency of 195.4125 THz (1535 nm). The frequency of the pilot lightwave is purposely chosen to be different from the frequency used in the THz wave generation system to avoid interference between the two signals. The pilot lightwave is then input into the MZI configuration at the OC. The lightwave is split at the WSS and directed through the upper path involving the OPM and the lower path involving the PS. As shown in figure, the input pilot lightwave into the THz wave generation has a power of -7.77 dBm while the output is -40.5 dBm. The pilot lightwave at the output of the THz wave generation system is of negligible magnitude to influence on the generation process. Instead,

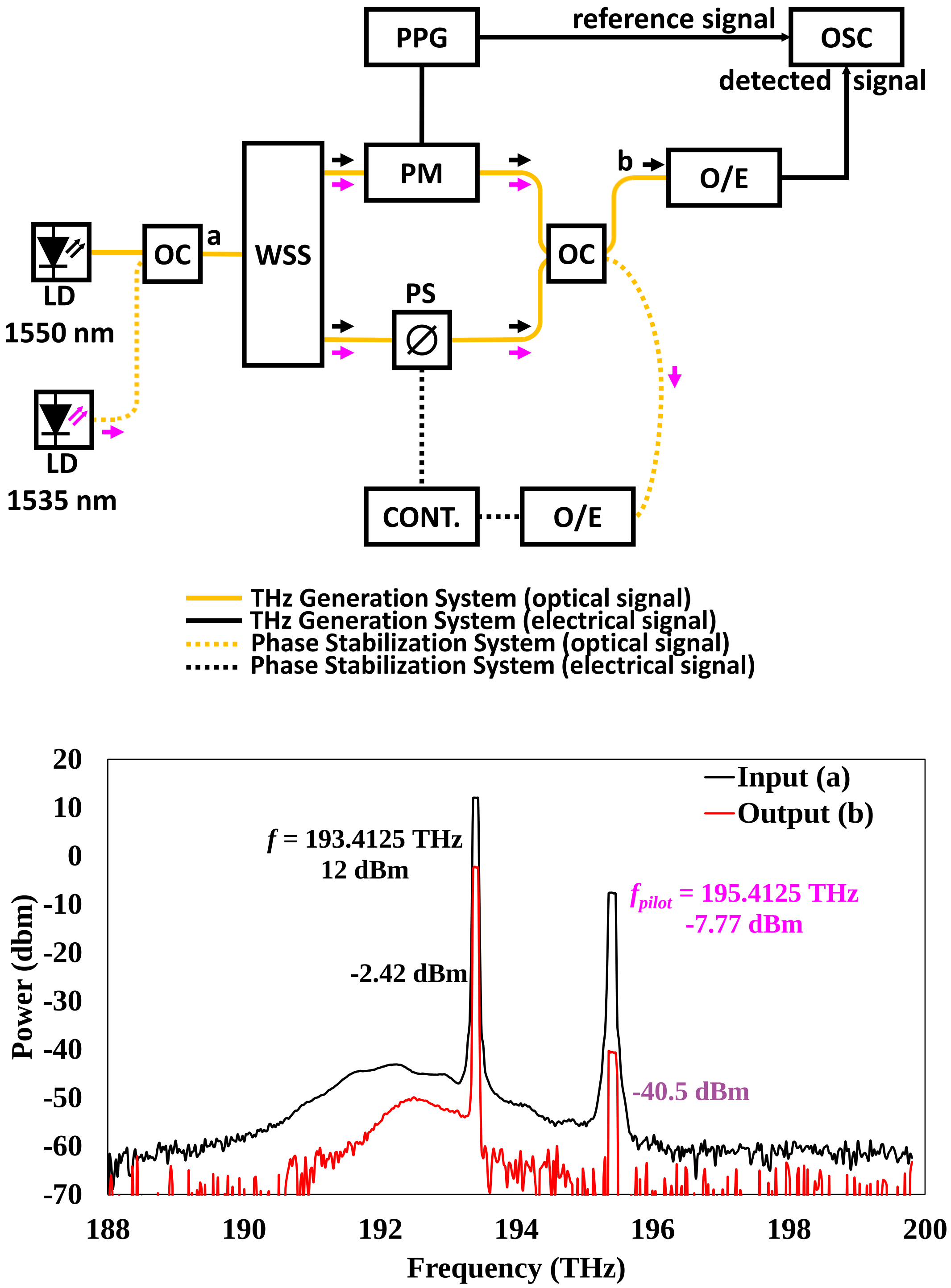

Figure 3.1 Experimental setup with forward pilot lightwave

after coupling at the OC, the pilot lightwaves interfere and pass through the other arm of the coupler to the optical-electrical (O/E) converter. The interference of the pilot lightwave enables the detection of phase fluctuations occurring by phase changes in the optical paths, particularly the optical fiber. The intensity of the interference is then measured using an O/E converter. The converted voltage is subsequently read by a feedback controller, which adjusts the PS to maintain a constant voltage. By precisely controlling and maintaining the intensity of the interfered pilot lightwave, the phase fluctuations in the THz wave generation system can be effectively eliminated, enabling the application of a high-sensitivity coherent detection at the output of the THz wave generation system.

3.2.2 Backward Pilot Lightwave System

Figure 3.2 shows the experimental setup featuring a phase stabilization system utilizing a backward-direction pilot lightwave. Similar to the forward-direction pilot lightwave system, a single lightwave is employed in the THz wave generation system (solid line). The input power a frequency *f* of 193.4125 THz in introduced into the THz wave generation system is 14.5 dBm and the output is -3.28 dBm , as shown in figure. The configuration of the phase stabilization system (dotted line) is positioned on the right side. In this setup, the pilot lightwave (light blue arrow) is introduced to the THz wave generation system from the backward direction, which is through the output of the setup. It is observed that the power of the pilot lightwave at the output of the THz wave generation system is -41.9 dBm, which is primarily due to the effects of total internal reflection at the OC (output). However, this power value is negligible and can be disregarded as it does not significantly impact the THz wave generation system. The pilot lightwave travels through the lower arm of the OC and splits into two paths. In the upper path, it passes through the PM, while in the lower path, it passes through the PS, both in the opposite direction. Then, the pilot lightwave is recoupled after the WSS. The coupled pilot lightwave is detected by the O/E converter. As the PM modulates the phase of the lightwave only when the lightwave and the electrical data signal travel in the same direction, the phase of the backward-direction pilot lightwave remains unmodulated. Hence, efficient interference is expected in this configuration.

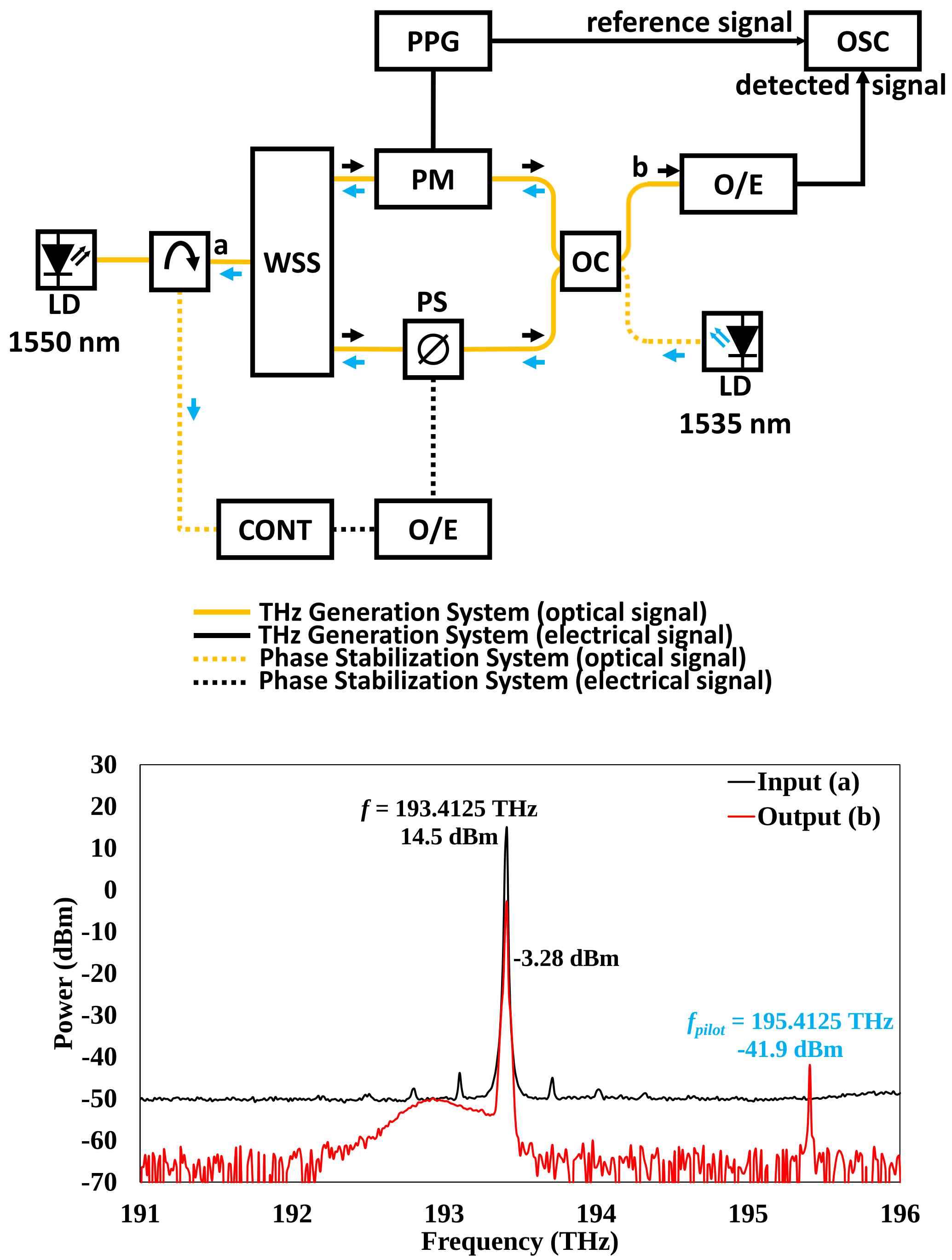

Figure 3.2 Experimental setup with backward pilot lightwave.

3.3 Result of Phase Stabilization System

The stabilization of the interfered intensity is observed. At first, the interfered intensity the pilot lightwave for the backward-direction pilot lightwave is observed at lower bit rate of 0.3, 0.5 and 3.0 Gbit/s. Figure 3.3 shows the voltage from the O/E converter that represents the interfered intensity of the pilot lightwave without (FB

OFF) and with (FB ON) the phase stabilization system at different bit rates applied to the PM. The interference is unstable and fluctuates without the phase stabilization system. On the other side, with the phase stabilization system applied, the interfered intensity becomes stable and almost no fluctuation.

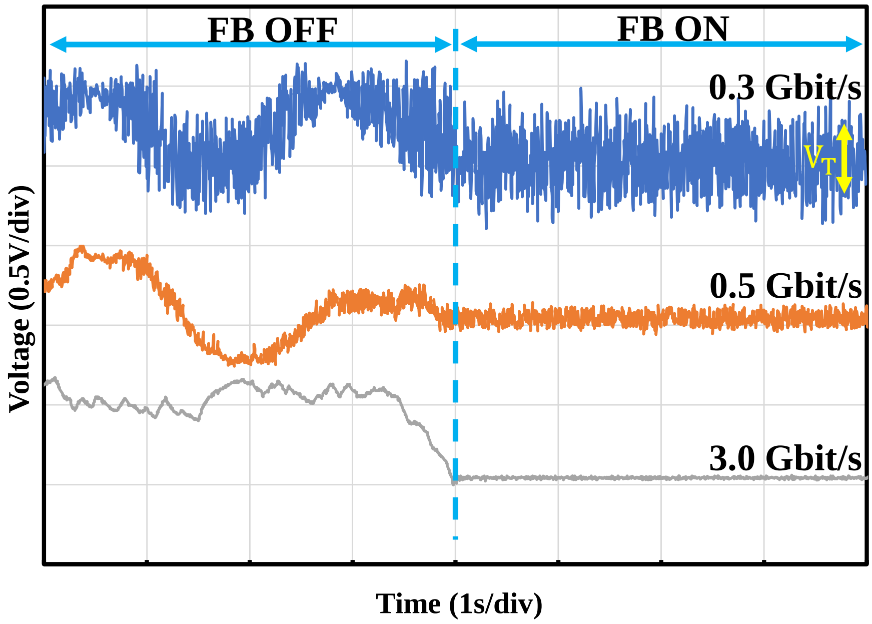

Figure 3.3 The detected interference signal with backward pilot lightwave system

Next, the experiment was repeated with an alternate oscilloscope capable of accommodating higher bit rates. The stabilization of the interfered intensity of the pilot lightwave at higher bit rates as depicted in Figure 3.4 and Figure 3.5. These figures present the voltage readings obtained from the O/E converter, which indicate the interfered intensity of both the forward-direction and backward-direction pilot lightwaves in the presence and absence of the phase stabilization system. The measurements were higher bit rates applied to the PM; 1, 3 and 10 Gbit/s.

Figure 3.4 shows the interference voltage value over the time when the phase stabilization system was employed for the forward-direction pilot lightwave in the case of the system OFF and ON. The interference voltage displayed instability and fluctuations in the absence of the phase stabilization system. However, even with the activation of the phase stabilization system, the interfered intensity failed to maintain a constant voltage across all modulation bit rates. The condition happened in all modulation rates 1, 3 and 10 Gbit/s. This behavior can be attributed to the blurring effect induced by the modulation of the pilot lightwave within the phase modulation system itself. In contrast, when employing the phase stabilization system with a backward-direction pilot lightwave, the interfered intensity achieved stability when the phase stabilization is ON, as shown in Figure 3.5.

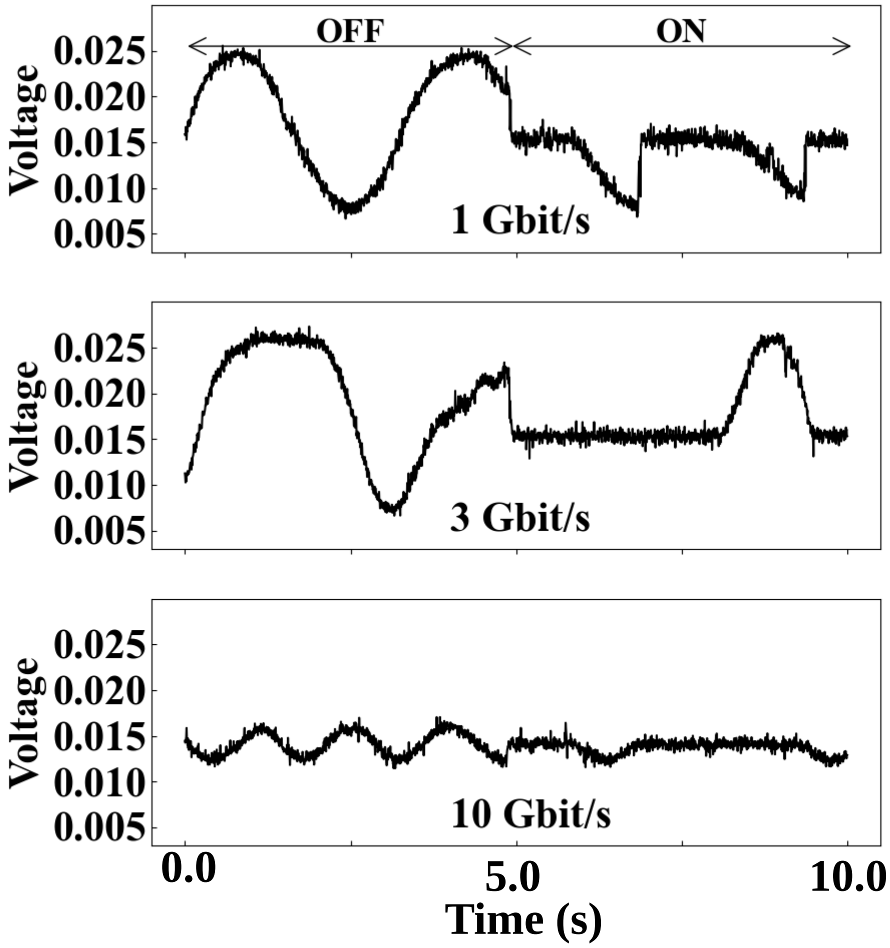

Figure 3.4 The detected interference intensity for forward-direction pilot lightwave

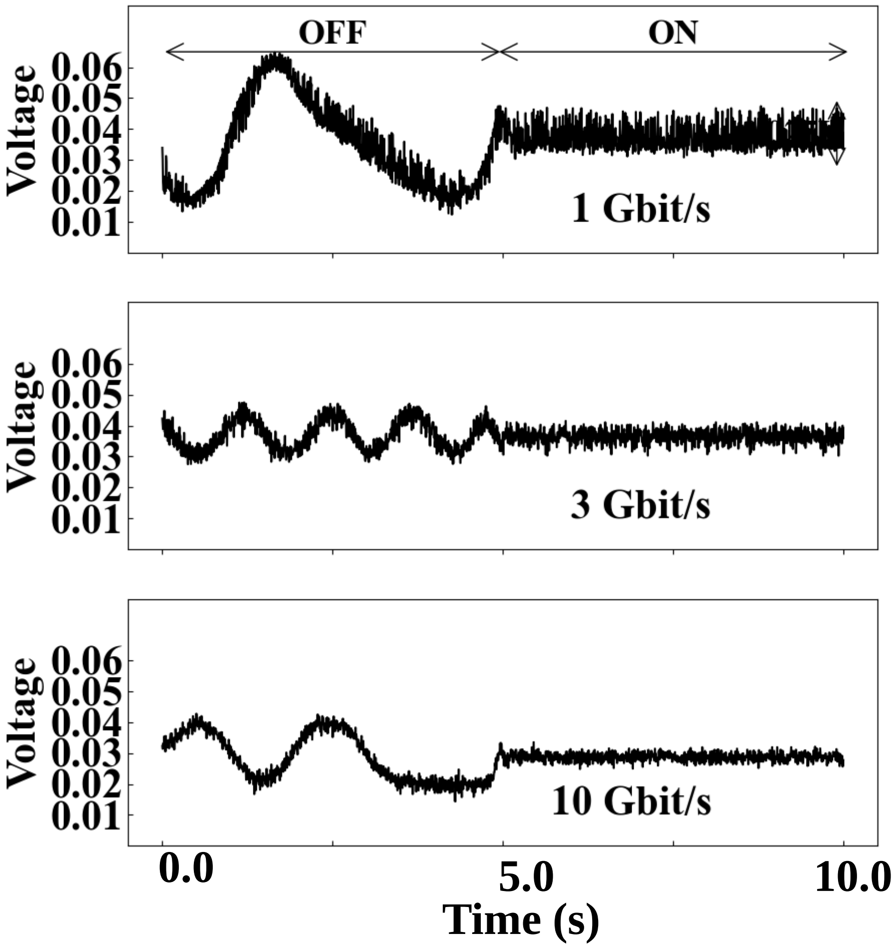

Figure 3.5 The detected interference intensity for backward-direction pilot lightwave

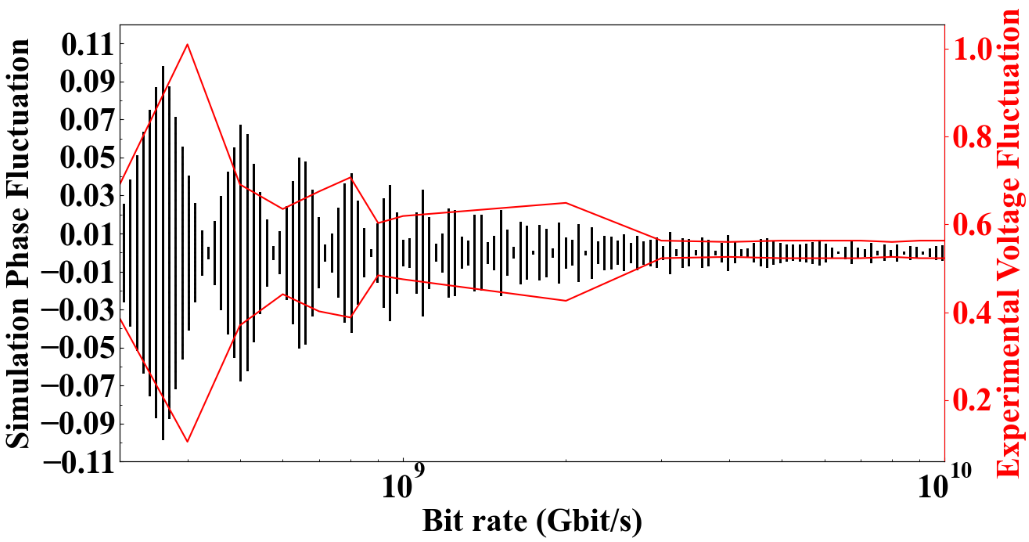

Figure 3.6 Simulation dan experimental result of phase fluctuation of the backward-direction pilot lightwave.

Furthermore, the vertical width of the interfered intensity, denoted as V_T, varied depending on the bit rate of the phase modulation. V_T decreased as the bit rate increased, indicating a reduced impact of phase modulation on the pilot lightwave at higher bit rates. Beyond 3 Gbit/s, V_T is significantly small, indicating that the phase modulation has minimal impact on the pilot lightwave at bit rates exceeding 3 Gbit/s. These experimental findings are in strong alignment with our simulation results, assuming that the voltage fluctuation values correspond to the phase fluctuation shown in Figure 3.8 and validated the efficacy of the backward-direction phase stabilization system. The simulation result did show the probability of the phase fluctuation of the pilot lightwave that passes through the phase modulator in the backward direction. It shows that the phase fluctuation has become smaller as the modulation bit rate increases.

3.4 Result of THz wave Generation System

3.4.1 Detected Interference Signal for THz wave Generation System

Next, the phase-modulated signal lightwave is observed and compared it with the modulation signal from the PPG for the backward- direction pilot lightwave setup.

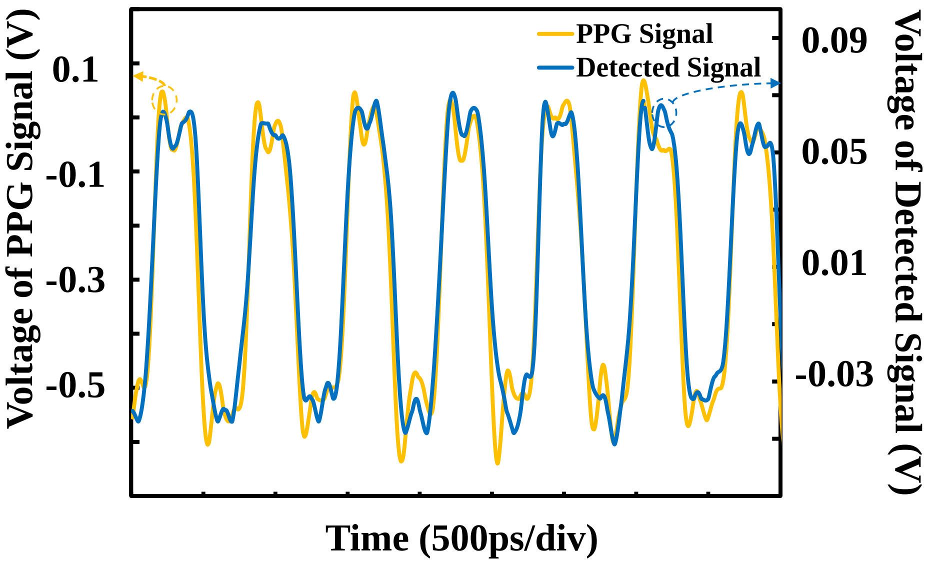

Figure 3.7 The signal from the PPG (yellow) and detected signal lightwave (blue) at 3.0 Gbit/s binary word pattern phase modulation.

Figure 3.7 shows the detected waveform (blue) as well as the modulation signal from PPG (yellow) as a reference for binary word pattern phase modulation. It was shown that the detected signal has a clear continuous data pattern. The detected phase-modulated signals are in phase as the modulation signal pattern from the PPG.

3.4.2 Stability of the Optical Domain

Next, the eye pattern of the phase modulated signal at the forward and backward pilot lightwave phase stabilization systems various bit rates. Figure 3.8 compares the forward and backward pilot lightwave phase stabilization system at 0.3, 0.4 and 0.5 Gbit/s. It is difficult to get a stable eye-opening for the forward pilot lightwave. In contrast, with the backward pilot light, the eye-opening is clear at above

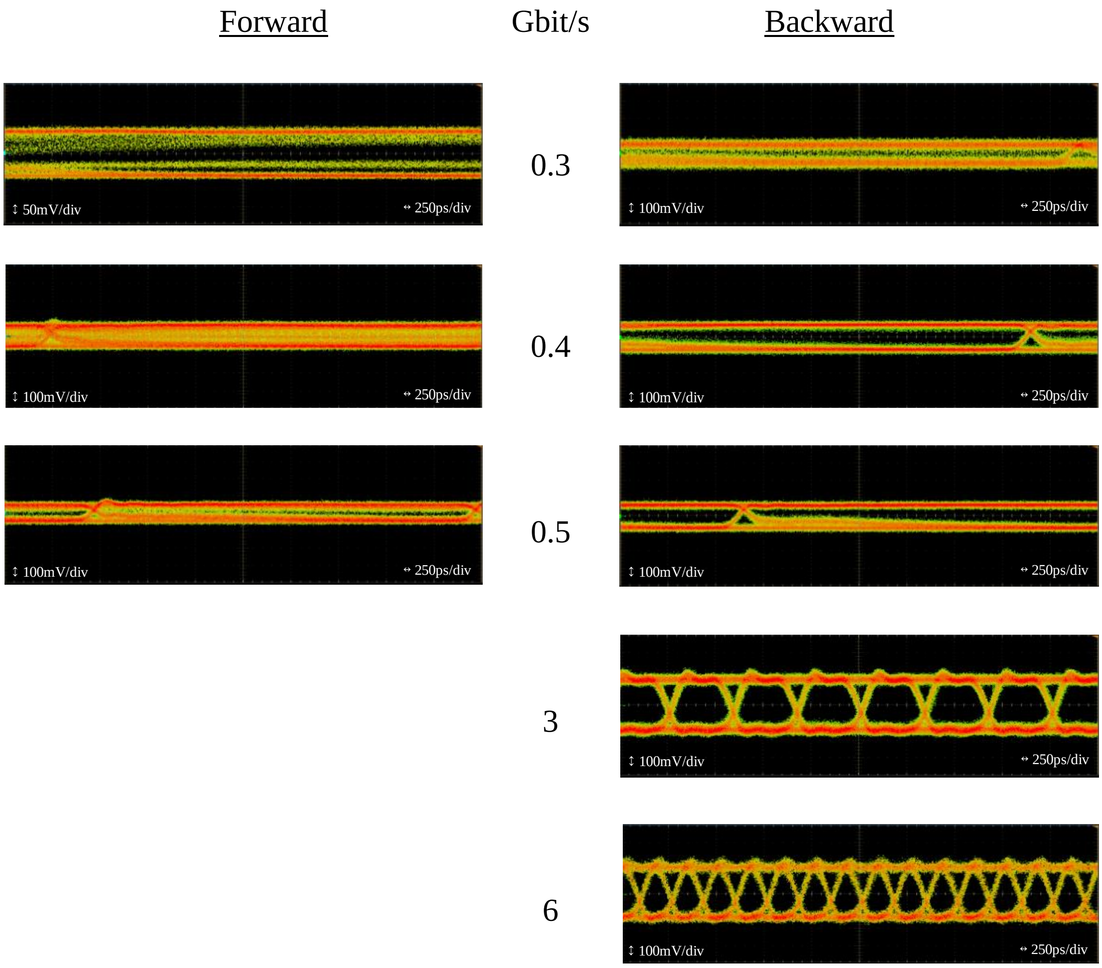

Figure 3.8 Comparison of eye pattern between forward pilot lightwave and backward pilot.

3 Gbit/s. These results confirmed that the phase stabilization with backward pilot lightwave is effective at a higher bit rate. At a lower bit rate, even with the backward direction, the phase of the pilot lightwave is modulated and cannot be interfered which prevents the feedback control for phase stabilization. After achieving successful results in the preliminary experiment, the experiment was repeated with an oscilloscope capable of accommodating higher bit rates. In this phase, the main focus was on achieving higher modulation bit rates for both the experimental setup for forward and backward directions of phase stabilization system.

Then, the phase stability of the optical domain was assessed by observing the eye pattern at different bit rates of 1, 3, and 10 Gbit/s, as depicted in Figure 3.9. A comparison of the performance between the forward-direction and backward-direction phase stabilization systems is presented in Figure 3.9(a) and (b), respectively. In both figures, the black dots represent the original modulation data from the PPG as a reference, while the red dots represent the detected signal. It is clear that the forward-direction phase stabilization system fails to achieve a stable eye-opening for each modulation signal. In the case of the backward-direction phase stabilization system, at lower bit rates, the pilot lightwave still undergoes modulation and cannot be interfered with, thus preventing feedback control for phase stabilization. Consequently, the resulting eye pattern exhibits an unclear eye-opening. However, a clear eye-opening is achieved at bit rates exceeding 3 Gbit/s. These findings provide experimental evidence supporting the effectiveness of phase stabilization using a backward-direction pilot lightwave, particularly at higher bit rates, thereby agreeing with our earlier theoretical predictions. These experimental results clearly demonstrate the adaptability and efficacy of the phase stabilization system employing the backward-direction pilot lightwave for the THz wave generation system.

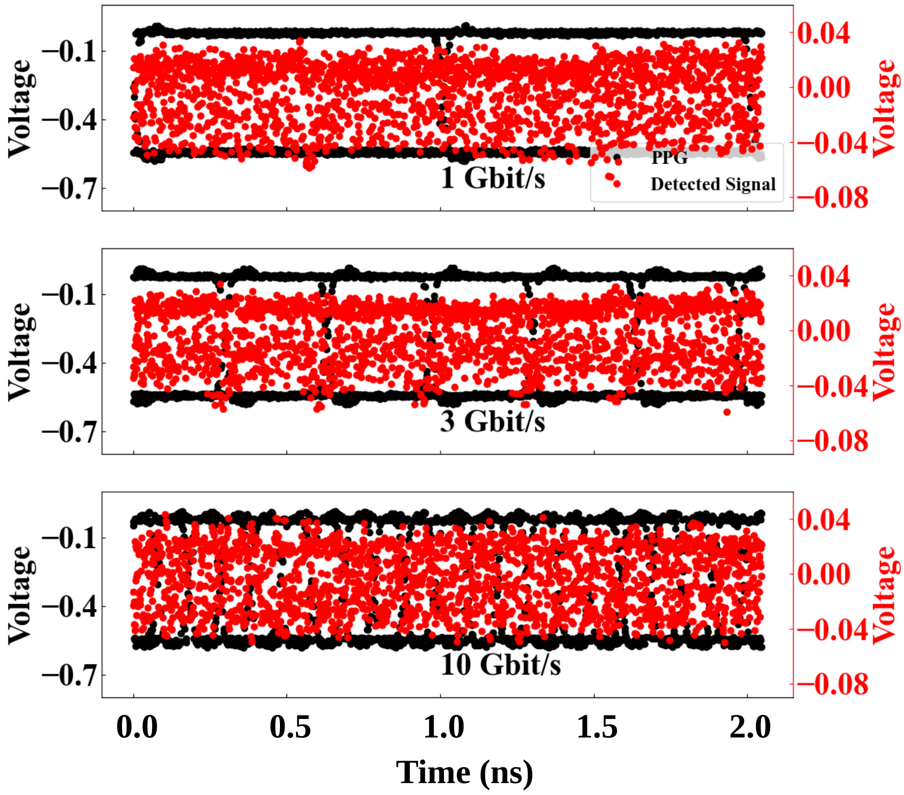

(a)

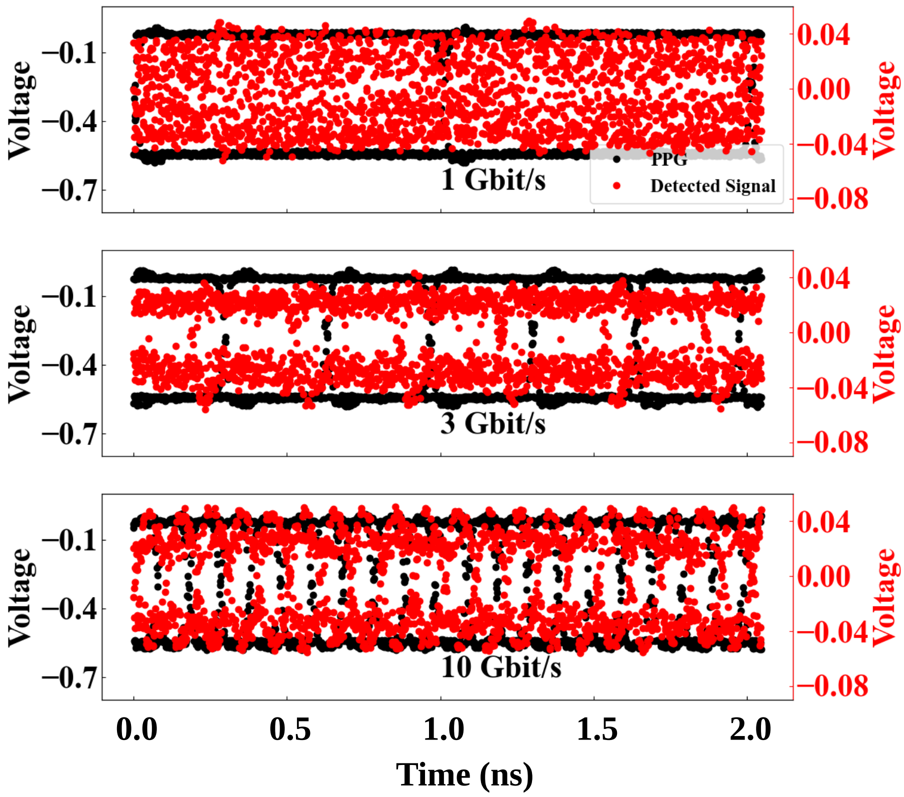

(a)

Figure 3.9 The eye pattern of the optical domain experimental setup with (a) forward-direction pilot lightwave and (b) forward-direction pilot lightwave at 1, 3 and 10 Gbit/s

3.5 Conclusion of This Chapter

The observed improvements in eye pattern stability emphasizes the importance of employing the appropriate pilot lightwave direction in achieving robust and reliable phase stabilization, especially at higher bit rates. Such improvements are crucial for realizing multilevel phase modulation for high data transmission in THz-wave applications. As a conclusion, the novel method of introducing the pilot lightwave from the backward direction of the THz wave generation system is applicable for generating a stabilized phase modulated THz wave.

REFERENCES

[1] I. Cisco Systems, “Cisco Visual Networking Index: Forecast and Trends, 2017–2022 White Paper,” *Cisco Forecast Methodol.*, pp. 2017–2022, 2019.

[2] S. Cherry, “Edholm’s law of bandwidth,” *IEEE Spectr.*, vol. 41, no. 7, p. 50, 2004.

[3] E. W. Paper, “6G spectrum - enabling the future mobile life beyond 2030,” no. March, 2023.

[4] Z. Li *et al.*, “Terahertz band range adjustable hyperbolic metamaterial refractive index sensor,” *Results Phys.*, vol. 49, no. April, p. 106477, 2023, doi: 10.1016/j.rinp.2023.106477.

[5] K. Tekbıyık, A. R. Ekti, G. K. Kurt, and A. Görçin, “Terahertz band communication systems: Challenges, novelties and standardization efforts,” *Phys. Commun.*, vol. 35, p. 100700, 2019, doi: 10.1016/j.phycom.2019.04.014.

[6] W. Hao, F. Zhou, M. Zeng, O. A. Dobre, and N. Al-Dhahir, “Ultra Wideband THz IRS Communications: Applications, Challenges, Key Techniques, and Research Opportunities,” *IEEE Netw.*, vol. 36, no. 6, pp. 214–220, 2022, doi: 10.1109/MNET.110.2100664.

[7] A. B. Belguidoum, M. L. Tounsi, and S. Mekaoui, “Analysis of 5G Radio Parameters and their Impact on the Peak Data Rate,” *Proc. - 2019 3rd Eur. Conf. Electr. Eng. Comput. Sci. EECS 2019*, pp. 66–71, 2019, doi: 10.1109/EECS49779.2019.00025.

[8] T. Nagatsuma, G. Ducournau, and C. C. Renaud, “Advances in terahertz communications accelerated by photonics,” *Nat. Photonics*, vol. 10, no. 6, pp. 371–379, 2016, doi: 10.1038/nphoton.2016.65.

[9] J. Yao and J. Capmany, “Microwave photonics,” *Sci. China Inf. Sci.*, vol. 65, no. 12, pp. 314–335, 2022, doi: 10.1007/s11432-021-3524-0.

[10] H. G. Yu, S. H. Choi, S. Jeon, and M. Kim, "300 GHz InP HBT amplifier with 10 mW output power," *Electron. Lett.*, vol. 50, no. 5, pp. 377–379, 2014, doi: 10.1049/el.2013.3288.

[11] M. Seo *et al.*, "InP HBT IC technology for terahertz frequencies: Fundamental oscillators Up to 0.57 THz," *IEEE J. Solid-State Circuits*, vol. 46, no. 10, pp. 2203–2214, 2011, doi: 10.1109/JSSC.2011.2163213.

[12] S. H. Kim, T. H. Jang, D. M. Kang, and C. S. Park, "A 120 GHz Wideband CMOS I/Q Transmitter for Short-Range Wireless Device-to-Device Communication," *Asia-Pacific Microw. Conf. Proceedings, APMC*, vol. 2020-Decem, pp. 39–41, 2020, doi: 10.1109/APMC47863.2020.9331594.

[13] T. A. Vu and M. Fujishima, "A 300 GHz CMOS transmitter front-end for ultrahigh-speed wireless communications," *Int. J. Electr. Comput. Eng.*, vol. 7, no. 4, pp. 2278–2286, 2017, doi: 10.11591/ijece.v7i4.pp2278-2286.

[14] J. V. Siles and J. Grajal, "Physics-based design and optimization of Schottky diode frequency multipliers for terahertz applications," *IEEE Trans. Microw. Theory Tech.*, vol. 58, no. 7 PART 2, pp. 1933–1942, 2010, doi: 10.1109/TMTT.2010.2050103.

[15] Y. Zhang, W. Zhao, Y. Wang, T. Ren, and Y. Chen, "A 220 GHz subharmonic mixer based on schottky diodes with an accurate terahertz diode model," *Microw. Opt. Technol. Lett.*, vol. 58, no. 10, pp. 2311–2316, Oct. 2016, doi: https://doi.org/10.1002/mop.30032.

[16] H. Hamada *et al.*, "300-GHz 120-Gb/s Wireless Transceiver with High-Output-Power and High-Gain Power Amplifier Based on 80-nm InP-HEMT Technology," *2019 IEEE BiCMOS Compd. Semicond. Integr. Circuits Technol. Symp. BCICTS 2019*, pp. 2019–2022, 2019, doi: 10.1109/BCICTS45179.2019.8972756.

[17] H. Hamada *et al.*, "300-GHz. 100-Gb/s InP-HEMT Wireless Transceiver Using a 300-GHz Fundamental Mixer," *IEEE MTT-S Int. Microw. Symp. Dig.*, vol. 2018-June, pp. 1480–1483, 2018, doi: 10.1109/MWSYM.2018.8439850.

[18] L. Hou, S. Tang, B. Hou, and J. H. Marsh, “Photonic integrated circuits for terahertz source generation,” *IET Optoelectron.*, vol. 14, no. 3, pp. 136–142, 2020, doi: 10.1049/iet-opt.2019.0089.

[19] W. Lee *et al.*, “Coherent terahertz wireless communication using dual-parallel MZM-based silicon photonic integrated circuits,” *Opt. Express*, vol. 30, no. 2, p. 2547, 2022, doi: 10.1364/oe.446516.

[20] G. Carpintero *et al.*, “Photonic integrated circuits for terahertz communication: The hybrid integrated microwave photonic approach,” *Opt. InfoBase Conf. Pap.*, no. Mmi, pp. 6–7, 2021, doi: 10.1364/ofc.2021.f4f.4.

[21] T. Alam *et al.*, “Wideband, high-resolution terahertz spectroscopy by light-induced frequency tuning of quantum-cascade lasers,” *Opt. Express*, vol. 27, no. 4, p. 5420, 2019, doi: 10.1364/oe.27.005420.

[22] H. W. Hübers, H. Richter, and M. Wienold, “High-resolution terahertz spectroscopy with quantum-cascade lasers,” *J. Appl. Phys.*, vol. 125, no. 15, 2019, doi: 10.1063/1.5084105.

[23] T. Shiramizu *et al.*, “Feasibility Demonstration of THz Wave Generation/Modulation Based on Photomixing Using a Single Wavelength-Tunable Laser,” *Photonics*, vol. 10, no. 4, 2023, doi: 10.3390/photonics10040369.

[24] S. Preu, G. H. Dhler, S. Malzer, L. J. Wang, and A. C. Gossard, “Tunable, continuous-wave Terahertz photomixer sources and applications,” *J. Appl. Phys.*, vol. 109, no. 6, 2011, doi: 10.1063/1.3552291.

[25] K. Li *et al.*, “16-QAM Vector Terahertz-Wave Signal Generation by Simple MZM-Based Optical Frequency Comb,” *IEEE Photonics J.*, vol. 13, no. 1, 2021, doi: 10.1109/JPHOT.2020.3045058.

[26] K. Kondo, M. Che, and K. Kato, “Generation and Enhancement of Pulsed THz Waves by Arrayed UTC-PDs,” *OECC/PSC 2022 - 27th Optoelectron. Commun. Conf. Conf. Photonics Switch. Comput. 2022*, no. 2, pp. 1–4, 2022, doi: 10.23919/OECC/PSC53152.2022.9849992.

[27] E. Peytavit, G. Ducournau, and J. Lampin, “THz Photomixers,” 2021, pp. 137–186.

[28] A. Morales, G. I. Nazarikov, S. Rommel, C. Okonkwo, and I. T. Monroy, “All-Photonic Heterodyne sub-THz Wireless Transmission at 80 GHz, 120 GHz and 160 GHz Carrier Frequencies,” in *2020 45th International Conference on Infrared, Millimeter, and Terahertz Waves (IRMMW-THz)*, 2020, pp. 1–2, doi: 10.1109/IRMMW-THz46771.2020.9370506.

[29] E. García-Muñoz *et al.*, “Photonic-based integrated sources and antenna arrays for broadband wireless links in terahertz communications,” *Semicond. Sci. Technol.*, vol. 34, no. 5, 2019, doi: 10.1088/1361-6641/aaf8f2.

[30] H. Yang *et al.*, “A THz-OAM Wireless Communication System Based on Transmissive Metasurface,” *IEEE Trans. Antennas Propag.*, vol. 71, no. 5, pp. 1–1, 2023, doi: 10.1109/tap.2023.3255539.

[31] S. Carpenter *et al.*, “A D-Band 48-Gbit/s 64-QAM/QPSK Direct-Conversion I/Q Transceiver Chipset,” *IEEE Trans. Microw. Theory Tech.*, vol. 64, no. 4, pp. 1285–1296, 2016, doi: 10.1109/TMTT.2016.2533491.

[32] P. Torkaman *et al.*, “A 5G/Sub-Terahertz Heterogeneous Communication Network,” *IEEE Access*, vol. 10, pp. 65572–65584, 2022, doi: 10.1109/ACCESS.2022.3184312.

[33] M. Sawaby, N. Dolatsha, B. Grave, C. Chen, and A. Arbabian, “A fully packaged 130-GHz QPSK transmitter with an integrated PRBS generator,” *IEEE Solid-State Circuits Lett.*, vol. 1, no. 7, pp. 166–169, 2018, doi: 10.1109/LSSC.2019.2895571.

[34] E. F. Garay, D. J. Munzer, and H. Wang, “A 150 GHz Lens-Free Large FoV Regenerative 2 × 2 Transceiver Array With 31% DC-to-EIRP Efficiency and -70 dBm Sensitivity for a 70 cm Bidirectional Peer-to-Peer Link,” *IEEE J. Solid-State Circuits*, vol. 57, no. 7, pp. 2102–2113, 2022, doi: 10.1109/JSSC.2022.3149526.

[35] Y. Kim *et al.*, “150-GHz CMOS TX/RX with Digitally Predistorted PAM-4

Modulation for Terahertz Contactless/Plastic Waveguide Communications," *IEEE Trans. Terahertz Sci. Technol.*, vol. 10, no. 4, pp. 370–382, 2020, doi: 10.1109/TTHZ.2020.2991303.

[36] L. Chen, M. Taba, A. Cathelin, and E. Afshari, "A Low-Power 20Gb/s 196GHz BPSK Wireless Transmitter with Energy Efficiency FoM of 0.15pJ/bit/cm," *Proc. Cust. Integr. Circuits Conf.*, vol. 2023-April, pp. 1–2, 2023, doi: 10.1109/CICC57935.2023.10121306.

[37] P. Rodriguez-Vazquez, J. Grzyb, B. Heinemann, and U. R. Pfeiffer, "A QPSK 110-Gb/s Polarization-Diversity MIMO Wireless Link with a 220-255 GHz Tunable LO in a SiGe HBT Technology," *IEEE Trans. Microw. Theory Tech.*, vol. 68, no. 9, pp. 3834–3851, 2020, doi: 10.1109/TMTT.2020.2986196.

[38] J. Grzyb, P. R. Vazquez, N. Sarmah, B. Heinemann, and U. R. Pfeiffer, "A 240 GHz high-speed transmission link with highly-integrated transmitter and receiver modules in SiGe HBT technology," in *2017 42nd International Conference on Infrared, Millimeter, and Terahertz Waves (IRMMW-THz)*, 2017, pp. 1–2, doi: 10.1109/IRMMW-THz.2017.8066869.

[39] C. Wang, J. Yu, X. Li, P. Gou, and W. Zhou, "Fiber-THz-Fiber Link for THz Signal Transmission," *IEEE Photonics J.*, vol. 10, no. 2, pp. 1–6, 2018, doi: 10.1109/JPHOT.2018.2809433.

[40] T. Hagiwara *et al.*, "A 258-GHz CMOS Transmitter with Phase-Shifting Architecture for Phased-Array Systems," *IEEE MTT-S Int. Microw. Symp. Dig.*, vol. 2021-June, pp. 705–708, 2021, doi: 10.1109/IMS19712.2021.9574976.

[41] K. Takiguchi, "PAM4 wireless communication in 300 GHz-band using integrated-optic PAM signal emulator," *2022 Conf. Lasers Electro-Optics, CLEO 2022 - Proc.*, pp. 1–2, 2022, doi: 10.1364/cleo_si.2022.stu5l.7.

[42] A. Oshiro *et al.*, "PAM4 48-Gbit/s wireless communication using a resonant tunneling diode in the 300-GHz band," *IEICE Electron. Express*, vol. 19, no. 2, pp. 1–6, 2022, doi: 10.1587/elex.18.20210494.

[43] I. Abdo, H. Hamada, H. Nosaka, A. Shirane, and K. Okada, "64QAM wireless

link with 300 GHz InP-CMOS hybrid transceiver," *IEICE Electron. Express*, vol. 18, no. 17, pp. 1–4, 2021, doi: 10.1587/ELEX.18.20210314.

[44] K. Maekawa, Y. Kawamoto, T. Nakashita, and T. Yoshioka, "300-GHz-band Wireless Link Using Photonics-based Ultralow-noise Transmitter and Receiver," *2023 Opt. Fiber Commun. Conf. Exhib.*, pp. 15–17, 2023, doi: 10.23919/OFC49934.2023.10116279.

[45] D. Pirrone *et al.*, "Metasurface-Based Filters for High Data Rate THz Wireless Communication: Experimental Validation of a 14 Gbps OOK and 104 Gbps QAM-16 Wireless Link in the 300 GHz Band," *IEEE Trans. Wirel. Commun.*, vol. 21, no. 10, pp. 8688–8697, 2022, doi: 10.1109/TWC.2022.3168399.

[46] S. Nellen *et al.*, "Coherent Wireless Link at 300 GHz with 160 Gbit/s Enabled by a Photonic Transmitter," *J. Light. Technol.*, vol. 40, no. 13, pp. 4178–4185, 2022, doi: 10.1109/JLT.2022.3160096.

[47] L. Yi *et al.*, "300-GHz-band wireless communication using a low phase noise photonic source," in *2019 49th European Microwave Conference (EuMC)*, 2019, pp. 816–819, doi: 10.23919/EuMC.2019.8910724.

[48] M. Qiao *et al.*, "60 Gbit/s PAM-4 wireless transmission in the 310 GHz band with nonlinearity tolerant signal processing," *Opt. Commun.*, vol. 492, no. June 2020, p. 126988, 2021, doi: 10.1016/j.optcom.2021.126988.

[49] J. Shi *et al.*, "4096-QAM OFDM THz-over-fiber MIMO transmission using delta-sigma modulation," *IEEE Photonics Technol. Lett.*, vol. 35, no. 13, pp. 741–744, 2023, doi: 10.1109/LPT.2023.3271907.

[50] Y. Tan *et al.*, "Transmission of High-Frequency Terahertz Band Signal Beyond 300 GHz Over Metallic Hollow Core Fiber," *J. Light. Technol.*, vol. 40, no. 3, pp. 700–707, 2022, doi: 10.1109/JLT.2021.3123473.

[51] J. Ding *et al.*, "104-m Terahertz-Wave Wireless Transmission Employing 124.8-Gbit/s PS-256QAM Signal," *Opt. InfoBase Conf. Pap.*, vol. 1, no. c, pp. 1–3, 2022, doi: 10.1364/ofc.2022.m3c.3.

[52] S. Jia *et al.*, "120 Gb/s multi-channel THz wireless transmission and THz receiver performance analysis," *IEEE Photonics Technol. Lett.*, vol. 29, no. 3, pp. 310–313, 2017, doi: 10.1109/LPT.2016.2647280.

[53] X. Li *et al.*, "120 Gb/s wireless terahertz-wave signal delivery by 375 GHz-500 GHz multi-carrier in a 2 × 2 MIMO system," *J. Light. Technol.*, vol. 37, no. 2, pp. 606–611, 2019, doi: 10.1109/JLT.2018.2862356.

[54] M. Zhao, W. Zhou, and J. Yu, "3.5 Gbit/s OOK THz signal delivery over 88 cm free-space at 441.504 GHz," *Microw. Opt. Technol. Lett.*, vol. 60, no. 6, pp. 1435–1439, 2018, doi: 10.1002/mop.31176.

[55] X. Li, J. Yu, K. Wang, W. Zhou, and J. Zhang, "Photonics-aided 2 × 2 MIMO wireless terahertz-wave signal transmission system with optical polarization multiplexing," *Opt. Express*, vol. 25, no. 26, p. 33236, 2017, doi: 10.1364/oe.25.033236.

[56] X. Li *et al.*, "132-Gb/s photonics-aided single-carrier wireless terahertz-wave signal transmission at 450GHz enabled by 64QAM modulation and probabilistic shaping," *Opt. InfoBase Conf. Pap.*, vol. Part F160-, pp. 10–12, 2019.

[57] X. Liu *et al.*, "Demonstration of 144-Gbps Photonics-Assisted THz Wireless Transmission at 500 GHz Enabled by Joint DBN Equalizer," *Micromachines*, vol. 13, no. 10, 2022, doi: 10.3390/mi13101617.

[58] Y. Yoshimizu, S. Hisatake, S. Kuwano, J. Terada, N. Yoshimoto, and T. Nagatsuma, "Wireless transmission using coherent terahertz wave with phase stabilization," *IEICE Electron. Express*, pp. 10–20130578, 2013.

[59] L. Gonzalez-Guerrero and G. Carpintero, "Coherent photonic Terahertz transmitters compatible with direct comb modulation," *Sci. Rep.*, vol. 12, no. 1, pp. 1–10, 2022, doi: 10.1038/s41598-022-13618-y.

[60] K. Sakuma *et al.*, "First demonstration of Mach-Zehnder-interferometric phase-stabilization at optoelectronic carrier generation for phase-shift keying signal," *2015 Opto-Electronics Commun. Conf. OECC 2015*, pp. 1–3, 2015, doi:

10.1109/OECC.2015.7340086.

[61] S. Takeuchi, K. Kato, Y. Yoshimizu, Y. Yasuda, S. Hisatake, and T. Nagatsuma, “Coherent sub-THz carrier frequency transmission with novel pseudo-Mach-Zehnder interferometric phase stabilization,” in *Microwave Photonics (MWP) and the 2014 9th Asia-Pacific Microwave Photonics Conference (APMP) 2014 International Topical Meeting on*, Oct. 2014, pp. 208–210, doi: 10.1109/MWP.2014.6994532.

[62] S. Takeuchi *et al.*, “Novel lightwave-interferometric phase detection for phase stabilization of two-tone coherent millimeter-wave/microwave carrier generation,” *IEICE Trans. Electron.*, vol. E99C, no. 9, pp. 1048–1055, 2016, doi: 10.1587/transele.E99.C.1048.

[63] M.-C. Lo *et al.*, “Foundry-fabricated dual-DFB PIC injection-locked to optical frequency comb for high-purity THz generation,” in *Optical Fiber Communication Conference*, 2019, pp. W1B-3.

[64] G. K. M. Hasanuzzaman, H. Shams, C. C. Renaud, J. Mitchell, and S. Iezekiel, “Photonic THz Generation using Optoelectronic Oscillator-driven Optical Frequency Comb Generator,” in *2018 International Topical Meeting on Microwave Photonics (MWP)*, 2018, pp. 1–4, doi: 10.1109/MWP.2018.8552892.

[65] T. Nagatsuma *et al.*, “Terahertz wireless communications based on photonics technologies,” *Opt. Express*, vol. 21, no. 20, pp. 23736–23747, Oct. 2013, doi: 10.1364/OE.21.023736.

[66] S. Takeuchi *et al.*, “Novel lightwave-interferometric phase detection for phase stabilization of two-tone coherent millimeter-wave/microwave carrier generation,” *IEICE Trans. Electron.*, vol. E99C, no. 9, pp. 1048–1055, 2016, doi: 10.1587/transele.E99.C.1048.

[67] Y. Ma, L. Stewart, J. Armstrong, I. G. Clarke, and G. Baxter, “Recent progress of wavelength selective switch,” *J. Light. Technol.*, vol. 39, no. 4, pp. 896–903, 2020.

[68] A. A. Ibrahim, T. Shiramizu, S. Ye, Y. Mikami, and K. Kato, “Pilot-Lightwave-based Terahertz Wave Phase Stabilization,” *Conf. Dig. - IEEE Int. Semicond. Laser Conf.*, vol. 2022-Octob, no. Ld, pp. 2022–2023, 2022, doi: 10.23919/ISLC52947.2022.9943347.

[69] T. Shiramizu, A. A. Ibrahim, S. Ye, Y. Mikami, and K. Kato, “Photonic Phase Stabilization Control System for Terahertz-Wave Phase Modulation,” in *2022 27th OptoElectronics and Communications Conference (OECC) and 2022 International Conference on Photonics in Switching and Computing (PSC)*, 2022, pp. 1–4, doi: 10.23919/OECC/PSC53152.2022.9850107.

[70] A. A. Ibrahim, H. Chen, T. Shiramizu, Y. Mikami, and K. Kato, “Terahertz-Wave Phase Modulation Enabled by Optical Interferometric Phase Stabilization,” in *2022 Asia-Pacific Microwave Conference (APMC)*, Nov. 2022, pp. 943–945.

CHAPTER 4
GENERATING AND DETECTING STABILIZED PHASE MODULATED THZ WAVE

4.1 Introduction

This chapter explore the implementation of phase stabilization techniques in a THz-wave PM generation and transmission setup. The experiment involves comparing both a backward direction phase stabilization system and a forward-direction phase stabilization system in the primary experiment while in the preliminary experiment only focus on the backward direction phase stabilization system only. The configuration is divided into two parts: the transmitter part, $T_{X,}$ where the THz wave is generated through photomixing using two different lightwaves, and the receiver part, $R_{X,}$ where the detected THz wave is down-converted and observed.

The purpose of this setup is to demonstrate the practical application of the phase stabilization system in an actual THz generation setup. It is begun with presented the configuration of the experimental THz generation setup, applying a phase stabilization system with the forward-direction and backward-direction pilot lightwaves. A detailed explanation of the experimental setup is provided, highlighting the components used for the photomixing and phase stabilization system. Additionally, the detected signal of the phase-modulated THz wave is investigated. Here, the experimental details that validate the effectiveness of the phase stabilization technique in the context of THz-wave PM generation is presented. Through this analysis, the aim is to contribute to the understanding and optimization of phase stabilization methods for PM THz wave applications.

4.2 Experimental Setup

4.2.1 THz-wave Generation System with Forward-direction Phase Stabilization System

Figure 4.1 illustrates the THz wave PM system equipped with a forward-direction phase stabilization system. The T_X initiates the process by introducing a single lightwave at a frequency of 193.4 THz from a laser diode (LD) on the left side of the configuration. An optical frequency comb generator (OFCG) generates a frequency comb with equally spaced spectral lines of 25GHz gap, allowing us to output specific optical frequencies with a 300 GHz difference at the Wavelength Selective Switch (WSS). In the upper path, the lightwave (red arrow) undergoes phase modulation using the optical phase modulator (PM) at different modulation bit rates, employing a return-to-zero (RZ) continuous signal from the pulse pattern generator (PPG). In the lower path (green arrow), the lightwave passes through the phase shifter (PS). The lightwaves from these two paths are combined at the optical coupler (OC), amplified, and directed to a uni-traveling carrier photodiode (UTC-PD) acting as a photomixer.

The input and output power of the THz wave generation system can be observed in figure. It shows that the output power of f_1 is -9.2 dBm while the f_2 is -10.2 dBm. Achieving power balance is crucial to ensure that both signals contribute equally to the mixing process. Despite the power differences between these two frequencies, as depicted in the graph, it is important to note that both frequencies have almost the same output power. This is because f_1 has undergone modulation, resulting in the total output power being equivalent to that of f_2. Consequently, the UTC-PD generates the phase-modulated THz wave, which is transmitted through the WR3.4 waveguide. As the carrier frequency of the THz signal is determined by the frequency difference between the lightwave, the output of the UTC-PD is radiated 300 GHz wave of 1, 5 and 10 Gbit/s Binary Phase Shift Keying (BPSK) signals.

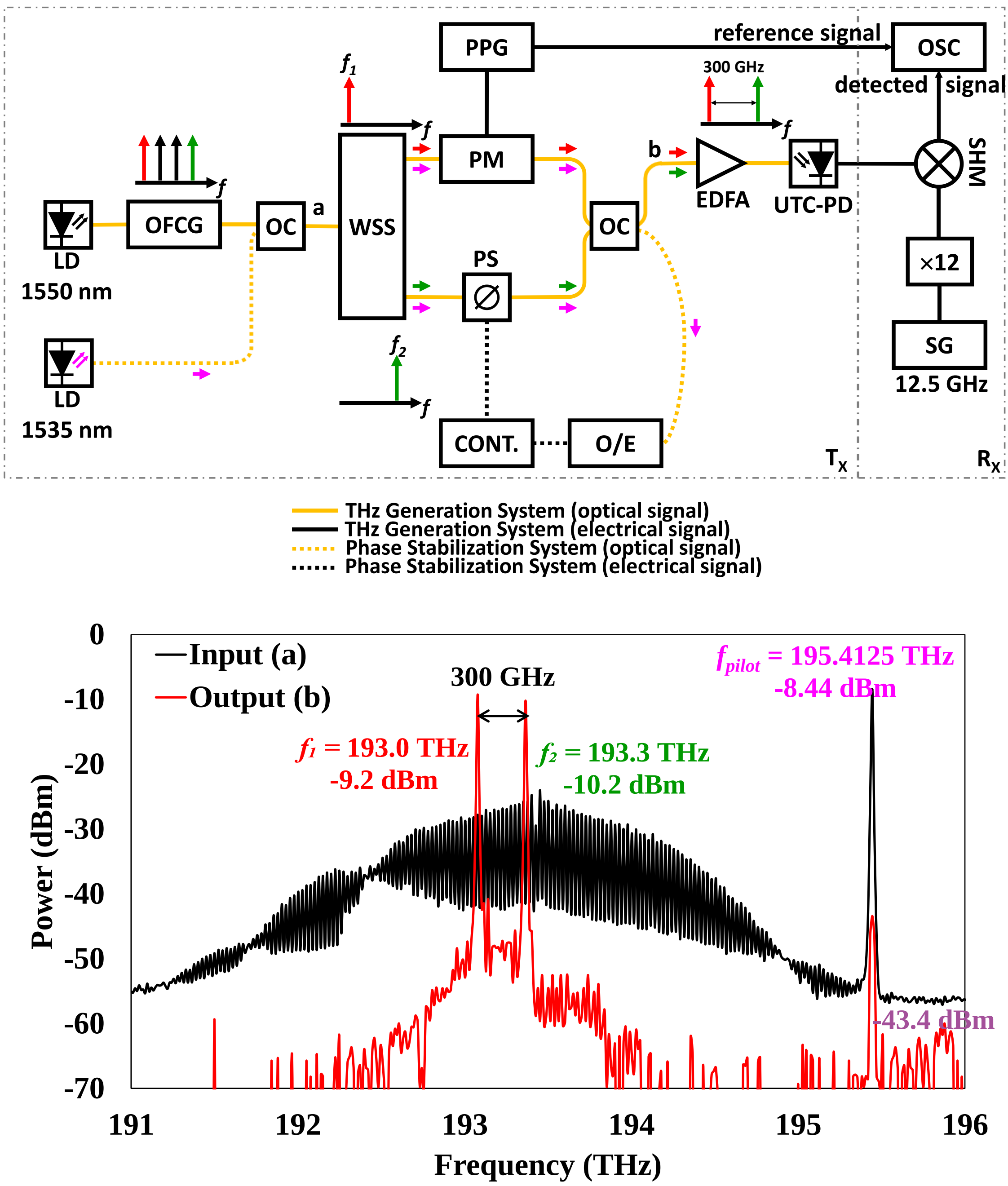

Figure 4.1 Experimental setup of THz wave generation system with forward-direction pilot lightwave and the graph of input and output lightwave of THz wave generation system

At the R_X, a sub-harmonic mixer (SHM) is utilized to down-convert the received THz wave by a local oscillator (LO). The LO, with a frequency of 12.5 GHz from the signal generator (SG), is first multiplied by 12 using an electrical multiplier and then further multiplied by 2 with the built-in multiplier in the SHM, resulting in a total LO frequency of 300 GHz. This LO signal is also synchronized with the signal generator of the OFCG at the transmitter, enabling the implementation of homodyne detection. The resulting waveform is observed on an oscilloscope (OSC).

In the phase stabilization system (dotted line), a pilot lightwave from a laser (pink arrow) with an optical frequency of 195.4125 THz is being introduced to the THz-wave generation system. The pilot lightwave power at the input of the THz wave generation system is -8.44 dBm and at the output is -43.4 dBm which can be negligible, as shown in the figure. This pilot lightwave is then split and directed through the upper path involving the PM and the lower path involving a PS. These lightwaves interfere after coupling at the optical coupler (OC), and the interference intensity is detected by an optical-to-electrical (O/E) converter. The resulting converted voltage is then read by a feedback controller, which maintains a constant interference intensity by controlling the phase shifter (PS).

4.2.2 THz-wave Generation System with Backward-direction Phase Stabilization System

Figure 4.2 depicts the THz wave PM system with the backward-direction phase stabilization system. This configuration utilizes the lightwave in a manner similar to the forward-direction pilot lightwave system. This time, the output power of f1 is -9.24 dBm while the f2 is -10.24 dBm as shown in the same figure. Moving on to the phase stabilization system, a pilot lightwave that originates from a laser diode is introduced from the right side of the THz wave PM system. The internal reflection at the OC is causing for the detection of the pilot lightwave at the output of the THz generation setup, but the power level is significantly low, measuring at -45.83 dBm. The pilot lightwave (light blue arrow) is split and then directed through the upper path involving the PM and the lower path involving the PS in a backward direction. These lightwaves interfere after passing through the WSS in reverse. Due to the absence of phase modulation in the backward-direction pilot lightwave at bit rates of 3 Gbit/s and higher, efficient interference is anticipated. The interference intensity is detected using an O/E converter, and the resulting voltage is read by a feedback controller responsible for maintaining a constant interference intensity by controlling the PS.

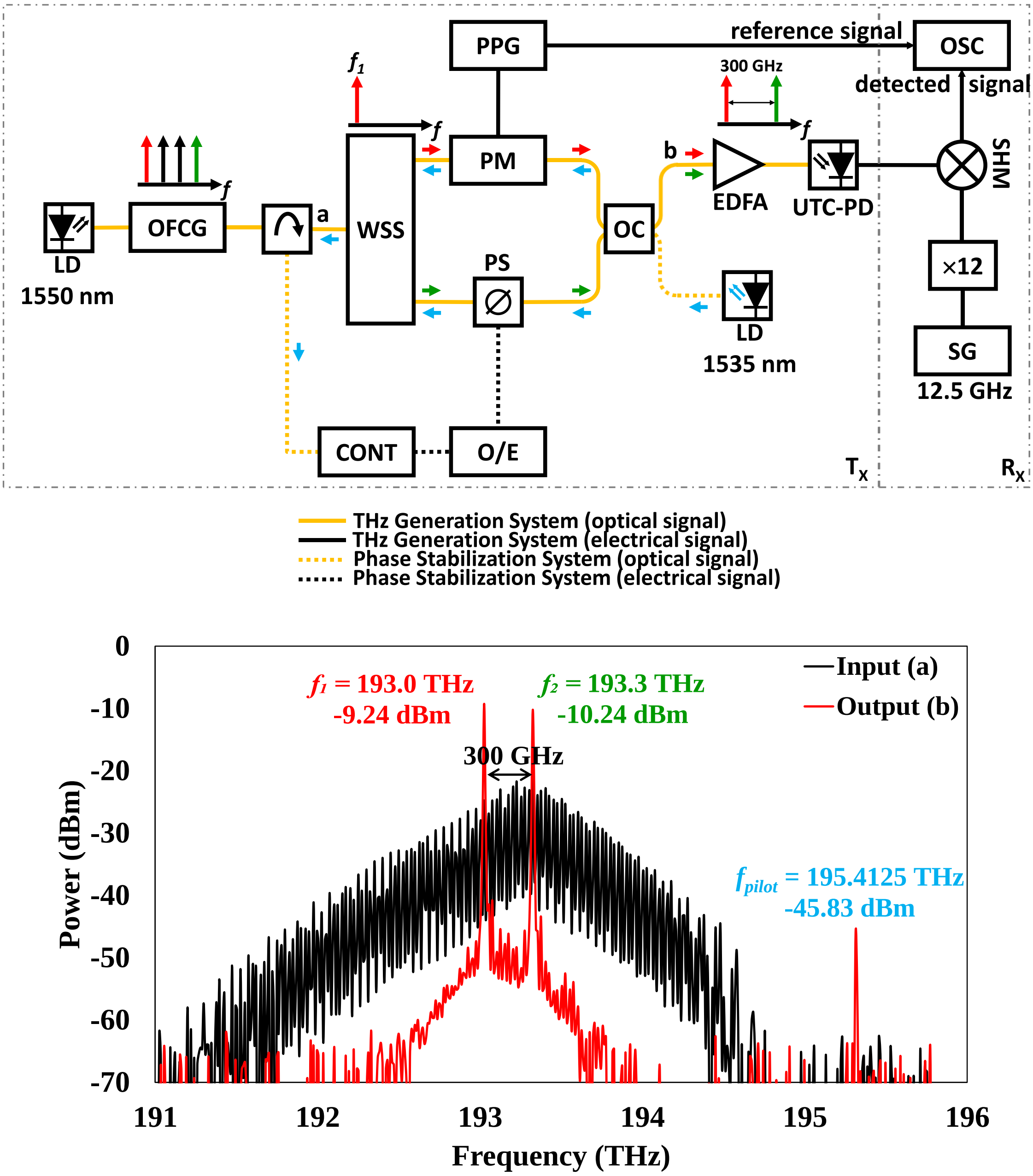

Figure 4.2 Experimental setup of THz wave generation system with backward-direction pilot lightwave and the graph of input and output lightwave of THz wave generation system

4.3 Detected Signal of Phase Modulated THz wave

The experiment then proceeded with the transmission of the phase-modulated 300-GHz wave and detected it using a sub-harmonic mixer equipped with a 300-GHz LO signal, employing coherent detection. Figure 4.3 presents the detected waveform (orange) alongside the initial modulation pattern generated by the PPG (black) for the phase-modulated THz wave generation system. Both forward-direction and backward-direction phase stabilization systems were represented in Figure 4.3 and Figure 4.4 respectively. The results demonstrate that the forward-direction phase stabilization system does not yield a distinct and continuous data pattern in the detected data signal. In contrast, the backward-direction phase stabilization system exhibits a noticeable and continuous data pattern at bit rates of 5 and 10 Gbit/s. The lower bit rate of 1 Gbit/s does not exhibit the same level of behaviour. These experimental findings corroborate our previously established theoretical results.

These observations provide valuable insights into the performance and limitations of the forward-direction and backward-direction phase stabilization systems in the context of phase-modulated THz wave transmission. The lack of a clear and continuous data pattern with the forward-direction system suggests potential

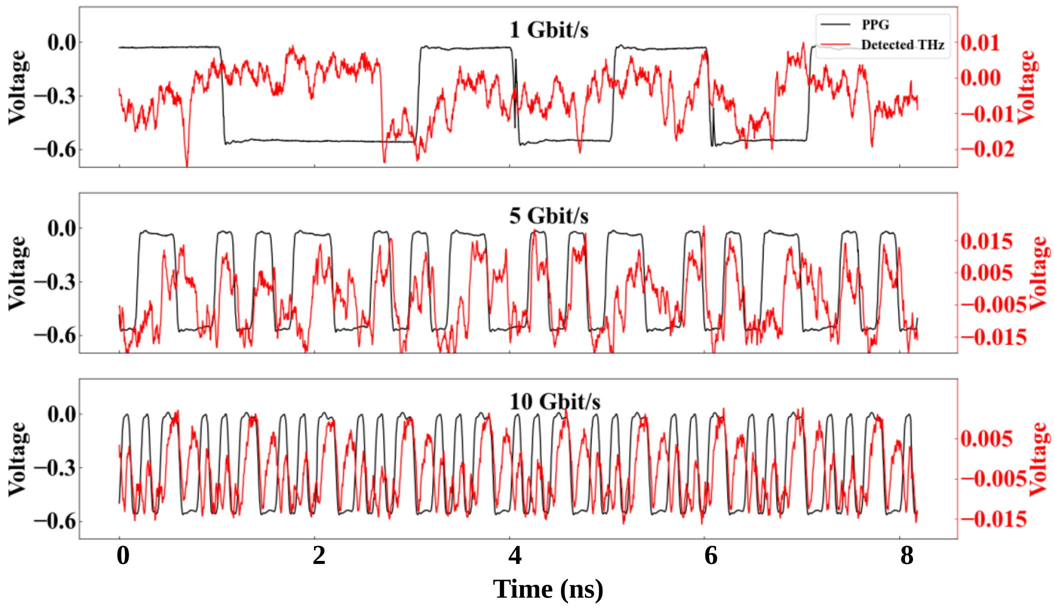

Figure 4.3 Detected waveform phase-modulated THz signal with forward-direction phase stabilization system at 1, 5 and 10 Gbit/s

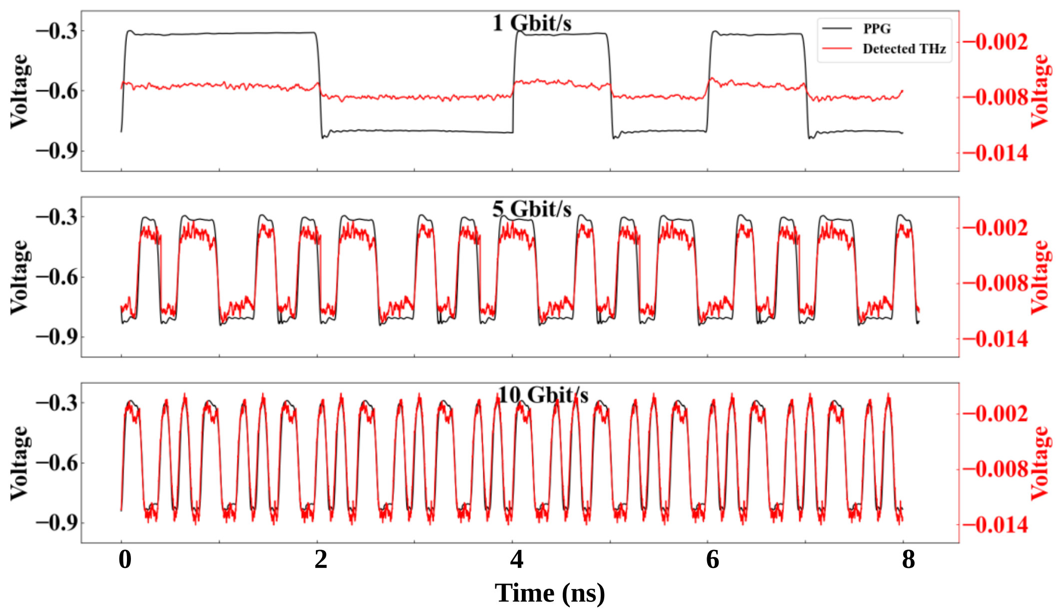

Figure 4.4 Detected waveform phase-modulated THz signal backward-direction pilot stabilization system at 1, 5 and 10 Gbit/s

challenges in achieving stable and reliable data transmission at higher bit rates. Conversely, the promising results obtained with the backward-direction system indicate its potential for supporting high-speed data transmission. These findings contribute to the efforts in optimizing and enhancing the stability and reliability of phase-modulated THz wave communication systems.

4.4 Conclusion of This Chapter

In conclusion, this research has successfully developed and compared a phase stabilization system for THz wave phase modulation using photomixing, employing both forward-direction and backward-direction approaches. The findings of this study highlight the effectiveness of the backward-direction phase stabilization method in achieving stable phase fluctuations between the two lightwaves while eliminating the impact of environmental disturbances. As a result, a stable 300-GHz phase-modulated wave is generated and transmitted at a bit rate of beyond 3 Gbit/s using the constructed system [70].

REFERENCES

[1] I. Cisco Systems, “Cisco Visual Networking Index: Forecast and Trends, 2017–2022 White Paper,” *Cisco Forecast Methodol.*, pp. 2017–2022, 2019.

[2] S. Cherry, “Edholm’s law of bandwidth,” *IEEE Spectr.*, vol. 41, no. 7, p. 50, 2004.

[3] E. W. Paper, “6G spectrum - enabling the future mobile life beyond 2030,” no. March, 2023.

[4] Z. Li *et al.*, “Terahertz band range adjustable hyperbolic metamaterial refractive index sensor,” *Results Phys.*, vol. 49, no. April, p. 106477, 2023, doi: 10.1016/j.rinp.2023.106477.

[5] K. Tekbıyık, A. R. Ekti, G. K. Kurt, and A. Görçin, “Terahertz band communication systems: Challenges, novelties and standardization efforts,” *Phys. Commun.*, vol. 35, p. 100700, 2019, doi: 10.1016/j.phycom.2019.04.014.

[6] W. Hao, F. Zhou, M. Zeng, O. A. Dobre, and N. Al-Dhahir, “Ultra Wideband THz IRS Communications: Applications, Challenges, Key Techniques, and Research Opportunities,” *IEEE Netw.*, vol. 36, no. 6, pp. 214–220, 2022, doi: 10.1109/MNET.110.2100664.

[7] A. B. Belguidoum, M. L. Tounsi, and S. Mekaoui, “Analysis of 5G Radio Parameters and their Impact on the Peak Data Rate,” *Proc. - 2019 3rd Eur. Conf. Electr. Eng. Comput. Sci. EECS 2019*, pp. 66–71, 2019, doi: 10.1109/EECS49779.2019.00025.

[8] T. Nagatsuma, G. Ducournau, and C. C. Renaud, “Advances in terahertz communications accelerated by photonics,” *Nat. Photonics*, vol. 10, no. 6, pp. 371–379, 2016, doi: 10.1038/nphoton.2016.65.

[9] J. Yao and J. Capmany, “Microwave photonics,” *Sci. China Inf. Sci.*, vol. 65, no. 12, pp. 314–335, 2022, doi: 10.1007/s11432-021-3524-0.

[10] H. G. Yu, S. H. Choi, S. Jeon, and M. Kim, “300 GHz InP HBT amplifier with 10 mW output power,” *Electron. Lett.*, vol. 50, no. 5, pp. 377–379, 2014, doi: 10.1049/el.2013.3288.

[11] M. Seo *et al.*, “InP HBT IC technology for terahertz frequencies: Fundamental oscillators Up to 0.57 THz,” *IEEE J. Solid-State Circuits*, vol. 46, no. 10, pp. 2203–2214, 2011, doi: 10.1109/JSSC.2011.2163213.

[12] S. H. Kim, T. H. Jang, D. M. Kang, and C. S. Park, “A 120 GHz Wideband CMOS I/Q Transmitter for Short-Range Wireless Device-to-Device Communication,” *Asia-Pacific Microw. Conf. Proceedings, APMC*, vol. 2020-Decem, pp. 39–41, 2020, doi: 10.1109/APMC47863.2020.9331594.

[13] T. A. Vu and M. Fujishima, “A 300 GHz CMOS transmitter front-end for ultrahigh-speed wireless communications,” *Int. J. Electr. Comput. Eng.*, vol. 7, no. 4, pp. 2278–2286, 2017, doi: 10.11591/ijece.v7i4.pp2278-2286.

[14] J. V. Siles and J. Grajal, “Physics-based design and optimization of Schottky diode frequency multipliers for terahertz applications,” *IEEE Trans. Microw. Theory Tech.*, vol. 58, no. 7 PART 2, pp. 1933–1942, 2010, doi: 10.1109/TMTT.2010.2050103.

[15] Y. Zhang, W. Zhao, Y. Wang, T. Ren, and Y. Chen, “A 220 GHz subharmonic mixer based on schottky diodes with an accurate terahertz diode model,” *Microw. Opt. Technol. Lett.*, vol. 58, no. 10, pp. 2311–2316, Oct. 2016, doi: https://doi.org/10.1002/mop.30032.

[16] H. Hamada *et al.*, “300-GHz 120-Gb/s Wireless Transceiver with High-Output-Power and High-Gain Power Amplifier Based on 80-nm InP-HEMT Technology,” *2019 IEEE BiCMOS Compd. Semicond. Integr. Circuits Technol. Symp. BCICTS 2019*, pp. 2019–2022, 2019, doi: 10.1109/BCICTS45179.2019.8972756.

[17] H. Hamada *et al.*, “300-GHz. 100-Gb/s InP-HEMT Wireless Transceiver Using a 300-GHz Fundamental Mixer,” *IEEE MTT-S Int. Microw. Symp. Dig.*, vol. 2018-June, pp. 1480–1483, 2018, doi: 10.1109/MWSYM.2018.8439850.

[18] L. Hou, S. Tang, B. Hou, and J. H. Marsh, “Photonic integrated circuits for terahertz source generation,” *IET Optoelectron.*, vol. 14, no. 3, pp. 136–142, 2020, doi: 10.1049/iet-opt.2019.0089.

[19] W. Lee *et al.*, “Coherent terahertz wireless communication using dual-parallel MZM-based silicon photonic integrated circuits,” *Opt. Express*, vol. 30, no. 2, p. 2547, 2022, doi: 10.1364/oe.446516.

[20] G. Carpintero *et al.*, “Photonic integrated circuits for terahertz communication: The hybrid integrated microwave photonic approach,” *Opt. InfoBase Conf. Pap.*, no. Mmi, pp. 6–7, 2021, doi: 10.1364/ofc.2021.f4f.4.

[21] T. Alam *et al.*, “Wideband, high-resolution terahertz spectroscopy by light-induced frequency tuning of quantum-cascade lasers,” *Opt. Express*, vol. 27, no. 4, p. 5420, 2019, doi: 10.1364/oe.27.005420.

[22] H. W. Hübers, H. Richter, and M. Wienold, “High-resolution terahertz spectroscopy with quantum-cascade lasers,” *J. Appl. Phys.*, vol. 125, no. 15, 2019, doi: 10.1063/1.5084105.

[23] T. Shiramizu *et al.*, “Feasibility Demonstration of THz Wave Generation/Modulation Based on Photomixing Using a Single Wavelength-Tunable Laser,” *Photonics*, vol. 10, no. 4, 2023, doi: 10.3390/photonics10040369.

[24] S. Preu, G. H. Dhler, S. Malzer, L. J. Wang, and A. C. Gossard, “Tunable, continuous-wave Terahertz photomixer sources and applications,” *J. Appl. Phys.*, vol. 109, no. 6, 2011, doi: 10.1063/1.3552291.

[25] K. Li *et al.*, “16-QAM Vector Terahertz-Wave Signal Generation by Simple MZM-Based Optical Frequency Comb,” *IEEE Photonics J.*, vol. 13, no. 1, 2021, doi: 10.1109/JPHOT.2020.3045058.

[26] K. Kondo, M. Che, and K. Kato, “Generation and Enhancement of Pulsed THz Waves by Arrayed UTC-PDs,” *OECC/PSC 2022 - 27th Optoelectron. Commun. Conf. Conf. Photonics Switch. Comput. 2022*, no. 2, pp. 1–4, 2022, doi: 10.23919/OECC/PSC53152.2022.9849992.

[27] E. Peytavit, G. Ducournau, and J. Lampin, “THz Photomixers,” 2021, pp. 137–186.

[28] A. Morales, G. I. Nazarikov, S. Rommel, C. Okonkwo, and I. T. Monroy, “All-Photonic Heterodyne sub-THz Wireless Transmission at 80 GHz, 120 GHz and 160 GHz Carrier Frequencies,” in *2020 45th International Conference on Infrared, Millimeter, and Terahertz Waves (IRMMW-THz)*, 2020, pp. 1–2, doi: 10.1109/IRMMW-THz46771.2020.9370506.

[29] E. García-Muñoz *et al.*, “Photonic-based integrated sources and antenna arrays for broadband wireless links in terahertz communications,” *Semicond. Sci. Technol.*, vol. 34, no. 5, 2019, doi: 10.1088/1361-6641/aaf8f2.

[30] H. Yang *et al.*, “A THz-OAM Wireless Communication System Based on Transmissive Metasurface,” *IEEE Trans. Antennas Propag.*, vol. 71, no. 5, pp. 1–1, 2023, doi: 10.1109/tap.2023.3255539.

[31] S. Carpenter *et al.*, “A D-Band 48-Gbit/s 64-QAM/QPSK Direct-Conversion I/Q Transceiver Chipset,” *IEEE Trans. Microw. Theory Tech.*, vol. 64, no. 4, pp. 1285–1296, 2016, doi: 10.1109/TMTT.2016.2533491.

[32] P. Torkaman *et al.*, “A 5G/Sub-Terahertz Heterogeneous Communication Network,” *IEEE Access*, vol. 10, pp. 65572–65584, 2022, doi: 10.1109/ACCESS.2022.3184312.

[33] M. Sawaby, N. Dolatsha, B. Grave, C. Chen, and A. Arbabian, “A fully packaged 130-GHz QPSK transmitter with an integrated PRBS generator,” *IEEE Solid-State Circuits Lett.*, vol. 1, no. 7, pp. 166–169, 2018, doi: 10.1109/LSSC.2019.2895571.

[34] E. F. Garay, D. J. Munzer, and H. Wang, “A 150 GHz Lens-Free Large FoV Regenerative 2 × 2 Transceiver Array With 31% DC-to-EIRP Efficiency and -70 dBm Sensitivity for a 70 cm Bidirectional Peer-to-Peer Link,” *IEEE J. Solid-State Circuits*, vol. 57, no. 7, pp. 2102–2113, 2022, doi: 10.1109/JSSC.2022.3149526.

[35] Y. Kim *et al.*, “150-GHz CMOS TX/RX with Digitally Predistorted PAM-4

Modulation for Terahertz Contactless/Plastic Waveguide Communications," *IEEE Trans. Terahertz Sci. Technol.*, vol. 10, no. 4, pp. 370–382, 2020, doi: 10.1109/TTHZ.2020.2991303.

[36] L. Chen, M. Taba, A. Cathelin, and E. Afshari, "A Low-Power 20Gb/s 196GHz BPSK Wireless Transmitter with Energy Efficiency FoM of 0.15pJ/bit/cm," *Proc. Cust. Integr. Circuits Conf.*, vol. 2023-April, pp. 1–2, 2023, doi: 10.1109/CICC57935.2023.10121306.

[37] P. Rodriguez-Vazquez, J. Grzyb, B. Heinemann, and U. R. Pfeiffer, "A QPSK 110-Gb/s Polarization-Diversity MIMO Wireless Link with a 220-255 GHz Tunable LO in a SiGe HBT Technology," *IEEE Trans. Microw. Theory Tech.*, vol. 68, no. 9, pp. 3834–3851, 2020, doi: 10.1109/TMTT.2020.2986196.

[38] J. Grzyb, P. R. Vazquez, N. Sarmah, B. Heinemann, and U. R. Pfeiffer, "A 240 GHz high-speed transmission link with highly-integrated transmitter and receiver modules in SiGe HBT technology," in *2017 42nd International Conference on Infrared, Millimeter, and Terahertz Waves (IRMMW-THz)*, 2017, pp. 1–2, doi: 10.1109/IRMMW-THz.2017.8066869.

[39] C. Wang, J. Yu, X. Li, P. Gou, and W. Zhou, "Fiber-THz-Fiber Link for THz Signal Transmission," *IEEE Photonics J.*, vol. 10, no. 2, pp. 1–6, 2018, doi: 10.1109/JPHOT.2018.2809433.

[40] T. Hagiwara *et al.*, "A 258-GHz CMOS Transmitter with Phase-Shifting Architecture for Phased-Array Systems," *IEEE MTT-S Int. Microw. Symp. Dig.*, vol. 2021-June, pp. 705–708, 2021, doi: 10.1109/IMS19712.2021.9574976.

[41] K. Takiguchi, "PAM4 wireless communication in 300 GHz-band using integrated-optic PAM signal emulator," *2022 Conf. Lasers Electro-Optics, CLEO 2022 - Proc.*, pp. 1–2, 2022, doi: 10.1364/cleo_si.2022.stu5l.7.

[42] A. Oshiro *et al.*, "PAM4 48-Gbit/s wireless communication using a resonant tunneling diode in the 300-GHz band," *IEICE Electron. Express*, vol. 19, no. 2, pp. 1–6, 2022, doi: 10.1587/elex.18.20210494.

[43] I. Abdo, H. Hamada, H. Nosaka, A. Shirane, and K. Okada, "64QAM wireless

link with 300 GHz InP-CMOS hybrid transceiver," *IEICE Electron. Express*, vol. 18, no. 17, pp. 1–4, 2021, doi: 10.1587/ELEX.18.20210314.

[44] K. Maekawa, Y. Kawamoto, T. Nakashita, and T. Yoshioka, "300-GHz-band Wireless Link Using Photonics-based Ultralow-noise Transmitter and Receiver," *2023 Opt. Fiber Commun. Conf. Exhib.*, pp. 15–17, 2023, doi: 10.23919/OFC49934.2023.10116279.

[45] D. Pirrone *et al.*, "Metasurface-Based Filters for High Data Rate THz Wireless Communication: Experimental Validation of a 14 Gbps OOK and 104 Gbps QAM-16 Wireless Link in the 300 GHz Band," *IEEE Trans. Wirel. Commun.*, vol. 21, no. 10, pp. 8688–8697, 2022, doi: 10.1109/TWC.2022.3168399.

[46] S. Nellen *et al.*, "Coherent Wireless Link at 300 GHz with 160 Gbit/s Enabled by a Photonic Transmitter," *J. Light. Technol.*, vol. 40, no. 13, pp. 4178–4185, 2022, doi: 10.1109/JLT.2022.3160096.

[47] L. Yi *et al.*, "300-GHz-band wireless communication using a low phase noise photonic source," in *2019 49th European Microwave Conference (EuMC)*, 2019, pp. 816–819, doi: 10.23919/EuMC.2019.8910724.

[48] M. Qiao *et al.*, "60 Gbit/s PAM-4 wireless transmission in the 310 GHz band with nonlinearity tolerant signal processing," *Opt. Commun.*, vol. 492, no. June 2020, p. 126988, 2021, doi: 10.1016/j.optcom.2021.126988.

[49] J. Shi *et al.*, "4096-QAM OFDM THz-over-fiber MIMO transmission using delta-sigma modulation," *IEEE Photonics Technol. Lett.*, vol. 35, no. 13, pp. 741–744, 2023, doi: 10.1109/LPT.2023.3271907.

[50] Y. Tan *et al.*, "Transmission of High-Frequency Terahertz Band Signal Beyond 300 GHz Over Metallic Hollow Core Fiber," *J. Light. Technol.*, vol. 40, no. 3, pp. 700–707, 2022, doi: 10.1109/JLT.2021.3123473.

[51] J. Ding *et al.*, "104-m Terahertz-Wave Wireless Transmission Employing 124.8-Gbit/s PS-256QAM Signal," *Opt. InfoBase Conf. Pap.*, vol. 1, no. c, pp. 1–3, 2022, doi: 10.1364/ofc.2022.m3c.3.

[52] S. Jia *et al.*, “120 Gb/s multi-channel THz wireless transmission and THz receiver performance analysis,” *IEEE Photonics Technol. Lett.*, vol. 29, no. 3, pp. 310–313, 2017, doi: 10.1109/LPT.2016.2647280.

[53] X. Li *et al.*, “120 Gb/s wireless terahertz-wave signal delivery by 375 GHz-500 GHz multi-carrier in a 2 × 2 MIMO system,” *J. Light. Technol.*, vol. 37, no. 2, pp. 606–611, 2019, doi: 10.1109/JLT.2018.2862356.

[54] M. Zhao, W. Zhou, and J. Yu, “3.5 Gbit/s OOK THz signal delivery over 88 cm free-space at 441.504 GHz,” *Microw. Opt. Technol. Lett.*, vol. 60, no. 6, pp. 1435–1439, 2018, doi: 10.1002/mop.31176.

[55] X. Li, J. Yu, K. Wang, W. Zhou, and J. Zhang, “Photonics-aided 2 × 2 MIMO wireless terahertz-wave signal transmission system with optical polarization multiplexing,” *Opt. Express*, vol. 25, no. 26, p. 33236, 2017, doi: 10.1364/oe.25.033236.

[56] X. Li *et al.*, “132-Gb/s photonics-aided single-carrier wireless terahertz-wave signal transmission at 450GHz enabled by 64QAM modulation and probabilistic shaping,” *Opt. InfoBase Conf. Pap.*, vol. Part F160-, pp. 10–12, 2019.

[57] X. Liu *et al.*, “Demonstration of 144-Gbps Photonics-Assisted THz Wireless Transmission at 500 GHz Enabled by Joint DBN Equalizer,” *Micromachines*, vol. 13, no. 10, 2022, doi: 10.3390/mi13101617.

[58] Y. Yoshimizu, S. Hisatake, S. Kuwano, J. Terada, N. Yoshimoto, and T. Nagatsuma, “Wireless transmission using coherent terahertz wave with phase stabilization,” *IEICE Electron. Express*, pp. 10–20130578, 2013.

[59] L. Gonzalez-Guerrero and G. Carpintero, “Coherent photonic Terahertz transmitters compatible with direct comb modulation,” *Sci. Rep.*, vol. 12, no. 1, pp. 1–10, 2022, doi: 10.1038/s41598-022-13618-y.

[60] K. Sakuma *et al.*, “First demonstration of Mach-Zehnder-interferometric phase-stabilization at optoelectronic carrier generation for phase-shift keying signal,” *2015 Opto-Electronics Commun. Conf. OECC 2015*, pp. 1–3, 2015, doi:

10.1109/OECC.2015.7340086.

[61] S. Takeuchi, K. Kato, Y. Yoshimizu, Y. Yasuda, S. Hisatake, and T. Nagatsuma, “Coherent sub-THz carrier frequency transmission with novel pseudo-Mach-Zehnder interferometric phase stabilization,” in *Microwave Photonics (MWP) and the 2014 9th Asia-Pacific Microwave Photonics Conference (APMP) 2014 International Topical Meeting on*, Oct. 2014, pp. 208–210, doi: 10.1109/MWP.2014.6994532.

[62] S. Takeuchi *et al.*, “Novel lightwave-interferometric phase detection for phase stabilization of two-tone coherent millimeter-wave/microwave carrier generation,” *IEICE Trans. Electron.*, vol. E99C, no. 9, pp. 1048–1055, 2016, doi: 10.1587/transele.E99.C.1048.

[63] M.-C. Lo *et al.*, “Foundry-fabricated dual-DFB PIC injection-locked to optical frequency comb for high-purity THz generation,” in *Optical Fiber Communication Conference*, 2019, pp. W1B-3.

[64] G. K. M. Hasanuzzaman, H. Shams, C. C. Renaud, J. Mitchell, and S. Iezekiel, “Photonic THz Generation using Optoelectronic Oscillator-driven Optical Frequency Comb Generator,” in *2018 International Topical Meeting on Microwave Photonics (MWP)*, 2018, pp. 1–4, doi: 10.1109/MWP.2018.8552892.

[65] T. Nagatsuma *et al.*, “Terahertz wireless communications based on photonics technologies,” *Opt. Express*, vol. 21, no. 20, pp. 23736–23747, Oct. 2013, doi: 10.1364/OE.21.023736.

[66] S. Takeuchi *et al.*, “Novel lightwave-interferometric phase detection for phase stabilization of two-tone coherent millimeter-wave/microwave carrier generation,” *IEICE Trans. Electron.*, vol. E99C, no. 9, pp. 1048–1055, 2016, doi: 10.1587/transele.E99.C.1048.

[67] Y. Ma, L. Stewart, J. Armstrong, I. G. Clarke, and G. Baxter, “Recent progress of wavelength selective switch,” *J. Light. Technol.*, vol. 39, no. 4, pp. 896–903, 2020.

[68] A. A. Ibrahim, T. Shiramizu, S. Ye, Y. Mikami, and K. Kato, "Pilot-Lightwave-based Terahertz Wave Phase Stabilization," *Conf. Dig. - IEEE Int. Semicond. Laser Conf.*, vol. 2022-Octob, no. Ld, pp. 2022–2023, 2022, doi: 10.23919/ISLC52947.2022.9943347.

[69] T. Shiramizu, A. A. Ibrahim, S. Ye, Y. Mikami, and K. Kato, "Photonic Phase Stabilization Control System for Terahertz-Wave Phase Modulation," in *2022 27th OptoElectronics and Communications Conference (OECC) and 2022 International Conference on Photonics in Switching and Computing (PSC)*, 2022, pp. 1–4, doi: 10.23919/OECC/PSC53152.2022.9850107.

[70] A. A. Ibrahim, H. Chen, T. Shiramizu, Y. Mikami, and K. Kato, "Terahertz-Wave Phase Modulation Enabled by Optical Interferometric Phase Stabilization," in *2022 Asia-Pacific Microwave Conference (APMC)*, Nov. 2022, pp. 943–945.

CHAPTER 5
CONCLUSION

5.1 Conclusion of the Thesis

In Chapter 1, the research background was discussed, which was based on Cisco's information about the global trend of device application. The significance of THz waves in meeting high-speed communication requirements was highlighted. Various methods of THz wave generation and the development trend in multilevel modulation techniques were explored. Finally, a method for generating phase-modulated THz waves using the photomixing approach was proposed.

Chapter 2 focused on the development of a new method for phase stabilization in the photomixing setup. The phase stabilization system using a Mach-Zehnder interferometer was studied, and wavelength selective switch channel settings techniques were examined. The mechanism of phase modulation was investigated, and a novel phase stabilization method involving introducing a pilot lightwave from the backward direction of the THz wave generation system was introduced.

In Chapter 3, the phase stabilization method was validated by implementing it in the THz wave generation system. The focus was on assessing the stability of the optical domain within the THz wave generation setup. Preliminary experiments were conducted, which successfully demonstrated the effectiveness of the proposed method. The primary experiment focused on higher bit rates, and the results obtained from both forward and backward direction phase stabilization methods were compared. Clear improvements in eye-opening at bit rates exceeding 3 Gbit/s were revealed.

Chapter 4 delved into the generation and detection of stabilized, phase-modulated THz waves. Preliminary experiments concentrated solely on the backward direction phase stabilization method, which yielded stable signals. The primary experiment prioritized higher bit rates, and the results obtained from both forward and backward direction phase stabilization were compared. The detected signals remained stable at higher modulation rates, specifically 5 Gbit/s and 10 Gbit/s for BPSK modulation.

Chapter 5 serves as the conclusive chapter of this thesis, summarizing the key findings and outcomes of the research. It brings together the discussions and results presented in the preceding chapters to draw meaningful conclusions.

5.2 Outlook

The findings of this research point to a bright future for signal transmission and communication technology. Following the successful integration of the system into a UTC-PD module system using waveguide transmission, several significant paths justify further investigation. Investigating the application of this experiment with chip antennas for signal transmission in the air has enormous potential in the near future. Chip antennas, noted for their small size and integration capabilities, have the potential to revolutionize wireless communication by enabling seamless data transfer in a wide range of devices and circumstances.

Furthermore, there is an urgent need to conduct additional studies in order to attain larger modulation rates and investigate higher levels of modulation. These initiatives are aimed at improving high-speed data transmission in order to meet the increasing demands of current data-intensive applications.

This research establishes a solid foundation for contributing to the creation of cutting-edge technologies that will determine the future of communication standards as we move beyond 5G communication. This research opens the door to a more connected and data-driven society where communication knows no bounds by seeking to overcome current limitations and embracing creative concepts.